Evaluating
Ligand Gated Human 5-HT_{3A} Receptor Variants
for Anesthetic Studies on Single Channel Level

Dissertation
zur Erlangung des Doktorgrades (Dr.rer.nat.) der
Mathematisch-Naturwissenschaftlichen Fakultät der
Rheinischen Friedrich-Wilhelms-Universität
Bonn

von
Kathrin Groeneveld, geboren in Wittlich

Bonn, 28.09.2015

Angefertigt mit Genehmigung der Mathematisch Naturwissenschaftlichen Fakultät der Rheinischen Friedrich-Wilhelms-Universität Bonn

Durchführung der experimentellen Arbeiten:

an der Klinik und Poliklinik für Anästhesiologie und operative Intensivmedizin der Universität Bonn
und im Fachbereich für Anästhesiologie der Universität Stony Brook, New York

1. Gutachter: Herr Prof. Dr. B. W. Urban
2. Gutachter: Herr Prof. Dr. V. Herzog
Verteidigt am 14.01.2016 in Bonn
Erscheinungsjahr 2016

Contents

Contents 3
List of Abbreviations 5
Introduction 6
Review 6
Ligand Gated Ion Channels 6
5-HT_3 Receptors and their Subunits 7
Actions of Anesthetics and Anesthetic Related Drugs on 5-HT_3 Receptors 13
Specific Aims 16
Materials and Methods 17
Molecular Biology 17
HEK-293 cells 17
Electrophysiology 20
Patch Clamp Method 20
Recording Protocols 23
Excluding Experimenter- and Setup Bias 26
Solutions 27
Software 28
Equipment 29
Analysis of Macroscopic Currents 30
Fitting Macroscopic Currents 31
Rundown 32
Analysis of Single Channel Currents 33
Excised Outside Out Mode 33
Cell Attached Mode 34
Statistics 39
Results 40
5-HT_{3A} wt– Basic Characterization (Without Drug) 40
Excised Outside-Out Patches 40
5-HT_{3AB} wt– Basic Characterization (Without Drug) 45
5-HT_{3A} QDA – Basic Characterization (Without Drug) 54
Excised Outside-Out Patches 54
5-HT_{3A}QDA - Cell-attached Patches 61
Amplitudes 63
Duration Histograms 65
Clusters 65
Cluster Durations 68
Quasi Macroscopic Currents 75
Openings in Clusters 77
Closings within Clusters 87
Closings Out of Clusters 89
5-HT_{3A} QDA – With Propofol 91

Excised Outside-Out Patches ... 91
Cell-Attached Patches ... 92
5-HT_{3A}QDA - With Phenol ... 100
Cell Attached Patches ... 100
Discussion ... 110
Comparing Three 5-HT_3R Variants to Find a Model for Single Channel Studies ... 110
5-HT_{3A} ... 111
5-HT_{3AB} ... 112
5-HT_{3A}QDA ... 116
h5-HT_{3A}QDA as a Model for Studying Single Channel Kinetics in wt h5-HT_{3A} ... 117
Determination of Clusters is a Crucial Step in Single Channel Analysis ... 118
Activity of h5-HT_{3A}QDA Channels Varies Between Patches and Over Time 119
Single Channel Kinetics Are 5-HT Concentration Dependent ... 120
Comparing the Kinetics of *Human* and *Mouse* 5-HT_{3A}QDA ... 122
Quasi Macroscopic Currents Resemble Recorded Macroscopic Currents ... 125
Effects of Substances on 5-HT_{3A}QDA Channels ... 126
5-HT_{3A} QDA – With Propofol ... 126
5-HT_{3A} QDA – With Phenol ... 128
Implications for Future Substance Studies on Single Channel Level ... 130
Conclusions ... 131
Abstract ... 132
Attachments ... 134
List of Figures ... 134
List of Tables ... 137
List of Formuli ... 138
References ... 140
Supporting Material ... 145
Time Constants and their Fractions for Combined Histograms ... 145
5-HT_{3A} QDA – With n-Hexanol ... 148
Excised Outside-Out Patches ... 148
Acknowledgment ... 151
Curriculum Vitae ... 152
Eidesstattliche Erklärung ... 153

List of Abbreviations

#	Number
2+ clusters	Clusters that include at least two openings
5+ clusters	Clusters that include at least five openings
5-HT	Serotonin
5-HT_{3A}	Homomeric serotonin gated receptor channel, formed by A subunits
5-HT_{3AB}	Heteromeric serotonin gated receptor channel, formed by A and B subunits
5-HT_{3A}QDA	High conductance mutant of homomeric serotonin gated receptor channel, formed by A subunits
$5HTR_3$	Serotonin gated receptor channel
A2D	Desensitized receptor bound to two agonists
A2R	Receptor bound to two agonists
A3D	Desensitized receptor bound to three agonists
A3R	Receptor bound to three agonists
Ach	Acetylcholin
AchR	Acetylcholin receptor
AD	Desensitized receptor bound to one agonist
A_i	amplitude of i^{th} peak
AR	Receptor bound to one agonist
C	Closed component
C(avg)	Weighted average of closed components
C_1	A closed component
C1-8	Closed components one to eight
C_2	Another closed component
Ca^{2+}	Calcium ion
cDNA	complementary Desoxyribonucleic acid
chi²	non parametric statistic test value to estimate the goodness of fits
Cl^-	Chloride ion
CNS	Central nervous system
CO_2	Carbon dioxide
Cs	Cluster component
Cs(avg)	Weighted average of cluster components
D	Desensitized receptor
DMSO	Dimethylsulfoxid
EC_{50}	50% enhancing concentration
ECS	Extracellular solution
FBS	fetal bovine serum
fr.amp.	Fractional amplitude
FRET	Förster resonance energy transfer
G (pS)	Conductance in pico Siemens
GABA	Gamma aminobutyric acid, a neurotransmitter
$GABA_A$	a ligand gated ion channel, responds to Gamma aminobutyric acid
GlyR	Glycine receptor
HEK293	Human embryonic kidney cell line 298
HEPES	4-(2-hydroxyethyl)-1-piperazineethanesulfonic acid , a buffer agent
HTR3A-E	Subunits A to E of the serotonin gated receptor channel
I (pA)	Current in pico Ampere
I_{0i}	mean current of i^{th} peak
IC_{50}	50% inhibiting concentration
ICS	Intracellular solution
I_{equil}	fraction of current remaining after both decays have equilibrated
Interval50	Time constant for 50 % channel recovery after desensitization
I_{ON}	current component, if full onset would be reached
I_{peak}	Maximum of a macroscopic current
I_t	current at time t (pA)
I-V	Current-Voltage relationship
k	curvature factor for the onset, k≥1
K^+	Potassium ion
M3	Membrane domain 3
M4	Membrane domain 4
MA	Amphipathic alpha helix within intracellular TM3-TM4 domain
medium (+AB)	medium includes antibiotics
n	Number of events
Na^+	Sodium ion
$NaHCO_3$	Sodium bicarbonate
n_{Hill}	Hill coefficient
O	Open component
O(avg)	Weighted average of open components
O_B	Brief open component
O_I	Intermediate open component
O_L	Long open component
PNS	Peripheral nervous system
p_{open}	Open probability
PSG	Penicillin/Streptomycin/Glutamine solution
$p_t = p_{total}$	Open probability in a complete recording
QMC	Quasi macroscopic current
R	Receptor
r	Spearman coefficient
rf	Rectification factor
rf	rectifying factor (calculated ba formula 14)
rs	molar refractivity
SD	Standard deviation
t	Time
t_{crit}	Critical time between clusters
$t_{crit\ long}$	Critical time between the shortest and the second to shortest cluster component
TM	Transmembrane
V (mV)	Voltage in milli Volt
$width_i$	width of i^{th} peak
wt	Wild type
τ_C	Time constant of closed component
τ_{Cs}	Time constant of open component
τ_{gap}	Critical gap time between two components
τ_O	Time constant of cluster component
τ_{OFF}	Timeconstant of recovery from desensitization
τ_{ON}	Onset of macroscopic current
$\tau_{recovery}$	Offset of macroscopic current
ω	fraction of decay due to second time constant

Introduction

Review

Although anesthesia has been practiced for over 150 years now – since the first successful surgery under ether induced anesthesia in 1846 - its molecular mechanisms are still fairly unknown. Anesthesia is a physiological state of variable patterns. Most general anesthetics induce immobility, unconsciousness and amnesia, but analgesia or muscle relaxation can be effects, too. As the group of substances, which can induce anesthesia, is chemically very diverse, the common belief for a long time was that anesthetics had nonspecific effects on cell membranes that produced changes in the function of membrane proteins.

Only when in the 1950s and 1960s new electrophysiological techniques provided new insights about pre- and post synaptic actions and their regulatory role on neural activity (Bonnet and Bremer, 1952; Bremer et al., 1954) (Eccles, 1964) (Hodgkin and Katz, 1949; Hodgkin and Huxley, 1952), this lead to findings of more specific actions of anesthetics on neurotransmitter receptors (Eccles et al., 1963).

Ligand Gated Ion Channels

Gamma aminobutyric acid ($GABA_A$), glycine (Gly), nicotinic acetylchlorine (Ach) and serotonin ($5\text{-}HT_{3)}$ receptors build a superfamily of ligand-gated ion channels. They share a basic topology of five individual subunits, each possessing four transmembrane stretches. The large extracellular domain contains the allosteric agonist binding sites nestled between subunits. Each subunit contributes to a central, transmembrane pore through which ions like Na^+, K^+, Ca^{2+}, or Cl^- permeate, depending on size and charge of the amino acid side chains that line the pore. Binding of a neurotransmitter to the binding pocket triggers a conformational change of the gate region, which lies within the pore (Figure 1, Unwin. 1993).

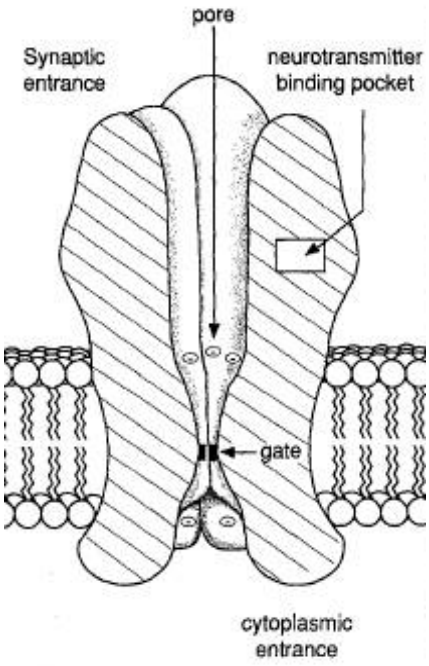

Figure 1: Basic features of a neurotransmitter-gated ion channel, taken from N. Unwin 1993.
A ring of subunits forms a pathway across the lipid bilayer that includes the pore and the gate; two neighboring subunits contribute to each binding pocket

Nerve cells express a large variety of ligand-gated ion channels with different ligand binding, ion selectivity and conductance. Many of them are promising molecular targets for the central nervous system effects of general anesthetics. Propofol for example decreases neuronal excitability by enhancing agonist induced activation of anion-selective inhibitory channels such as $GABA_A$Rs and GlyRs (Zeller et al., 2008; Nguyen et al., 2009) and inhibiting cation-selective excitatory channels such as 5-HT_3Rs and nAChRs (Rusch et al., 2007).

5-HT_3 Receptors and their Subunits

5-Hydroxytryptamin$_3$ (5-HT_3) receptors are ligand gated cation channels that can be found in both the peripheral and central nervous systems (Tecott et al., 1993; Kapeller et al., 2011). One well established physiological role of these receptors in humans is their modulation of the vomiting reflex. 5-HT_3 antagonists such as ondansetron are used clinically to prevent anesthesia induced nausea and vomiting (Gyermek, 1995). They are also known to play roles in cognition, pain and psychological disorders and can be found in according areas in the central (CNS) and in the peripheral nervous system (PNS).

During a stable transfection of HEK-293 cells with human 5-HT_{3A} encoding DNA (performed by Dr. Boenisch's group), several clones were produced (see page 19:

Stable Transfection of HEK-293 Cells). Dr. Urban's group had the opportunity to electrophysiologically test several of those clones (data not shown). Although the same plasmid was used to construct the clones, the expressed protein showed a variety of serotonin induced currents. In addition to differences in the number of functional channels that were expressed at the plasma membrane, the kinetics of the channels varied. Some clones produced currents with slow activation- and decay constants. These were assumed to have introduced a spontaneous mutation and were not used for further experiments. The homomeric 5-HT_{3A} clone that was used in this group was the one that showed a maximum expression of channels, assumed by a maximum peak current that was reached when applying serotonin to outside-out patches from those cells.

This 5-HT_{3A} clone was used in Dr. Urban's group for about 15 years now and reliably showed reproducible results (Barann et al., 2000a, 2000b, 2008; Urban et al., 2006a). This way a very detailed characterization and pharmacological studies of about 100 substances could be done.

Naturally Occurring 5-HT_3 Subunits

Functional 5-HT_3 receptors can be assembled as a homomer of A subunits, or as a heteromer of A and either B, C, D, or E subunits. As 5-HT_{3A} was the first detected and cloned subunit, the homomer is the functionally best studied version. Introducing another subunit alters electrophysiological properties (Niesler et al., 2007), which could explain differences between studies investigating 5-HT_{3A} receptor function in cell lines compared with native subunit heterogeneous tissues.

Comparative expression analysis of HTR3A, B, C, D and E genes showed HTR3D expression to be restricted to kidney, colon and liver and HTR3E expression to colon and intestine, whereas all other genes are widely expressed in many tissues including brain (Niesler et al., 2003).

5-HT$_{3A}$ Subunit

5-HT$_{3A}$ is the only known homomeric pentamer of the 5-HT$_3$ family that forms a functional ion channel. Subunit homogeneity simplifies the molecular biological properties of the pentamer, so that kinetic and molecular models with fewer variants can be built. Compared to other ion channels of their family, 5-HT$_{3A}$ channels show slow kinetic constants, so that influences of substances on channel opening and closing phases are better to detect and quantify.

The 5-HT$_{3A}$ stably transfected HEK cell line used in the present study has been used since many years and showed a stable protein expression as well as reproducible channel activity. This made it possible to build up a data pool of over 100 macroscopic substance studies on 5-HT$_{3A}$ (Barann et al., 2000a, 2008; Decker, 2010; Meiboom et al., 2013). Because the single channel conductance of 5-HT$_{3A}$ is too small to detect, alternatives are needed for studies that relate macroscopic substance studies to single channel behavior.

Baptista-Hon et al (Baptista-Hon et al., 2013) described a membrane associated MA-stretch between the M3 and M4 region, which has 114 residues and plays an important role for the single channel conductance and for the rectification of the 5-HT$_3$ channel. Within that area there's a structurally still unresolved stretch of 85 residues. When truncating this area to 75 residues, Baptista-Hon et al create a functionally wild type like channel. When truncating the area to only 70 residues, rectification is abolished and single channels show a higher conductance. The M3-M4 loops of human cys-loop receptors all exceed 70 residues. This length seems to be fundamental.

5-HT$_{3B}$ Subunit

One serotonin channel variant that occurs in native cells is the heteromeric 5-HT$_{3AB}$, which shows a higher single channel conductance compared to 5-HT$_{3A}$ (Hapfelmeier et al., 2003; Stewart et al., 2003). Higher single channel conductances resemble conductances that were found in native neurons (Hussy et al., 1994a).

Because of past positive experiences with the stably transfected 5-HT$_{3A}$ line, one goal here was to establish a stable transfected 5-HT$_{3AB}$ line as well. When an according clone was built, a basic electrophysiological characterization was the first step to identify similarities and differences to the already characterized homomer.

When expressed in *xenopus* oocytes, the serotonin EC$_{50}$ for homomeric channels is 1.8 µM, for heteromeric 5-HT$_{3AB}$ 20 µM, and AB shows a faster decay (Stevens, 2005).

Homomeric 5-HT$_{3A}$ channels and heteromeric 5-HT$_{3AB}$ channels differ in several basic characteristics (Baptista-Hon et al., 2013): while A is outward rectifying, AB shows a linear IV. Macroscopic AB currents show a faster decay than A and lower calcium permeability. Also the single channel conductance of AB channels is much higher. While A single channel currents are too small to be resolved, AB reaches 16 pS.

When it comes to the prediction of the stoichiometry of heterogeneous channels, opinions differ. Barrera and group purified 5-HT$_{3AB}$ receptor proteins with antibody-decorated subunits and based on atomic force microscopic images of resulting receptors predict a A2B3 (BBABA) stoichiometry (Barrera et al., 2005a). Docking experiments using homology models of 5-HT$_{3A}$ and 5-HT$_{3AB}$ channel binding sites predict that serotonin binds to the interfaces between A subunits (Lochner and Lummis, 2010). This means within heteromeric channels, two A subunits must be adjacent to each other and supports the idea of a A3B2 stoichiometry with nonadjacent B subunits that (Miles et al., 2013) predict, based on fluorescence intensity ratios and Förtster resonance energy transfer (FRET) efficiencies of heterogenic 5-HT$_3$ receptor proteins in isolated plasma membrane-sheets. Da Costa and Sine showed a dependence of binding kinetics on the subunit composition of pentameric ion channels as well (daCosta and Sine, 2013).

High Conductance Mutant 5-HT$_{3A}$ QDA Receptor Channels

Mutation of three arginine amino acids within the MA-stretch of the 5-HT$_{3A}$ subunit to the according residues of the B subunit (Q, D, A) produces a high conductance homomer, the 5-HT$_{3A}$QDA (Kelley et al., 2003a).

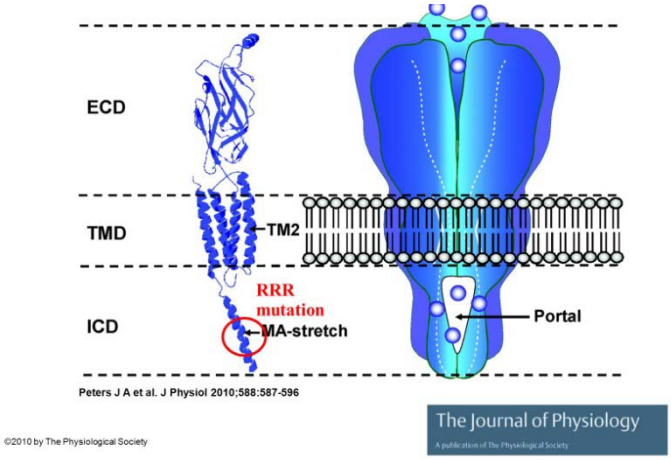

Figure 2: The architecture of the eukaryotic members of the pentameric ligand-gated ion channel super family.
Left: a homology model of a human 5-HT$_{3A}$ receptor subunit constructed by Hales et al. (Hales et al., 2006), indicating the position of the MA-stretch and the RRR mutation that leads to the high single channel conductance mutant 5-HT$_{3A}$QDA.

The human isoform has a conductance of 42 pS and a linear I-V at low extracellular Ca^{2+} concentration. Inward currents depend on extracellular Ca^{2+} concentration, which leads to Ca^{2+} dependent changes in channel conductance and rectification.

Kinetic Models for 5-HT$_{3A}$ QDA Receptor Channels

First schemes for receptor channel activation of ligand gated cys-loop channels were conducted on the nicotinic acetylcholine-receptor (AChR) channel (Sine and Steinbach, 1987). AChR single channel recordings at low agonist concentrations did show one open component and two closed components, so that it was assumed that the channel activation follows a simple sequential kinetic scheme with two agonist bound but closed channel states (AR and A2R) that lead to an openings series (burst), where openings are separated by short closures (A2R').

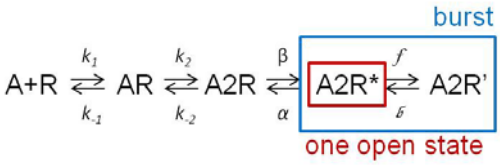

Figure 3: Kinetic scheme for opening and closing of AChR

The scheme can be described by three rate constants: the channel opening rate (β), the channel closing rate (α), and the agonist dissociation rate (k_{-2}). β and k_{-2} are comparable in magnitude, so that on average the channel opens and closes several times once the receptor channel opens. β is also much larger than α such that the doubly occupied receptor has a high probability of being open (β / β + α = 0 93).

Glycine receptor (GlyR) kinetic models include more than one open state and assume that each open state corresponds to a different state of ligation (Beato et al., 2004). Such a model cannot describe the experimental dwell times of 5-HT_{3A}QDA (Bouzat et al., 2008). They suggest that three classes of openings arise from a fully liganded closed state, but include preceding binding steps.

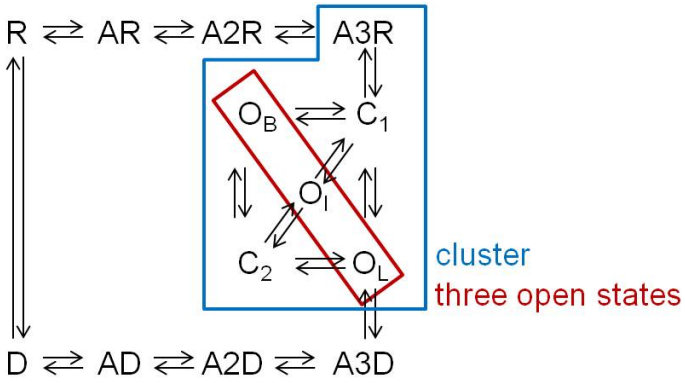

Figure 4: Kinetic scheme for opening and closing of mouse 5-HT_{3A}QDA channels, taken from (Corradi et al., 2009).
Colored squares are own modifications. R = receptor, AR, A2R, A3R = agonist(s) bound to receptor, but receptor still in a closed state; D = desensitized receptor state; AD, A2D, A3D = agonist bound desensitized receptor states; O = open receptor states (brief, intermediate, long); C = closed receptor states within a cluster.

Actions of Anesthetics and Anesthetic Related Drugs on 5-HT_3 Receptors

5-HT_3 receptor antagonists such as ondansetron are used clinically to prevent nausea during chemotherapy and anesthetic induced nausea and vomiting (AINV) (Gyermek, 1995). Some anesthetics, such as the volatile anesthetic ethanol, tend to increase the incidence of AINV but others, such as the intravenous anesthetic propofol, decrease the incidence of AINV.

Anesthetics also have differential effects on 5-HT_3 receptor currents. The anesthetic induced modulation of agonist-elicited currents correlates with the molecular volume of anesthetics (rs = -0.962, (Stevens, 2005)). Small molecules potentiate, large molecules inhibit and intermediate ones have a minimal effect on 5-HT_{3A} and 5-HT_{3AB} channels. This leads to the conclusion, that 5-HT induced currents are enhanced by binding to a small binding site that physically limits binding to molecular volumes smaller than 110 $Å^3$. Additionally, a larger binding site is proposed by Stevens et al (2005). When larger compounds bind there, inhibitory actions are mediated. The small binding site does not seem to be effected by the presence of B subunits, the large site does.

It is widely accepted that a detailed study of drug effects on voltage-gated channels requires voltage protocols that test for effects on different states of the channel. Similarly, with ligand-gated channels we use different application protocols to study effects of a drug on the different states of these channels.

The integrated current response takes into account changes in onset, peak current and desensitization of the current response and thus may provide the best estimate of how a drug affects synaptic communication. But to gain detailed information about molecular mechanisms between agonist and receptor proteins, a quantification of the individual effects on macroscopic currents was done. To separate wash-in time constants of these effects, macroscopic experiments were performed in different application modes. In open channel mode, the drug is applied simultaneously with the agonist, so that fast effects on the open channel are detected. In closed channel experiments, the drug is applied for a certain duration to the closed channel, before application of the agonist opens it. This way effects on the closed channel conformation are detected. The equilibrium mode experiments combine all effects of the drug by continuously applying it before and during agonist application. This mode might be

closer to physiological conditions, but would be hard to interpret without previously described experiments, because many effects with different time constants overlap.

Propofol is a clinically widely used anesthetic. To investigate its depressing actions on 5-HT_3 receptors, detailed macroscopic electrophysiological studies have been done on 5-HT_{3A} receptor channels. Propofol doesn't seem to effect the onset, but produces a concentration dependent acceleration of desensitization (in equilibrium application). Propofol shows significant effects at concentrations as low as 3 µM and less, which is close to the concentration where 50% of patients show no motor response to tracheal intubation (2 µM, (Kazama et al., 1998)).

The net effect at a synapse can be estimated as the effect on the integrated current, which represents the total charge passing into the postsynaptic membrane. Propofol suppresses ion flux through excitatory ion channels (Belelli et al., 1996; Pistis et al., 1997; Urban et al., 2006) and causes less emesis (Borgeat and Stirnemann, 1998).

Because anesthetic potency is generally related to drug hydrophobicity, series of compounds are examined. Meyer-Overton relations have been used to estimate anesthetic potencies arising from nonspecific hydrophobic actions (Barann et al., 2008). When applied under equilibrium condition, propofol inhibits serotonin induced currents in tranfected HEK 293 cells with an IC_{50} of 18 µM. 2-Isopropylphenol has an IC_{50} of 17 µM, phenol 1.6 mM. All three substances show two effects, one with fast and the other with slow kinetics. Propofol increases desensitization rate, 2-isopropylphenol decreases it. With propofol, both the fast as the slow effects are inhibitory, whereas with phenol and 2-isopropylphenol there is a fast potentiating effect and a slow inhibitory effect (Barann et al., 2008). The fast effects are serotonin concentration and anesthetic concentration dependent. Inhibition by propofol requires more than a few milliseconds to develop, similar to muscle type ACh receptors (Dilger et al., 1994). The time constant for peak current inhibition by propofol (220 ms) is similar to the time constant for 5-HT induced desensitization (250 ms).

In order to explore the differences in molecular actions of propofol to molecular actions of inhalation anesthetics such as ethanol, macroscopic electrophysiological studies with a homologous series of n-alkanols have been performed on human 5-HT_{3A} receptors (Decker et al., 2015). Just like propofol, N-alcohols did show fast and slow effects on currents over 5-HT_{3A}, which depend on exposure time, concentration and

chain-length. N-hexanol will serve in the following study as representative substance of the n-alkanol group, as it has physicochemical properties intermediate between phenol and ethanol. Under equilibrium condition, n-hexanol reduces the current with an IC_{50} of 1.5 mM. The fast and the slow inhibiting effect occur with the time constants 21 ms and 11.6 ms, respectively. N-hexanol accelerates both onset and decay of macroscopic currents.

Effects of anesthetics and anesthetic related substances on 5-HT_3 receptors are complex and versatile. Above described studies were conducted on macroscopic level, meaning the sum of many activated ion channels was observed. To be able to resolve the many overlapping effects of substances, single channel studies are necessary. Being able to relate changes in single channel kinetics to macroscopic changes will give further inside to possible binding sites of 5-HT_3 channels.

In the case of the aromatic propofol, the strategy is to look at compounds that share some, but not all, of the chemically active moieties of the drug. The lesser hydrophobic propofol derivative phenol is structurally related, but has only one reactive OH-group. N-Hexanol is a closely related open chain derivative with one OH-group. Thus, phenol and n-hexanol are the compounds of choice to start a series of substance studies on single channel level and explore the different molecular actions of individual moieties of anesthetic related substances.

Specific Aims

Members of the ligand-gated ion channel super family are promising molecular targets for the effects of general anesthetics on central nervous system. There is extensive electrophysiological data on the effects of anesthetics and related compounds on 5-HT_{3A} receptor channels serving as a homomeric model for ligand-gated ion channels. Almost all those studies were done on the macroscopic level. Information on the single channel level is required in order to obtain details of the molecular interactions of anesthetics with their protein targets. However, 5-HT_{3A} receptor channels have too low a conductance to be resolved with current electrophysiological techniques. The present study examines two alternate forms of 5-HT_3 receptors with high conductance and evaluates their usefulness for kinetic analysis of anesthetic interactions with channels.

Aim 1 was to characterize human 5-HT_{3AB} channels as they are physiologically occurring heteromeric variants of 5-HT_3 receptors known to have a sufficiently large single channel conductance to be easily resolved.

Aim 2 was to characterize human 5-HT_{3A}QDA channels as an alternative which although not occurring physiologically has the advantage of being the least modified mutant of 5-HT_{3A} that shows high single channel conductance, and also being homomeric like the wild-type.

Aim 3 was to perform pharmacological single channel studies on the more suitable high-conductance form of the 5-HT_3 receptor channel.

Materials and Methods

Molecular Biology

HEK-293 cells

Human Embryonic Kidney 293 cells, originally derived from human embryonic kidney cells in the early 70's. They are easily transfected with cDNA coding for a variety of proteins and are commonly used in cell biology research.

Cell Culture

Cell culture methods included passing, plating, freezing and thawing of HEK 293 cells. All cell culture methods followed standard procedures. All solutions, media and material were sterile. Cells were kept in cell culture flasks in an incubator at 37°C, 95% humidity and 5% CO_2. For experimental use cells were seeded in 35 mm cell culture dishes.

Media Used For Cell Culture

For Cells for Transient Transfections:

Based on Dulbecco's MEM Nutrient Mix (4.5g/D Glucose, + D-Glutamine)

Growth medium without antibiotics (-AB):

- 10% fetal bovine serum (FBS)
- 15mM HEPES

Growth medium with antibiotics (+AB):

- 10% FBS
- 15 mM HEPES
- 5 µg/ml Plasmocin (to prevent mycoplasma)
- 1% Gibco PenStrep 10,000

Growth medium (+AB): to use for one week after newly defrosted cells have recovered (= use for first passage)

10% FBS

15 mM HEPES

5 mg/ml Plasmocin (recommended dose to eliminate mycoplasma from infected cells)

1% Gibco PenStrep 10,000

Cryoprotectant medium:

10% FBS

5% (v/v) DMSO

For 5-HT_{3A} Stable Transfected Cells:

Based on Dulbecco's MEM Nutrient Mix (4.5g/D Glucose, - D-Glutamin)

Growth medium with antibiotics (+AB):

10 % FBS

3 % $NaHCO_3$

1% PSG (10,000 U/ml penicillin, 10,000 U/ml streptomycin, 29.2 mg glutamine)

1.5 % PANecitin (=Geniticin)

Cryoprotectant medium:

10% FBS

5% (v/v) DMSO

For 5-HT_{3AB} Stable Transfected Cells:

Based on Dulbecco's MEM Nutrient Mix (4.5g/D Glucose, - D-Glutamin)

Growth medium with antibiotics (+AB):

10 % FBS

500 µg/ml Zeocin

1.5 % PANecitin (=Geniticin)

Cryoprotectant medium:

10% FBS

5% (v/v) DMSO

Stable Transfection of HEK-293 Cells

The procedure of the stable transfection was kindly done by Dr. Boenisch's group at the Institut für Pharmakologie und Toxikologie in Bonn.

Human 5-HT3A cDNA was transfected into HEK 293 cells via calcium phosphate transfection (Chen and Okayama, 1987) using the pCDNA3 vector, which is 5.4kb long and includes codes for geniticin and ampicillin resistance. 5-HT3A cDNA integration into the cell genome was nonspecific. Transfected cells were selected by the addition of 800ug/ml geneticin to the cell medium about two days after transfection. This causes non transfected cells to die, which can then easily be discarded by changing cell media every two days. Vital cells stay attached to the flask bottom, unhealthy and dead cells are floating in the discarded medium. The surviving cells were plated in petri dishes and appearing cell clusters separated by clone barrels (*Klonzylinder*, by Sigma) and plated in 24well culture plates (Falcon), where they were cultivated to reach a high confluence. 20-40 of those transfected colonies were then tested via [14C]Guanidinium Influx and binding of the selective 5-HT_{3A} receptor antagonist [3H]GR 65630 [3-(5-methyl-1H-imidazol-4-yl)-1(1-metzhyl-1H-indol-3-yl)-1-propanone] for their expression of human 5-HT3A cDNA. Or specific [3H]5-HT intake experiments were performed. Only positively tested clones – one of which was used for all h5-$HT3_A$ experiments in this work - were conserved.

Transient Transfection of HEK293 Cells

HEK 293 cells were transiently transfected with cDNA that encodes the 5-HT_{3A}QDA subunits. The cDNA was inserted into the cells via transfection reagents fugene (promega) or genejuice (emd-millipore) according to the manufacturer recommended protocols. Cells that were transfected via fugene were co-transfected with CD8 cDNA, to mark successfully transfected cells with CD8 beads before patch clamp experiments.

Electrophysiology

Patch Clamp Method

The patch clamp method to study multiple and single channels was developed by Erwin Neher and Bert Sakmann in 1976 (Neher et al., 1978). It makes it possible to study the excitation of ion channels in a patch of cell membrane under controlled conditions.

As an electrode, one uses a glass micropipette with a tip diameter of about one micrometer. This pipette gets sealed onto the surface of the cell membrane by touching the surface and applying some negative pressure. Such a sealed membrane area is called a patch. To make sure that the pipette tip is smooth and wont poke through the surface, the tip is heat polished.

When the micropipette tip is sealed tightly to the membrane surface area, this results in a very high electrical resistance greater than one gigaohm. One has reached the so called ‘cell-attached’ configuration. From here one has two possibilities. If one moves the pipette upwards, away from the cell, the sealed patch will rip out of the cell membrane and form an ‘inside-out’ patch. But if one rips the membrane surface open first by adding negative pressure, the ‘whole-cell’ configuration is reached. This configuration is a pre step to the ‘outside-out’ configuration. If one moves the micropipette away from the cell surface after forming a ‘whole cell’ patch, the edges of the membrane will stay attached to the edges of the pipette tip and the ripped of flaps of the membrane that are attached to those edges will find each other again and form a closed patch of membrane. This patch will be positioned at the pipette tip in such a way that the former extracellular side will face away from the pipette tip (‘outside out’).

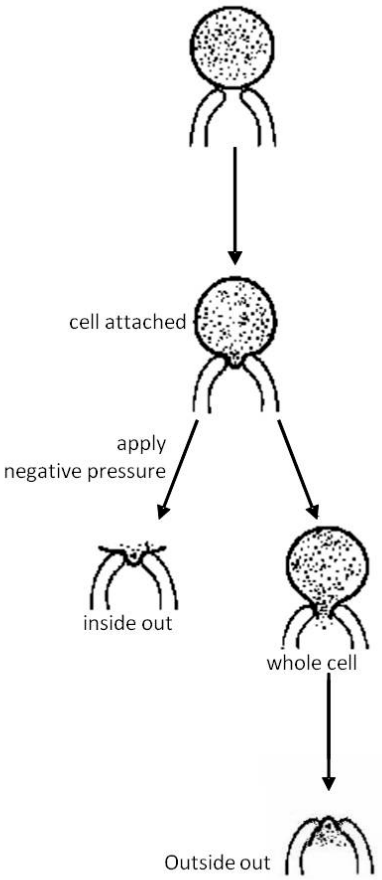

Figure 5: patch clamp configurations

Within this study, only ‘cell attached’ and ‘outside out’ conformations were used.

A chlorided silver wire is placed inside the pipette and brought into contact with the ICS. The wire conducts detected electric currents to the head stage and the connected amplifier. Because of the high resistance of the seal, it is possible to isolate currents across the patch from other electrical noise.

To be able to set the zero current level of voltage, a bath electrode of chlorided silver wire is positioned into the extracellular solution (ECS) that fills the cell dish. The differential amplifier clamps the voltage between the two electrodes to zero and uses the voltage that is needed to do so to observe the current changes over the patch. Therefore the gain by the amplifier is given in mV/pA.

The Cell Attached Configuration

When working with the cell attached configuration, the whole cell stays attached to the ground and there are no solution changes possible with the here used solution exchange system.

Detected are currents over the membrane patch between the inside of the cell and the inside of the pipette. That means the bath electrode cannot be used to clamp the membrane potential of the patch to zero. The membrane potential naturally mainly is determined by the resting potential for potassium. When we fill the micro pipette with extracellular solution (ECS), which includes a potassium chloride concentration (145 mM) close to the inner cell potassium concentration, we force the chemical potential at the cell membrane to zero.

The cell-attached configuration is used to record very small single channel currents. To reduce the background noise as far as possible, the capacity of the recording pipettes is reduced by coating it with Sylgard. This way the glass on the pipette tip is more insulated.

The cell attached configuration leaves the cell surface intact and allows for long stable recordings under equilibrium conditions.

In this study the cell attached configuration is used to record single channel events in a patch under stable conditions for long time periods.

The Outside Out Configuration

When an outside out patch is formed, the glass pipette is filled with intracellular solution (ICS), which mimics the ionic composition of cytoplasm. The pipette with the patch at its tip can be positioned in front of solution application systems. Because the former outside of the cell membrane is facing out of the pipette, agonist and antagonists can be applied to extracellular parts of the channel. The outside out configuration is less stable than the cell attached configuration, but allows for multiple solution changes at the same patch. This way each experiment can be compared to its own control, so that fewer experiments are necessary to reach statistically strong results.

In this study the outside out configuration is used to record multiple few second long traces of macroscopic currents under different conditions at one patch.

Recording Pipettes

Glass capillaries with the inner diameter of 1.12 mm and the outer diameter of 1.5 mm were pulled by a vertical puller into recording pipettes with resistances between 2.5-5.5 MΩ. For cell-attached experiments, the narrow shanks of the pipette tips were coated with Sylgard (Dow Corning Corporation, USA). The Sylgard coat was dried under a heat lamp for 30-60 min.

Patch Life Time

Patch life time varies a lot. Sometimes patches would last only seconds. Every now and then a patch would last hours.

The life time of a patch doesn’t only depend on how stable of a patch could be formed. Depending on the conducted experiments, the patch is exposed to different stress factors. Application of certain substances that influence membrane lipids and proteins will lead to decreasing patch quality, including higher membrane noise and a larger electrical leak. So does the application of large voltages. In some cases this makes it hard to reach the same number of patches for those experiments.

When conducting single channel level experiments, the duration is crucial for the following analysis, because one needs many individual events to reach proper statistics. Generally cell attached patches are more stable than excised ones. The membrane and the cytoskeleton are still intact. This is why for the present study cell attached patches were formed when recording single channel events. For these experiments the holding potential was reduced for the same reason. This way it was possible to record minutes, often 20-30 minutes of channel activity in one patch under one condition.

Still different patch durations mean different numbers of experiments on excised patches and different numbers of recorded single channel events on cell attached patches. Depending on the way gained data are processed and analyzed more stable patches might gain more statistical weight within the data pool. For single channel level experiments, this is hard to be avoided, as individual events of different patches need to be pooled to gain sufficient numbers of events for single channel analysis. For macroscopic currents, domination of results by long lasting patches is avoided by always averaging all experiments of one patch into one data point.

Recording Protocols

The Rapid Solution Changer RS-200 is an up to nine tube system that allows for a computer controlled application of multiple solutions to a whole cell or excised patch. The nine tubes are attached to a rotating head. One tube is positioned in front of the patch (or cell). The software allows for individual protocols that synchronize pinch valves to open and close solution filled tubes and the movement of those tubes in front of the positioned patch.

To reach a maximum response to an agonist pulse it is important to give the channels in a patch sufficient recovery time between pulses by bathing the patch in agonist free ECS for 60 s.

To elicit high currents, excised outside out patches were clamped to -100 mV briefly (0.6 s) before the agonist was applied until the current recording stopped. In between agonist applications, the patch was clamped to 0 mV in order to increase patch longevity.

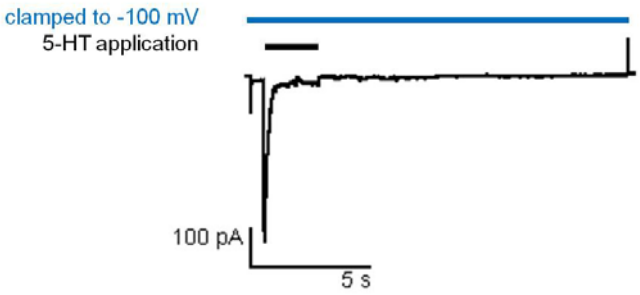

Figure 6: Voltage application on the example of a 5-HT_{3A}QDA transfected excised outside out patch to record macroscopic currents.
Shown is the example of a control experiment without substance application.

Single channel activity from cell attached patches was recorded continuously and requiring a continuous voltage clamp. To reduce the stress on the clamped membrane and prolong the time that a patch stays stable, a less negative voltage of -80 mV was chosen.

Standard Conditions for Control Currents

For macroscopic currents on excised outside out patches, concentration of 30 µM 5-HT was chosen as standard agonist pulse for control currents, to elicit a reproducible maximal response. If not mentioned otherwise, excised patches were clamped to -100 mV.

Cell attached patches are clamped to -80 mV. Control experiments were patched with pipettes filled with 30 nM 5-HT, to elicit as many individual channel events as possible, but avoid overlapping activities of multiple channels.

Concentration Response Curves on Excised Patches

For serotonin:

To determine the agonist concentration dependence of 5-HT_3 channels, different serotonin concentrations were applied to the same patch, while the patch was clamped to one voltage (-100 mV). For display of concentration responses, resulting peak currents were normalized to 30 µM peaks.

For substances:

When applying substances one can differentiate between open channel (-+) and equilibrium (++) application. During an open channel application, substance and agonist are applied simultaneously for 1200 ms. During an equilibrium application, the substance application is started 60 s before the agonist pulse is given.

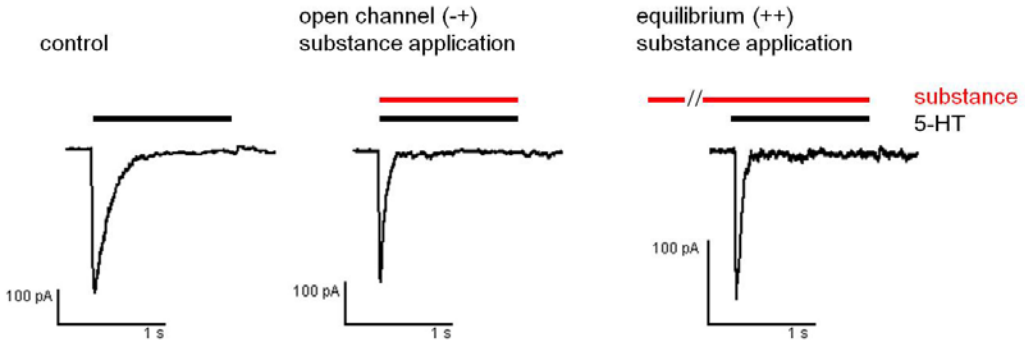

Figure 7: Different solution application modes on excised outside out patches on the example of a 5-HT_{3A}QDA transfected patch.
The patch was clamped to -100 mV, exposed to 30 µM 5-HT for 1200 ms (black bar) and 18 µM propofol (red bar, different durations).

Current-Voltage Dependence (I-V) on Excised Patches

To determine the dependence of 5-HT_3 channels on the voltage at the membrane, a patch was clamped to different voltages and simultaneously perfused by a constant serotonin concentration (30 µM). For I-V display, resulting peak currents were normalized to -100 mM peaks.

Double-Pulse Experiments on Excised Patches

To evaluate the recovery time of 5-HT_3 channels from desensitization, double-pulses with varying interpulse intervals were given. Currents obtained after a 60 s interval served as control.

Flow Rate

In all set ups solution change systems depending on gravity are used. By adjusting the reservoir height and valve positions, the flow rate of solutions can be changed. Generally a high flow rate is preferred, to make sure substances reach all in the patch present ion channels immediately and kinetics are not obscured by slow arrival of substances to binding sites. Limiting factor though is the mechanical stress that high flow rates expose the patches to, which might lead to loss of the seal.

High rack position flow rate is 2.3 ± 0.08 ml/min, lowest rack position 1.6 ± 0.09 ml/min. Most of the time only valves that trigger the flow speed in only ECS containing tubes were shifted to reduce the speed.

It can be assumed, that within this study, flow rates are sufficiently adjusted and don't vary.

Excluding Experimenter- and Setup Bias

Selective macroscopic current experiments on stable 5-HT_{3A} transfected HEK cell membranes were performed as in previous studies (Barann et al., 2000b). Current kinetics with τ_{ON} of 7.6 ± 3.7 and τ_{OFF} of 156.6 ± 154.1 (ms ± SD) did confirm the macroscopic current shape that was found constantly during the last 15 years. So did other electrophysiological properties that were checked for in the present study, like the EC_{50} for serotonin (here 8.9 µM) and the refractory time needed for a 50 % recovery (here 19.94 s ± 2.63 SD). This way it was assured that experimenter bias or changes in the experimental setup do not alter the resulting channel properties and therefore future single channel analysis can be corresponded to past macroscopic properties without being concerned about these potential impacts. Patches and their electrophysiological performances depend highly on many equipment and execution details (Suchyna et al., 2009a), which makes it advisable for every new experimenter or newly combined setup to check for a few properties on the well known 5-HT_{3A} channel before starting experiments on unknown channel variants.

Rundown correlated changes of kinetics over time (the decay phase gets faster by 1.7 % per minute) were not surprising either. Rundown and related changes over time

are a common, yet still not understood phenomenon within the patch clamp community (Suchyna et al., 2009b). Loss of activatable channels in a patch would explain the amplitude reduction, but not the changes of τ_{OFF} over time. By always relating the experimental current to its own framing control and washout currents, rundown effects do not alter the relative effects of substances or different agonist concentrations.

Solutions

Extracellular solution (ECS) contains (mM):
NaCl (150), $CaCl_2$ (1.8), $MgCl_2$ (1), HEPES (10), KOH (5.4), NaOH to adjust the pH to 7.4

High potassium-extracellular solution (ECS) contains (mM):
KCl (145), NaCl (5), $CaCl_2$ (1.8), $MgCl_2$ (1), HEPES (10), KOH (5.4), NaOH to adjust the pH to 7.4

Intracellular solution (ICS) contains (mM):
KCl (140), $MgCl_2$ (5), HEPES (10), EGTA (5), KOH (10), KOH to adjust the pH to 7.4

For excised outside out experiments, 5-HT and substances were dissolved in ECS.
For cell attached experiments, 5-HT and substances were dissolved in ICS, substances were additionally dissolved in high potassium ECS.

Serotonin (5-hydroxytryptamin):
By Sigma-Aldrich.
250 µM stock was made first and kept frozen until usage.

Propofol (2,6-di-isopropylphenol):
By Sigma-Aldrich, 97% purity.
1M ethanol stock was made first.
Final solution was stirred over night before used for experiments.

Phenol:

By Sigma-Aldrich, ≥ 99.5% purity.

Was directly dissolved in ECS/ICS.

Final solution was stirred over night before used for experiments.

2-n-hexanol:

By Sigma-Aldrich, 99% purity.

10mM ethanol stock was made first.

Final solution was stirred over night before used for experiments.

Software

Table 1: List of used software

software	provider	origin
RSC-200	Bio-Logic, Science Instruments	France
pClamp, ClampFit, ClampEx	Axon Instruments, Molecular Devices Corporation	CA, USA
patchmaster	HEKA	NY, USA
QuB	SUNY Buffalo (Nicolai and Sachs, 2014)	NY, USA
IGOR Pro	Wave Metrics Inc.	OR, USA
Microsoft Office	Microsoft Corporation	CA, USA
GraphPadPrism	GraphPad	CA, USA

Equipment

Table 2: List of equipment for the different setups that the experiments were conducted at.

			tool	manufacturer	origin	features
all set ups			tubes, flexible	cole parmer	Vernon Hills, IL	ID: 0.5 mm, OD: 2.1 mm
			tubes	Reichelt Chemietechnik	Heidelberg, Germany	PTFE-Chemieschlauch 2.4 x 3.0mm
			Glas capillaries for rotating head	Science Products GmbH	Hofheim, Germany	0.78 x 1.0 x 80mm
			RSC-200 rapid solution changer	Bio-Logic SAS	Claix, France	
			perfectum gastight syringes	popper & sons, inc.	New Hyde Park, NY	glas
	Bonn		Electrode wires	Science Products GmbH	Hofheim, Germany	silver
			Glas capillaries for electrodes	World Precision Instruments, Inc.	Sarasota, FL	1.5 mm OD, 1.12 mm ID
			L/M-3P-A vertical puller	List Medical	Darmstadt, Germany	
			L/M-CPZ 101 heat polisher	List Medical	Darmstadt, Germany	
			ID 03 Microscope	Zeiss	Jena, Germany	
			Axiovert 25 Microscope	Zeiss	Jena, Germany	1.5 mm OD, 1.12 mm ID
			BB 6060 incubator	Heraeus	Hanau, Germany	
		set up I	EPC 7 amplifier	List Medical	Darmstadt, Germany	
			Bessel low pass filter	Frequency Devices	Massachusets, USA	
			TL-1 DMA interface	Axon Instruments Inc.	Union City, CA	
		set up II	Axopatch 200 amplifier	Axon Instruments Inc.	Union City, CA	50 ccm, 100 ccm
			LPBF-48DG filter	npi electronic GmbH	Tamm, Germany	
			Digidata 1200 Series Interface	Axon Instruments Inc.	Union City, CA	
	Stony Brook		glas capillaries for electrodes	A-M Systems	Sequim, WA	1.5 mm OD, 1.12 mm ID
			MF-83 heat polisher	Narishige Scientific Instrument Lab.	Tokyo, Japan	
			PIP5 vertical puller	HEKA	Bellmore, NY	
			Nikon microscope	Modulation Optics Inc.	Greenvale, NY	silver
			EPC 10 amplifier	HEKA	Bellmore, NY	
			incubator	Thermo Scientific	Waltham, MA	

Analysis of Macroscopic Currents

Macroscopic currents show the activity of the sum of many ion channels in one patch. Simultaneous voltage and agonist pulses are given, usually at a time point that all ion channels of the patch are in an activatable state, so that the on- and the offset of macroscopic currents describe the activation and decay time constants (τ_{ON} and τ_{OFF}) of the ion channels. Binding of 5-HT results in conformational changes of the channel protein, which then opens its pore. Positively charged ions (i.e. Na^+ or K^+) can pass from the extracellular to the intracellular. By convention inward current of positive charge is displayed downward (Figure 8).

As long as the agonist is still applied, the decay phase is a combination of desensitization and deactivation of the ion channels.

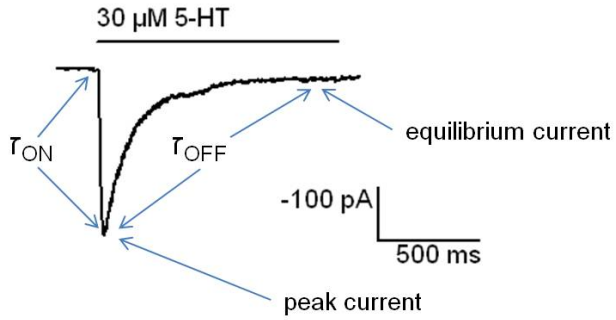

Figure 8: Example for a macroscopic current of 5-HT_{3A} channels in an excised outside out patch, induced by 30 µM 5-HT.

For the present study, all macroscopic currents were recorded on excised outside out patches.

Fitting Macroscopic Currents

In previous studies, onset and offset were fitted separately (Witten, 2009; Decker, 2010). Those fits would depend a lot on the fitting range that was chosen for each phase. Formula (1) and (2) fit the onset and the decay phase (offset) of the current in one step. The fraction of overlap between onset and offset phase depends on k, which describes the extend of 's' shape that the onset takes. I_{ON} does not represent the actual peak current, but an estimate of the current that would be reached by the onset phase of the fit. Due to the nature of the used exponential formula, the time constants represent the time that is needed for the current to change by 1/e ≈ 36.8 %.

During the further analysis, the actual peak amplitudes (pA) and the time constants (ms) of onset and decay phase were used to describe macroscopic currents and to indicate changes. Macroscopic currents could be fitted with two decay constants, using the formula

$$I(t) = I_{ON} * \left(1 - e^{-t/\tau_{ON}}\right)^k * \left((1-w) * e^{-t/\tau_{OFF1}} + w * e^{-t/\tau_{OFF2}} + I_{equil}\right) \quad (1)$$

With

$I_{(t)}$ = current at time t (pA)
I_{ON} = current component, if full onset would be reached (pA)
t = time (ms)
τ_{ON} = activation time constant (ms)
k = curvature factor for the onset, k≥1
ω = fraction of decay due to second time constant
τ_{OFF1} = first decay time constant (ms)
τ_{OFF2} = second decay time constant (ms)
I_{equil} = fraction of current remaining after both decays have equilibrated

For some currents, two decay constants could not be resolved, thus they were fitted with just one (τ_{OFF}), using the formula

$$I(t) = I_{ON} * \left(1 - e^{-t/\tau_{ON}}\right)^k * \left(e^{-t/\tau_{OFF}} + I_{equil}\right) \quad (2)$$

When comparing fits containing one decay constant with those containing two decay constants, for the latter, a single time constant was calculated according to the formula.

$$\tau_{OFF} = \tau_{OFF1} * (1 - w) + \tau_{OFF2} * w \quad (3)$$

Rundown

A well known yet not understood phenomenon is the so called rundown. This describes a loss off current over the same patch over time. To subtract the effect of rundown from the analysis of experiments, experimental traces (application of drugs or different agonist concentrations etc.) are always framed by traces taken under standard conditions. Those framing traces are averaged. Assuming that a rundown happens continually, one can compare the experimental trace now with the averaged framing controls and assume that the rundown effect was subtracted. A threshold of 25 % for excepted rundown was set. Meaning that whenever the loss of current (pA) between framing control traces was more than 25 %, the experiment was not analyzed.

Analysis of Single Channel Currents

Excised Outside Out Mode

When there are resolvable single channel events in the equilibrium phase of macroscopic currents, first step to analyze their amplitudes is to determine a range of the respective current that shall be analyzed. This should be a range that includes as many events as possible, but as few multiple channel openings as possible.

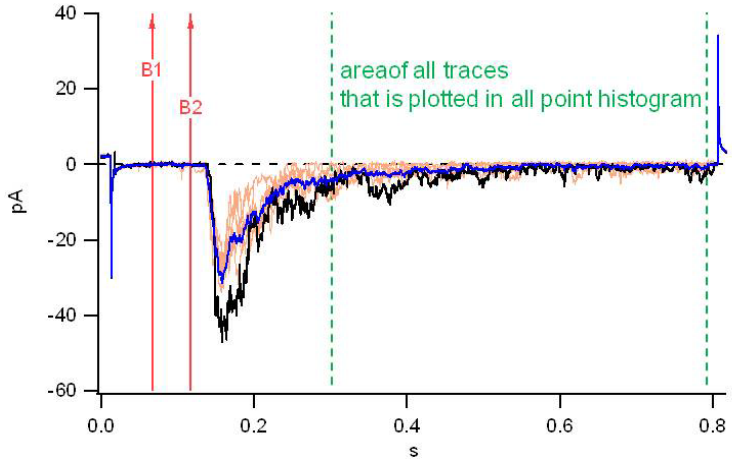

Figure 9: Six traces of one 5-HT_{3AB} transfected patch, induced by 30 µM 5-HT at -100 mV. Indicated by red lines (B1 and B2): area to determine baseline, by green lines: area that is plotted in an all points histogram (Figure 10). The currently active trace is black, the mean of all six traces is blue.

The higher the fraction of still active channels that contribute to the recording, the noisier the recording will be. High noise levels though will prevent distinct peaks in the resulting all point histograms. Figure 9 shows an example of a series of six recordings over 5-HT_{3AB} and the area that was chosen for all points histogram analysis.

Figure 10 shows the respective all-points-histogram, which plots the frequencies of current values and can be expected to show distinct peaks for different levels of multiple channel openings. First such peaks are located, which then are fitted to a sum of n Gaussian distributions to determine their means, using the formula

$$counts(I) = \sum_{i=1}^{n} A_i exp\left[-\left(\frac{I - I_{0i}}{width_i}\right)^2\right] \quad (4)$$

A_i = amplitude of i^{th} peak, I_{0i} = mean current of i^{th} peak

$width_i$ = width of i^{th} peak (width = $\sqrt{2}\sigma$, σ= standard deviation)

These means provide estimates of the amplitude levels of one or multiple channel openings and the differences between these levels represent a single channel current amplitude.

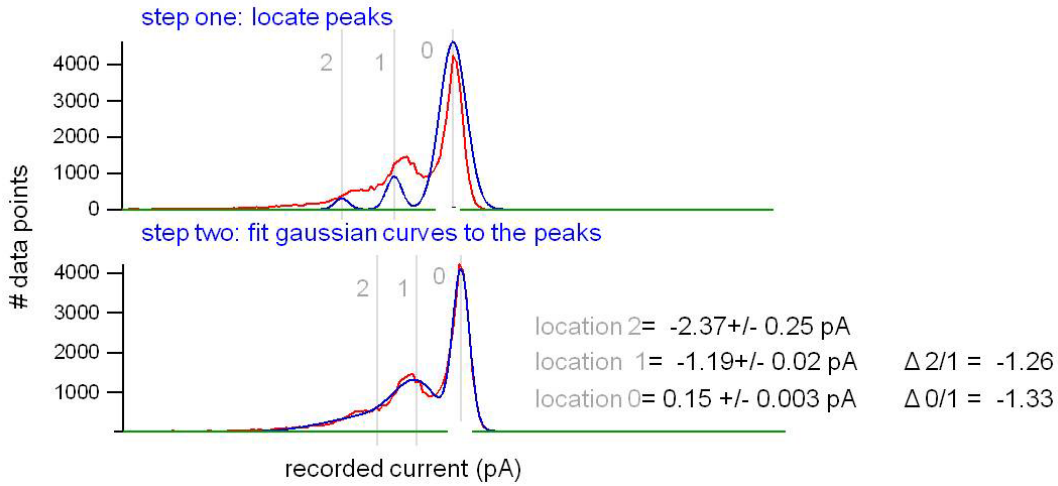

Figure 10: All points histogram by plotting traces shown above.
First, potential peaks are located, then the histogram is fitted by Gaussian curves (formula 4), respective peaks represent the current of 0, 1 or 2 open ion channels.

Cell Attached Mode

Preparing Single Channel Data for Further Analysis

Single channel recordings were processed and analyzed with QuB and IGOR Pro. QuB was used for the first evaluation of each recording. After subtracting the leak current and adding a 3 kHz filter to the recording, single channel events were detected by using a 50% threshold method (Colquhoun and Sigworth 1995 in Neher and Sakmann 1995). A dead time of 60 µs was applied to reduce false positive detection of events. The resulting idealization of the recording into closed, one channel opening, two channel opening and three channel opening stretches is then loaded into IGOR Pro and aligned with the original recording.

Processing Single Channel Data via Personalized IGOR Pro Procedures

The fraction of false positive detection was still too high, for example due to stretches with high membrane noise that was detected as channel activity. This is why each recording had to go through further processing before being analyzed. Stretches that are too noisy to be analyzed are deleted, so are multiple channel openings.

To each stretch that was idealized as a single channel opening, IGOR Pro detects a current amplitude. Those are plotted in a histogram, which is fitted by a Gaussian distribution. The mean of resulting distribution is the mean single channel current of the analyzed recording. Events within the recording that show a current below 50% of the mean single channel current are deleted.

IGOR Pro procedures also detect the duration of each opening and closing event. Those durations are then plotted in histograms. Duration histograms are fitted by a number of exponential curves using a maximum likelihood procedure (Colquhoun and Sakmann, 1985). Histograms are fitted with multi exponential curves of the equation

$$f(t) = \sum_{i=1}^{n} fr.amp._i \, (e^{-\tau_i t}) \tag{5}$$

n = number of components, fr.amp = fractional amplitude of each component and τ = time constant for each component.

Because we plot the histograms on a log binned scale, we actually use the formula

$$f(t) = \sum_{i=1}^{n} fr.amp._i \{e[t - \ln(\tau_i) - e(t - \ln(\tau_i))]\} \tag{6}$$

see (Sigworth and Sine, 1987), equation 8 for details.

Exponential distributions depend only on amplitudes and time constants; there is no other value that describes the distribution further (as the width of a distribution for Gaussian curves for example). So for every exponential component that can be fitted into the duration histogram, one obtains two values: its position on the duration scale τ (ms) and its amplitude fr.amp. (given as a fraction of all events of the analyzed histogram).

When fitting individual experiments, often there aren't enough events to resolve all components. Or the lack of a sufficient number of events leads to superimposed

components. Therefore criteria are needed, to decide rather a component is to be kept or not. One criterion is the ability of alignment. When pooling the dwell times of recordings obtained at the same conditions, the resulting histogram was fit. The duration histograms for the individual patches can show fewer components, but those components that are found should represent the ones found in the combined histogram. Another criterion is the fraction of one component. If a component makes up less than 10% of the analyzed cluster durations, the risk of it being a superimposed component is very high. Open and cluster components with fractions less than 0.1 are therefore ignored and the fit is repeated with one fewer component

Open probabilities of entire traces (%) are calculated including multiple channel openings by counting double and triple opening durations times two or three respectively:

$$p_T = \sum (n_i * t_i)/T_T \quad (7)$$

p_T probability over total time, n_i number of channels open, t_i duration of opening, T_T total time

To calculate open probabilities within clusters T_T is the duration of the cluster and n_i equals one.

All procedures in IGOR Pro were written and kindly provided by James P. Dilger, Ph.D. from Stony Brook University, Stony Brook, NY, USA.

Normalizing Combined Duration Histograms

Within a series of recordings at the same experimental conditions, individual patches were found that differed significantly in one or more single channel characteristic. When such an exceptional recording includes a large number of events it can shift results of combined duration histograms towards exceptional values.

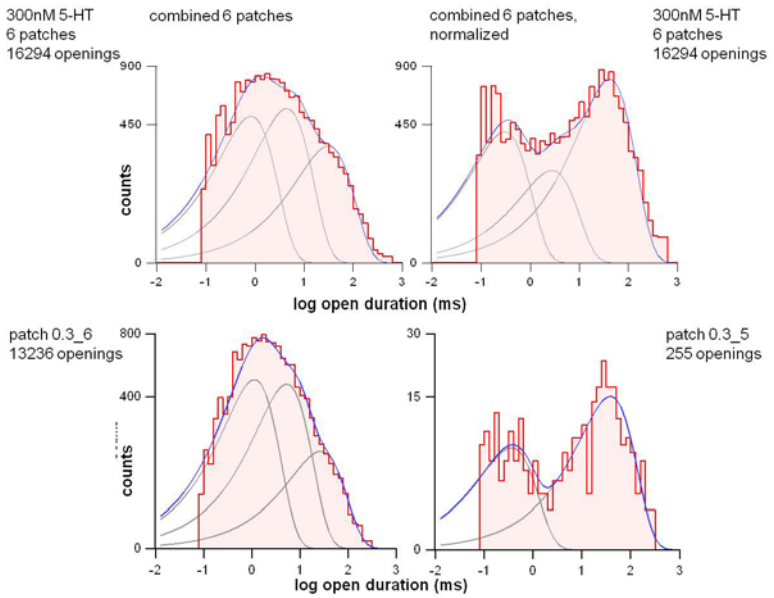

Figure 11: Combined histograms of the same six 300 nM 5-HT recordings.
Top row: Combined histograms of all six patches, left: each opening is weighted equally, right: each patch is weighted equally. Bottom row: Individual histograms for two of the six recordings, left: for a recording that includes many events and shows exceptional histogram characteristics, right: for a recording that includes fewer events and shows representative histogram characteristics like all other recordings of the series do, including the dip between the two components

Figure 11 shows this on the example of combined open durations of six 300 nM 5-HT recordings: All patches of that series except patch 0.3_6 (bottom left) show two components that are separated by a dip in their open duration histograms (bottom right). Because the exceptional patch 0.3_6 includes many more events than the other recordings do, the combined histogram resembles the one without the otherwise characteristic dip (top left). This phenomenon is avoided by normalizing open event durations in a way so that each patch is weighted equally (top right).

Cluster Determination

To determine a critical closed duration that represents the time between individual clusters (where a cluster is assumed to arise from one single channel) (t_{crit}), the closed duration histograms were first fit to multiple exponential distributions (formula 6). The results are shown in Figure 12. The two fastest components of closed duration histograms (C1, C2) are very reproducible from patch to patch and are similar at all 5-HT concentrations. Component C3 is consistent for 5-HT concentrations of 100 nM and above. However, C3 is somewhat slower at 30 nM 5-HT. Components larger than C3 also show concentration dependence.

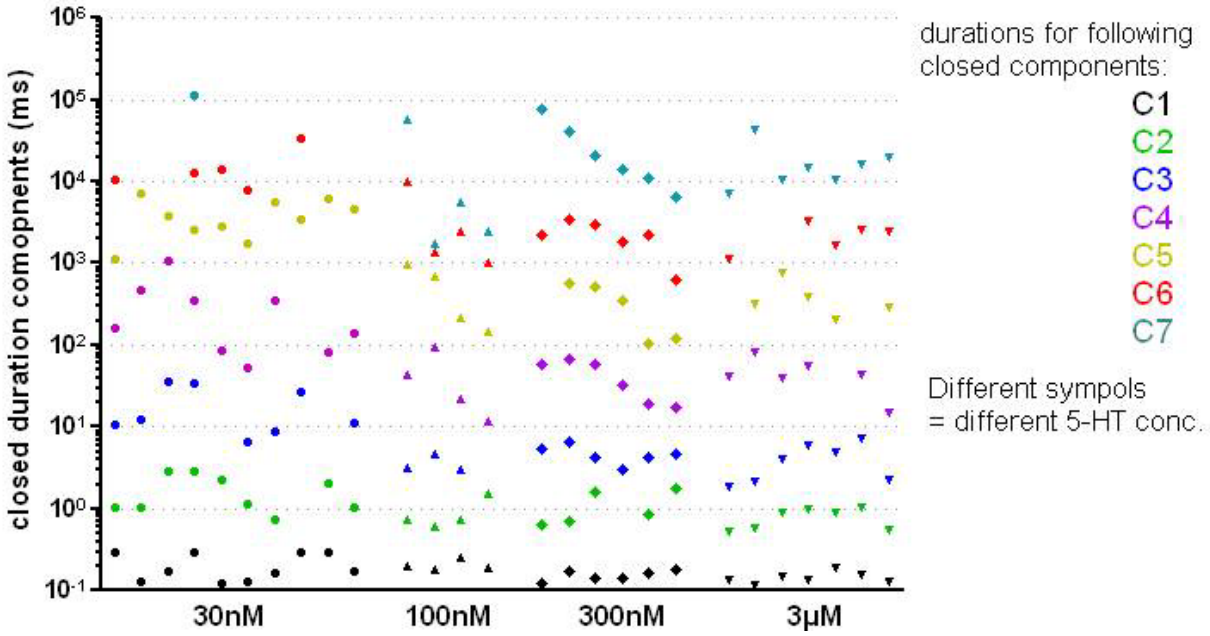

Figure 12: Duration components (ms) resulting from multiple exponential fits (formula 6) of closed duration histograms for individual patches at different serotonin concentrations.

There are several systematic ways to define the midpoint between two exponential distributions, here the method by Colquhoun and Sakmann (Colquhoun and Sakmann, 1985) was used. In this method, the critical gap time (t_{gap}) is chosen so that equal proportions of short and long intervals are misclassified by the fit, as described by the formula

$$e^{-t_{gap}/\tau C_2} = 1 - e^{-t_{gap}/\tau C_1} \quad (8)$$

Figure 13 shows the gap times (t_{gap}) between each adjacent pair of closed components. The two shortest gap times are very reproducible at all 5-HT concentrations. The gap times between the third and the fourth closed components (blue, C3-C4) show a distinct concentration dependence and patch-to-patch variability. This suggests that the C3-C4 gap depends on the number of active channels.

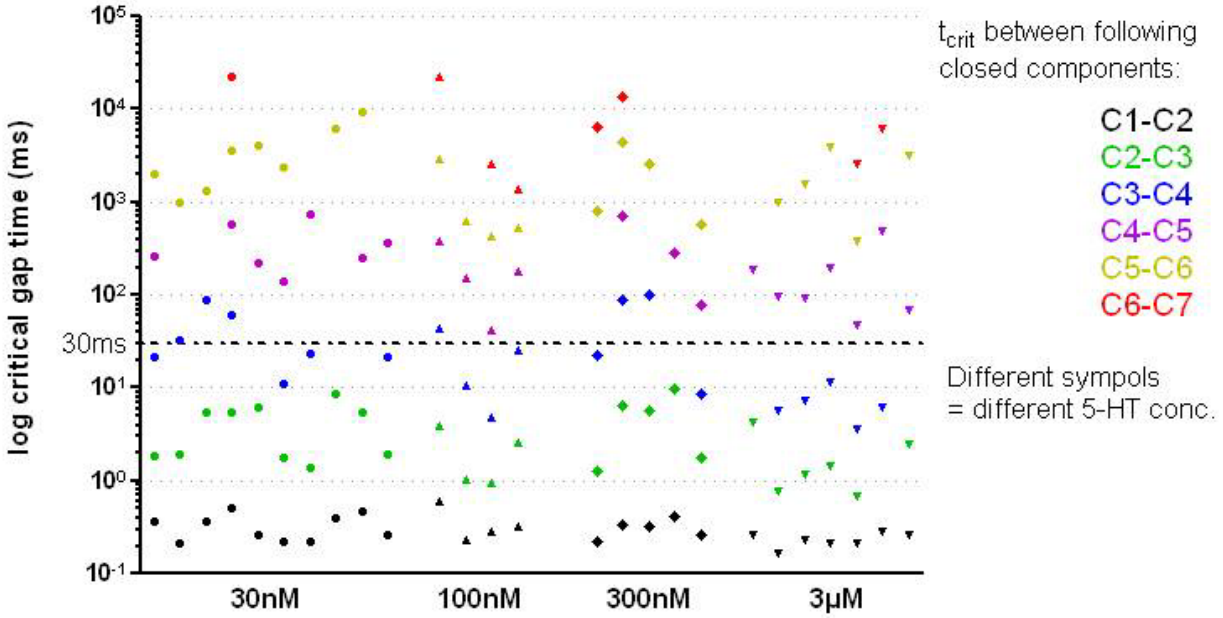

Figure 13: Critical gaps (t_{gap}) between closed time components (C1-C7)
Gap times were obtained using the Colquhoun definition of critical times (Colquhoun and Sakmann, 1985) (formula 8), after fitting closed duration histograms for several patches to up to seven components.

Closed duration components and critical gap times between these suggest that the critical time between clusters is between the third and the forth closed component. One approach would be to define a cluster based on the critical gap time for each patch. However, because we wanted to combine results from different patches, we chose to define a single critical gap time to be used for each experimental condition. Figure 13 suggests that we could also use the same critical gap time of 30 ms for all 5-HT concentrations. The determination of critical gap time was assessed when studying the effect of substances on the channel.

Statistics

Statistical tests were done via GraphPadPrism and included Student's *t* tests and one way ANOVA tests with statistical significance set at $p = 0.05$. Significant one way ANOVA tests were followed by Tukey's Multiple Comparison.

Results

5-HT_{3A} wt– Basic Characterization (Without Drug)

5-HT_{3A} channels have been characterized and used for extensive pharmacological studies for many years now (Barann et al., 2000b, 2008; Meiboom et al., 2013). As one goal of the present study was to evaluate a single channel model to explain macroscopic phenomena on 5-HT_{3A}, a selective characterization of 5-HT_{3A} was done first, to confirm properties that were found before and to make sure experimenter and setup bias will not alter values.

Excised Outside-Out Patches

If not mentioned otherwise, all following 5-HT_{3A} properties are based on macroscopic currents induced by a 1.2 ms application of 30 µM 5-HT at -100 mV, recorded from outside-out patches that were excised from HEK cells stably transfected with 5-HT_{3A}.

Typical Current Traces

30 µM 5-HT pulses induced expected typical currents with a fast onset and a slower offset on stably 5-HT_{3A} transfected patches, an example is shown in Figure 14.

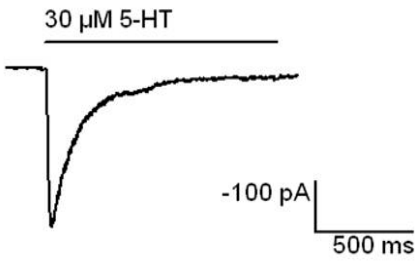

Figure 14: representative current trace over a stably 5-HT_{3A} transfected cell patch, induced by 30 µM 5-HT at -100 mV

Macroscopic currents were fitted with formula 1 or formula 2, to evaluate their peak amplitudes and their activation and decay time constants (τ_{ON} and τ_{OFF}).

Current Amplitudes

Mean peak amplitudes were -174 ± 459 pA (n = 42 patches ± SD) for the first recorded currents of each patch. No patch did show resolvable single channel openings.

When recordings could be repeated, the peak current decreased over time. The degree of this so called rundown is shown in Figure 15, where peak currents were normalized, so that the first one of each patch equals 100 %.

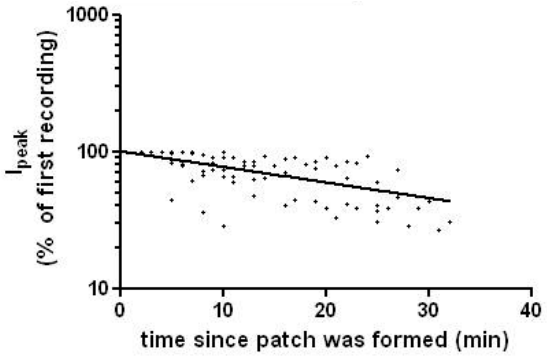

Figure 15: I_{peak} of 5-HT induced currents over 5-HT_{3A} expressing membrane patches (n=15). 30 µM 5-HT pulses were given at -100 mV with at least 60 s recovery time in between. Peaks are normalized, so that the value of the first pulse equals 100 %. The decrease of I_{peak} was fitted by formula 9, resulting in a Half Life Time of 26.4 min.

The decrease of Ipeak was fitted by a single exponential decay

$$I_{peak}(t) = (100\% - 0.13\%) * e^{-t/38min} + 0.13\% \quad (9).$$

The relative peak amplitudes of macroscopic 5-HT_{3A} currents decreased with a Half Life Time of 26.4 min.

To evaluate the influence of rundown on onset and offset of macroscopic currents, these where determined over longer time periods as well.

Time Constants τ_{on} and τ_{off}

Macroscopic currents did show fast onsets with an average τ_{ON} of 7.6 ± 3.7 ms and a slower decay with an average τ_{OFF} of 157 ± 154 ms (n = 42 patches ± SD) for the first recorded traces of each patch. Along with the current amplitude reduction sometimes came a change of kinetics. Figure 16 shows the changes of τ_{ON} and τ_{OFF} over time of 15 individual patches.

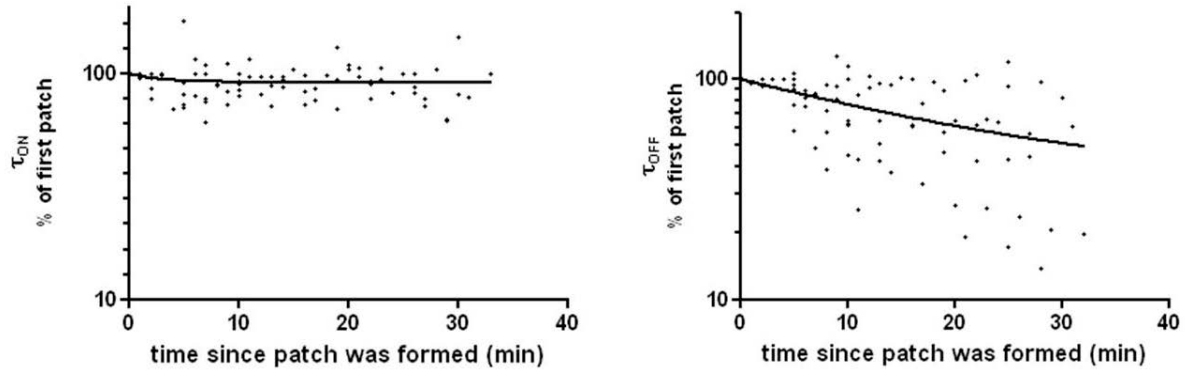

Figure 16: τ_{ON} and τ_{OFF} of 5-HT induced currents over 5-HT_{3A} expressing membrane patches (n=15) over the time since the patch was formed.
30 µM 5-HT pulses were given at -100 mV with at least 60 s recovery time in between. **τ**s were normalized, so that the value of the first pulse equals 100 %. The decrease of the onsets of currents was fitted with formula 10, resulting in a Half Life Time (ln(2)/2.8min) of 1.9 min.
The decrease of the offsets of currents was fitted with formula 11, resulting in a Half Life Time (ln(2)/24min) of 17 min.

The rundown effect on τ_{ON} was fitted with

$$\tau_{ON}(t) = (100\% - 92\%) * e^{-t/2.8min} + 92\% \quad (10)$$

It only shows a decrease to a plateau at 92 %, so that the effect, which occurs with a Half Life Time of only 1.9 min, is negligible.

τ_{OFF} was fitted with

$$\tau_{OFF}(t) = (100\% - 32\%) * e^{-t/24min} + 32\% \quad (11)$$

And decreases with a Half Life Time of 17 min down to a relative τ_{OFF} of 32 %.

Recovery from Desensitization

Double-pulse experiments were performed as described (page 25: Double-Pulse Experiments on Excised Patches), where currents after 60 second intervals did serve as control and were conducted between test pulses after different shorter intervals (3,10,30 seconds). Patches that did not show rundown exceeding 25 % were used to determine recovery.

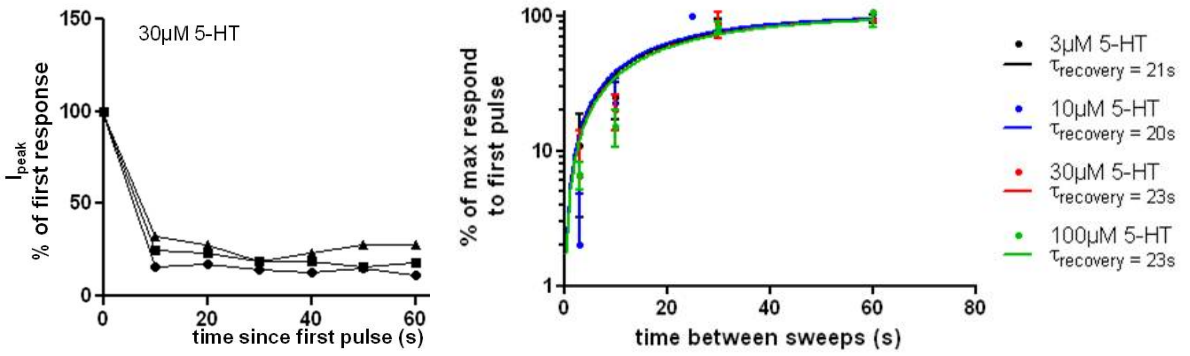

Figure 17: Recovery of 5-HT$_{3A}$ from desensitization.
Stably 5-HT$_{3A}$ transfected HEK293 cells. Responses to different interpulse lengths (time between sweeps). First pulse equals 100 %. **Left:** current amplitudes (normalized to the first response) from experiments with three patches, in which 30 µM 5-HT was applied for 1s (is this right?) every 10s. **Right:** percentage of desensitization at different interpulse lengths (3, 10, 30 and 60 s between sweeps). Symbols show the average for each concentration including SD, n (3, 10, 30, 100 µM 5-HT) = 4, 5, 3, 3 respectively, lines show the respective single exponential fits.

Figure 17 on the left shows the responses of three patches after a repeated 10 s pulse interval. They keep reaching peak amplitudes (I_{peak}) of around 25 % of the first pulse at repeated 10 s interval pulses.

On the right different 5-HT concentrations are compared. The recovery time of 5-HT$_{3A}$ (20-23 s) does not change with 5-HT concentration, when fitting the four data sets to a singular exponential

$$normalize\ I_{peak}(t) = 100(1 - exp(-t/\tau_{recovery})) \quad (12)$$

5-HT Concentration Response

Stable 5-HT_{3A} transfected HEK cells were patched and different serotonin concentrations (3, 10, 30, 100 µM) applied. The resulting peak currents were normalized, so that the amplitude induced by 30 µM 5-HT equals 100 %. The resulting sigmoidal dose response curve was fitted to

$$I_{normalized}(c) = \frac{100\%}{1 + \left(\frac{EC_{50}}{c}\right)^{n_{Hill}}} \tag{13}$$

and reveals an EC_{50} of 5-HT_{3A} channels for 5-HT of 10.8 µM.

Figure 18 shows a comparison of these data with respective data collected by several experimenters on the 5-HT_{3A} channel over several years as presented in (Brünker, 2010).

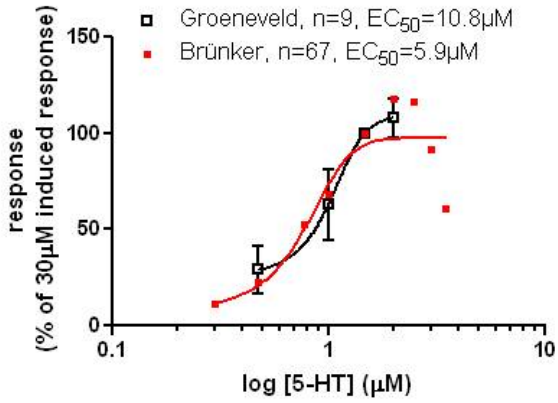

Figure 18: 5-HT concentration responses of stably 5-HT_{3A} transfected cell patches. Normalized to the response at 30 µM, bars show standard deviation. Used fit is shown in text above (formula 13). Hill coefficient was 2.1 in both cases. Both data sets were obtained under standard conditions (page 24:Standard Conditions for Control Currents), they differ only in the experimenters.

5-HT_{3AB} wt– Basic Characterization (Without Drug)

The following sections will describe the basic electrophysiological characteristics of stably 5-HT_{3AB} transfected cell patches, in order to evaluate 5-HT_{3AB} as a possible model channel to explain single channel kinetics in 5-HT_{3A} receptors.

Typical Current Traces from Excised Outside-Out Recordings

Cells were patched at least four days after seeding, to make sure they were attached to the bottom. The rate for successful patches (forming a sealed patch of a membrane area that produces typical 5-HT_{3AB} currents) did not change with dish age and was around 44% (71 patch trials resulted in 40 patches, 31 of which produced currents).

Different types of traces could be distinguished. In Figure 19 a typical of a trace is displayed which shows clearly distinguishable single channel events, identifiable by large rectangular steps (about 1.3 pA) within the current trace. Those are best visible after the decay phase, when the patch reaches a steady state and only one or a few channels open and close at a time. Even the magnified trace displayed in Figure 20 does not show such obvious single channel events. One can see some membrane noise, but no rectangular steps.

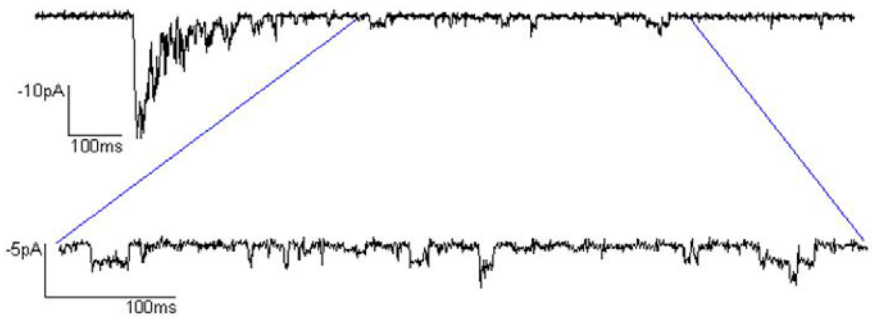

Figure 19: representative trace of an outside out patch of stable 5-HT_{3AB} transfected HEK cell

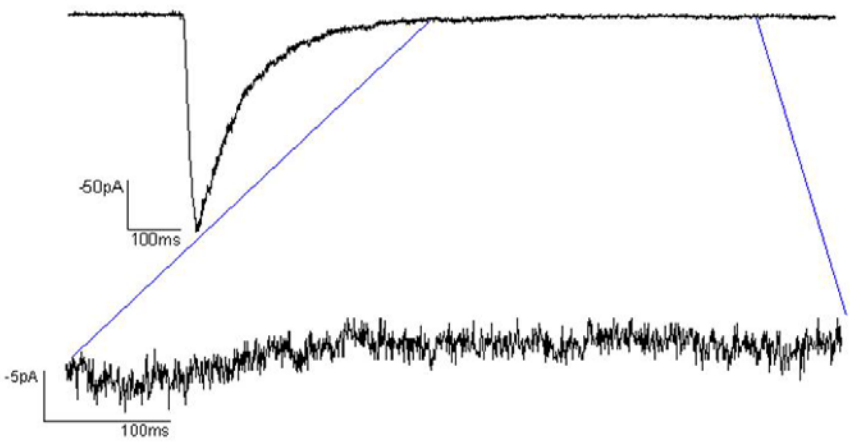

Figure 20: representative trace of an outside out patch of stable 5-HT_{3AB} transfected HEK cell

The individual patches were divided into two groups by their appearance. First a group of traces that did show distinguishable single channel events of typical rectangular shape and second, a group of traces that did not.

Current Amplitudes

In Figure 21 peak amplitudes (30 µM 5-HT) are plotted against the interval between cell seeding and cell patching. The amplitudes did not significantly increase with the cell age after seeding. The averaged (n patches =33) macroscopic peak current was -65 pA and showed a wide range with a standard deviation of ± 69 pA.

As described above and shown in Figure 19 and Figure 20, single channel events were not always visible within the macroscopic traces. When they were, their current amplitudes could be evaluated by finding the peaks of all-points-histograms (page 33: Analysis of Single Channel Currents). Single channel current amplitude was 1.3 ± 0.2 pA (± SD) at -100 mV (n patches = 6), which corresponds to a conductance of 13.4 ± 1.6 pS (see Figure 22).

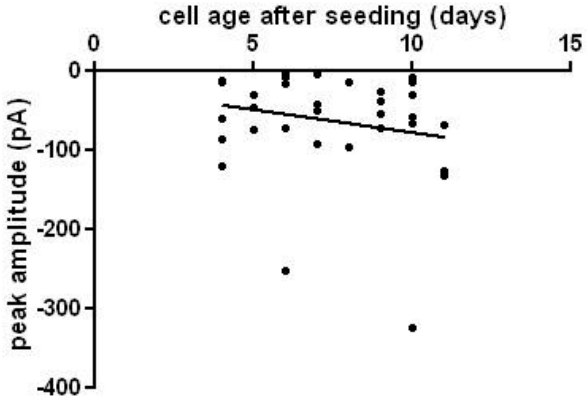

Figure 21: 30 µM 5-HT induced peak currents (pA) at different dish ages (days).
Each data point represents the mean peak current of one patch (n = 33patches). The line represents a linear regression with a slope of -5.7 pA per day (Ipeak = 5.7*cell age-21.4), which is not significant (p = 0.078).

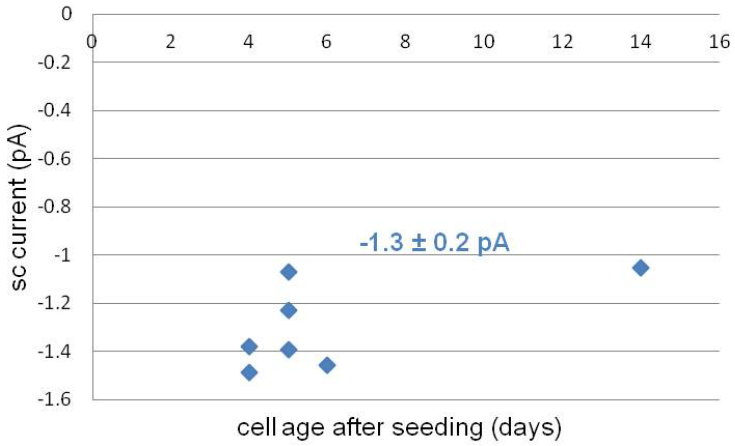

Figure 22: Current amplitudes (pA) of single channel (sc) openings induced by 30 µM 5-HT at -100 mV.
n = 7 patches.

Time Constants τ_{on} and τ_{off}

Macroscopic currents of 5-HT_{3AB} transfected cell patches showed a fast onset with a τ_{ON} of 7.5 ± 4.5 ms and a decay phase with a τ_{OFF} of 61 ± 78 ms (n = 13 patches ± SD).

Recovery from Desensitization

In order to measure recovery from desensitization, double-pulse experiments were performed (page 25: Double-Pulse Experiments on Excised Patches). Figure 23 plots the normalized peak amplitude of the current following the second pulse.

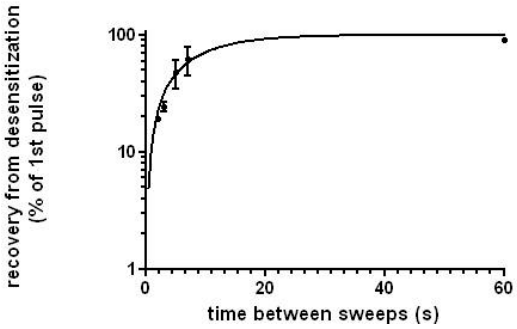

Figure 23: Recovery from desensitization of 5-HT_{3AB} transfected cell patches.
The recovery was fitted with formula (12), resulting with a $\tau_{recovery}$ of 8s.

Normalized peak amplitudes after different recovery times were fitted with formula (12). The resulting recovery curve shows a recovery constant of 8 s.

Voltage Dependence

I-V curves were obtained as described (page 25: Current-Voltage Dependence (I-V) on Excised Patches).Figure 24 shows I-V curves recorded between -100 mV and 100 mV for eleven individual 5-HT_{3AB} patches. Although all I-V curves show a reversal potential around zero, they show different I-V characteristics. Some patches show a nearly linear voltage dependence (red), others are rectifying (blue). Two individual patches are highlighted to emphasize these differences.

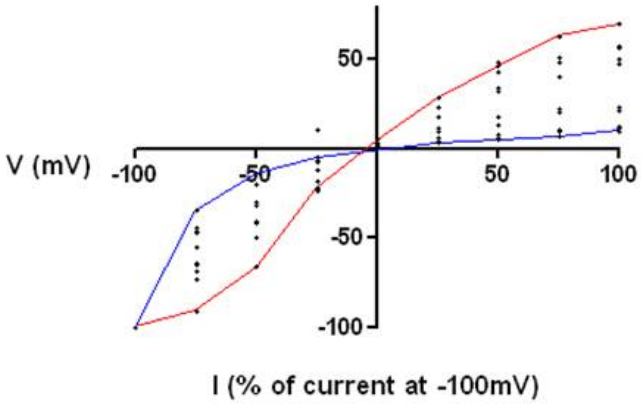

Figure 24: Voltage dependence of currents of eleven 5-HT_{3AB} stably transfected cells induced by 30 µM 5-HT.
Peak currents normalized at -100 mV are shown. All different holding potentials (changed in 25 mV steps) were given to the same patch. Two individual patches are highlighted, to emphasize the different slopes.

One factor correlating with those differences is the number of cell passages after transfection. Patches from cells that were passaged more often tend to show stronger rectifying characteristics. Figure 25 shows the average I-V curves recorded after few passages and many passages, respectively. +100 mV currents of cells that

were not passaged often (O) show a decrease to 56 ± 9% of -100 mV currents. For patches after many passages (□) currents reached 13 ± 5 % of currents at -100 mV when the membrane is clamped to 100 mV (± SD).

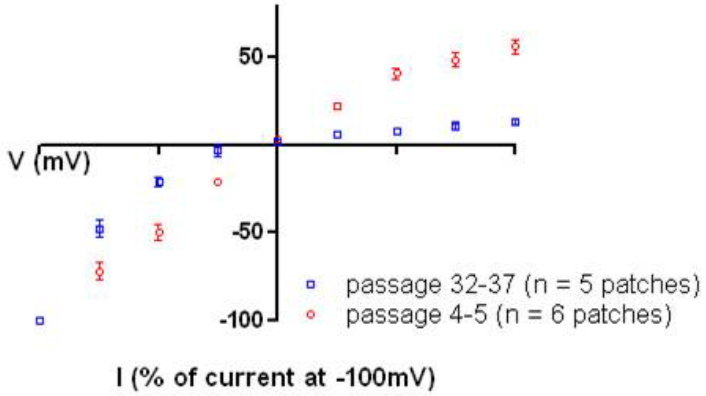

Figure 25: Voltage dependence of 5-HT_{3AB} currents induced by 30 µM 5-HT compared to different numbers of passages that cells went through before getting patched.
Averaged peak currents normalized at -100 mV are shown, bars represent SD. The complete voltage range in 25 mV steps was given to each patch. Same patches as in Figure 24.

Another factor correlating with the rectification of 5-HT_{3AB} transfected cell patches was the presence of resolvable single channel openings.

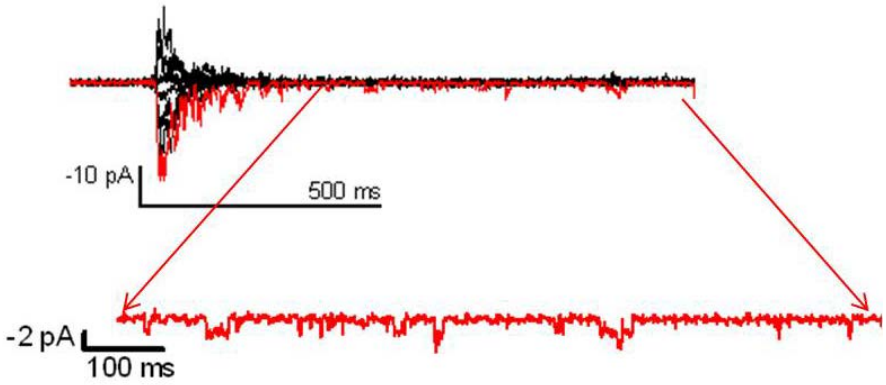

Figure 26: 5-HT_{3AB} transfected cell, traces of a patch at different voltages (-100 mV to +100 mV**)**. Red trace at -100 mV was enlarged, single channel openings directed downwards.

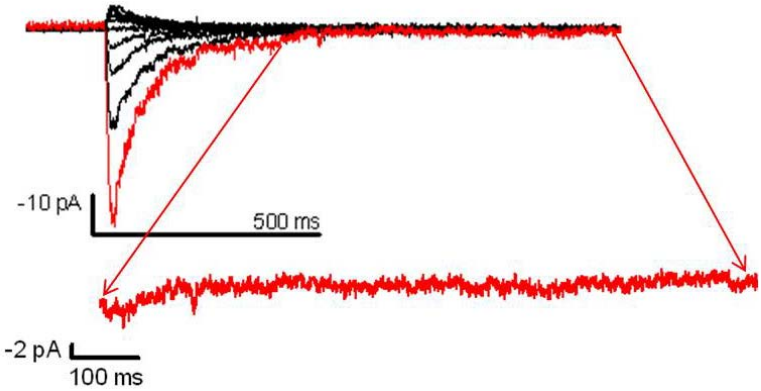

Figure 27: 5-HT_{3AB} transfected cell, traces of a patch at different voltages (-100 mV – 100 mV**)**. Red trace at -100 mV was enlarged.

Figure 26 shows overlay superposition of nine macroscopic currents recorded from the same patch at nine voltages between -100 mV and +100 mV. The peak amplitude at -100 mV is nearly as large as the peak amplitude at +100 mV. The steady state current at -100 mV is magnified to show single channel openings, which are clearly visible.

A different example can be seen in Figure 27, where a cell of the same passage (but a different cell dish) was patched and the same voltage protocol as described above was applied. The peak amplitudes at positive voltages are much smaller than those at negative voltages, indicating a strongly outwardly rectifying voltage dependence of the channels within the patch. The magnified steady state current of the -100 mV trace does not show any distinguishable single channel openings.

Rectifying factor (rf)

To quantitate the voltage dependence of 5-HT_{3AB} transfected cell patches without having to apply the whole range of voltages to each patch, a rectifying factor (rf) was introduced. This factor was defined by the absolute ratios of peak current response to 30 µM 5-HT at -100 mV and at +100 mV.

$$rf = \frac{-I(-100\ mV)}{I(100\ mV)} \tag{14}$$

An rf = 1 indicates a symmetric I-V relation, in other words no rectification. The larger rf, the more outward rectification does the I-V curve of the respective patch show.

Figure 28 shows rectifying factors of 36 patches of 5-HT_{3AB} transfected cells. The experiments were done on cell batches that were defrosted at two different time points (▲/▲ January 2010 and ●/● Summer 2010), but origin from the same stable transfection line. Before analyzing the rectifying factors, it was determined if the traces did show resolvable single channel events like the trace in Figure 26. Respective rectifying factors are depicted in red (▲ and ●).

5-HT_{3AB} transfected cell patches of the batch that was defrosted Summer 2010 (circles) show a range of current rectification (rf = 1.7 - 9). Those cells that indicate resolvable single channel events (red) were clearly less rectifying than the ones that didn’t (black).

The batch that was defrosted January 2010 (triangles) started out with small rectifying factors, but showed an increase of rectification with the number of passages the cells went through. Because over time it became clear that 5-HT_{3AB} expression in the cells was not stable over time, the second batch (circles) was not passaged as often anymore. Thus there are no data points for this batch at higher passages.

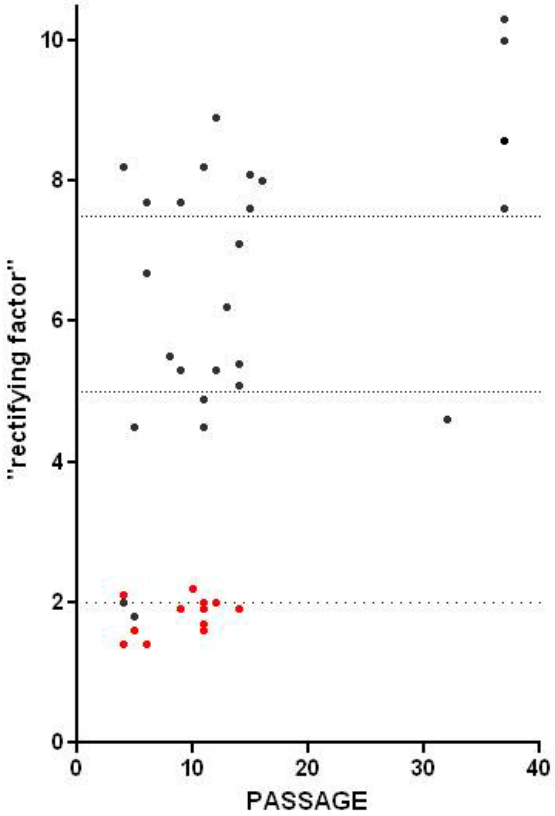

Figure 28: 'rectifying factor' as calculated by formula (14) at different passages of different cell batches.
Every point represents one patch. They were determined between those patches that showed rectangular single channel openings (red) and those that did not (black). Triangles: cell batch defrosted January 2010. Dots: cell batch defrosted summer 2010.

All the patches that show distinguishable single channel openings show very reduced rectification. Intermediate forms of rectification can be found too, though none of those patches showed clearly resolvable single channel events.

5-HT Concentration Response of Macroscopic Currents

Stable 5-HT_{3AB} transfected HEK cells were patched and different serotonin concentrations (3, 10, 30, 100 µM) applied to the same patch. The resulting peak currents were normalized, so that the amplitude induced by 30 µM 5-HT equals 100 %. In Figure 29, the resulting dose response curves for 20 patches are shown. The curves for two patches are highlighted to emphasize different slopes.

Many patches reach a response that is close to maximum when 30µM 5-HT is applied (blue highlighted patch). But there are also several patches that seem to have a shifted sensitivity for serotonin. Their current amplitude still increases under higher concentrations (red highlighted patch). This leads to a wide variety of curve shapes.

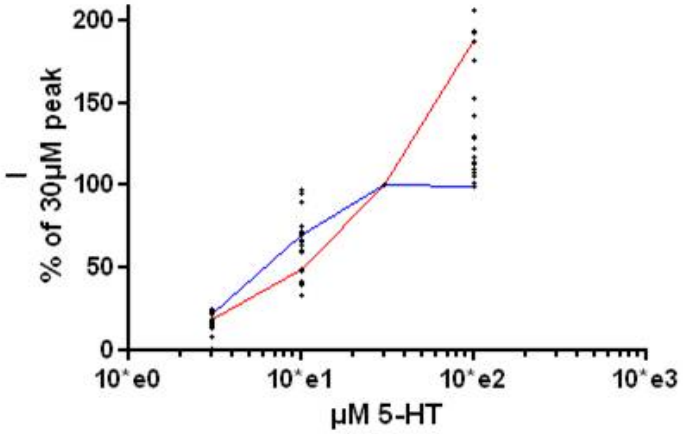

Figure 29: Concentration response curves for 20 individual patches of 5-HT_{3AB} stably transfected HEK293 cells.
Individual curves were normalized to peaks at 30 µM. Two individual patches are highlighted, to emphasize the different slopes.

I-V characteristics and single channel occurrence are used in Figure 30 to separate the pool of 20 patches into three populations. Black triangles represent the averages of these patches that had a high rf (> 6.5) and no resolvable single channel events (n = 9). Grey diamonds represent the averages of the patches that showed lesser rectification (rf up to 6.5) and no resolvable single channel events (n = 5). Red squares represent the averages of the patches that did not show much rectification (rf < 2), but resolvable single channel events (n = 6). Those populations are then fitted with formula 13. The resulting variables are listed in Figure 30.

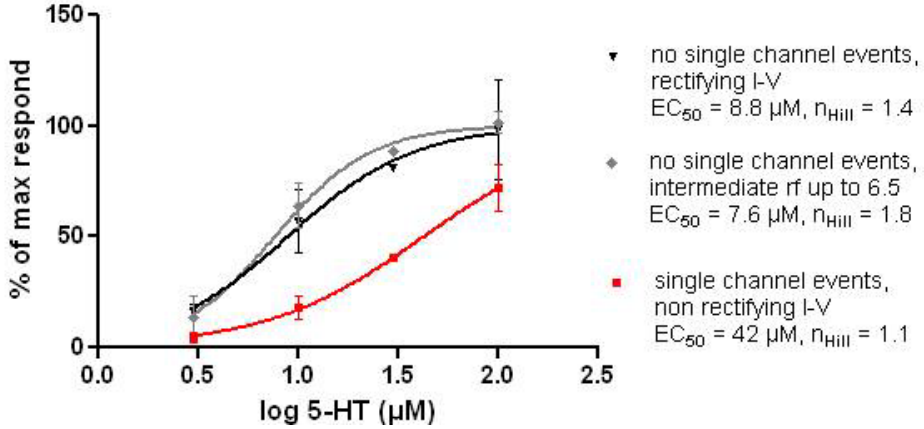

Figure 30: Concentration response curves for different populations of patches of 5-HT_{3AB} stably transfected HEK293 cells.

Slopes of the dose response curves of the first two populations look very similar (1.4 and 1.8). Also the EC_{50}s don't differ much (8.8 µM and 7.6 µM). The third population though, the one that showed single channel events in the individual traces, reveals a more shallow shape with a shifted EC_{50} for 5-HT to higher concentrations (42 µM) in comparison to the other populations.

5-HT_{3A} QDA – Basic Characterization (Without Drug)

The following chapters will describe the electrophysiological characterization of 5-HT_{3A}QDA. All experiments were conducted patching 5-HT_{3A}QDA transiently transfected HEK cells. Most cells were co-transfected with CD8, to be able to identify successfully transfected cells by binding CD8 beads to their surface.

Excised Outside-Out Patches

Outside-out patches of 5-HT_{3A}QDA transfected HEK cells were exposed to different voltages and agonist concentrations.

Typical Current Traces

Serotonin induced currents from 5-HT_{3A}QDA transfected cell patches did show typical currents with a fast activation and a slower decay phase. Within the steady-state phase (enlarged window in Figure 31), between 2-3 pA large single channel events were distinguishable.

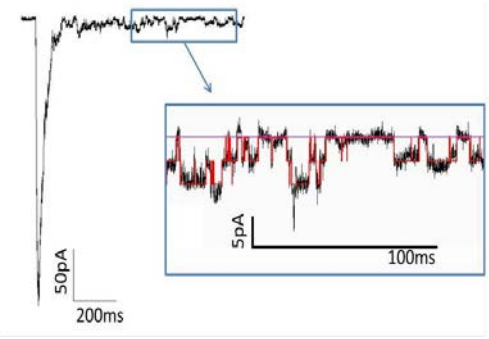

Figure 31: 30 µM 5-HT induced current in an excised outside-out patch of a 5-HT_{3A}QDA transiently transfected HEK 293 cell at -100 mV.
Blue frame: magnified steady-state phase of trace to emphasize distinguishable single channel events. Pink: baseline (= no open channel), red: idealization of single channel levels by QuB.

Current Amplitudes

The pulses (30 µM 5-HT, -100 mV) of 34 5-HT$_{3A}$QDA transiently transfected patches right after forming the patch did induce an average peak current amplitude of -860 ± 923 (pA ± SD). Many patches did show a rundown of currents.

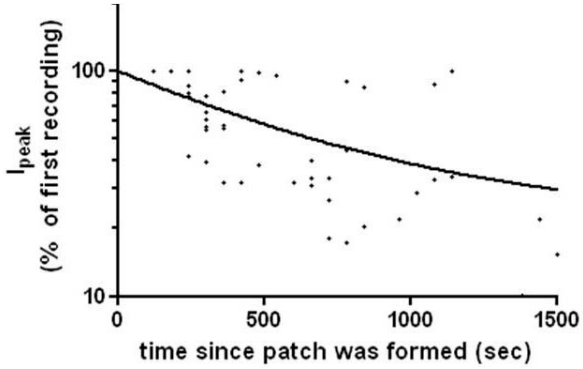

Figure 32: I_{peak} of 5-HT induced currents over 5-HT$_{3A}$QDA expressing membrane patches (n=9). 30 µM 5-HT pulses were given at -100 mV with at least 60 s recovery time in between. Peaks are normalized, so that the value of the first pulse equals 100 %. The decrease of I_{peak} was fitted by formula 15, resulting in a Half Life Time of 449 sec.

Figure 32 shows the normalized (max equals 100 %) peak amplitudes of macroscopic currents of nine 5-HT$_{3A}$QDA transfected patches that could be detected over longer time periods. The decrease of I_{peak} was fitted by

$$I_{peak}(t) = (100\% - 22\%) * e^{-t/648sec} + 22\% \quad (15)$$

The relative peak amplitudes of macroscopic 5-HT$_{3A}$QDA currents decreased with a Half Life Time of 449 sec (=7.5 min).

To evaluate the impact of this phenomenon on the channels kinetics, on- and offset were watched over time as well (Figure 31).

Time Constants τ_{on} and τ_{off}

5-HT$_{3A}$QDA transfected cell patches did show fast onsets of 30 µM serotonin induced currents. 34 patches showed an average onset of 6.8 ± 5.5 ms (± SD) and a decay phase with an offset of 73 ± 56 ms (± SD). Figure 33 Shows an example of 5-HT induced currents over a 5-HT$_{3A}$QDA transfected cell patch at three different time points after forming the outside-out patch. Not only did the peak amplitude decrease over the duration of a patch, but with the time constants changed, too.

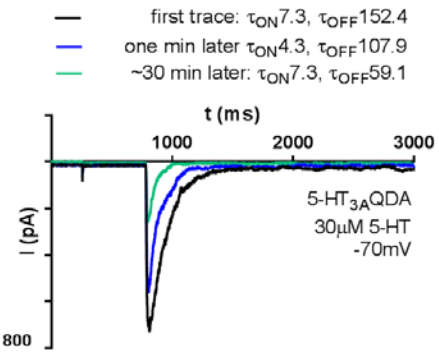

Figure 33: Three 5-HT$_{3A}$QDA traces recorded over a time period of 30 minutes.
30 µM 5-HT induced currents over an outside out patch of a 5-HT$_{3A}$QDA transfected HEK cell. τ_{ON} und τ_{OFF} in ms.

The macroscopic kinetics of nine patches could be detected over longer time periods. Plotted on the left in Figure 34 are the onsets of the same nine patches that are plotted above in Figure 32 over time.

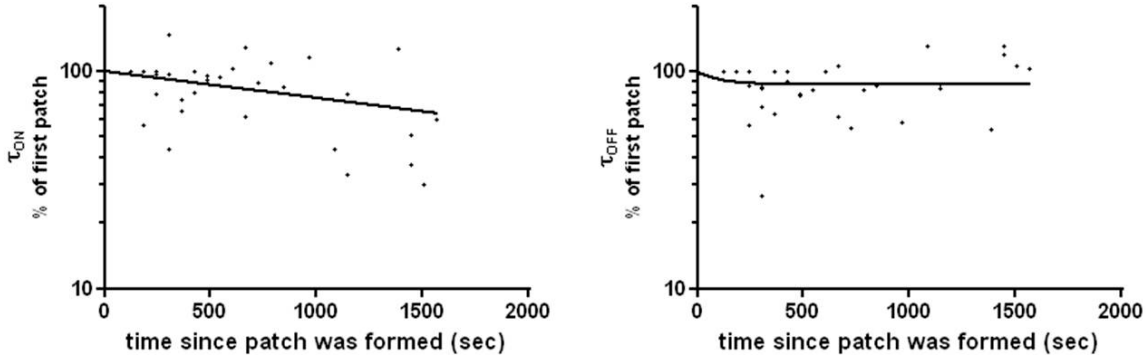

Figure 34: τ_{ON} and τ_{OFF} of 5-HT induced currents over 5-HT$_{3A}$ expressing membrane patches (n=9) over the time since the patch was formed.
30 µM 5-HT pulses were given at -100 mV with at least 60 s recovery time in between. τs were normalized, so that the value of the first pulse equals 100 %. The decrease of the onsets of currents was fitted with formula 16, resulting in a Half Life Time (ln(2)/2.8min) of 2430 sec. The decrease of the offsets of currents was fitted with formula 17, resulting in a Half Life Time (ln(2)/24min) of 72 sec.

The left graph in Figure 34 shows onset time constants of nine patches over the time that the patch did last, normalized to the onset of the first recording. The rundown effect on τ_{ON} was fitted with

$$\tau_{ON}(t) = (100\% - 9.9e^{-10}\%) * e^{-t/3505sec} + 9.9e^{-10}\% \quad (16)$$

and shows a very slow decrease to a plateau close to 0 %, reaching its Half Life Time after 2430 sec (40 min).

τ_{OFF} was fitted with

$$\tau_{OFF}(t) = (100\% - 87\%) * e^{-t/103sec} + 87\% \quad (17)$$

And decreases with a Half Life Time of 72 sec (1.2 min) down to a relative τ_{OFF} of 87 %.

Figure 35 compares on- and offsets and peak amplitudes of previously described native 5-HT_3 channel variants with the ones of its high conductance mutant. While the onset time constants are similar, the decay time constant of both 5-HT_{3AB} and 5-HT_{3A}QDA are faster by about 2fold. The average peak amplitude of macroscopic 5-HT_{3A}QDA currents is larger than the one for the native channel currents.

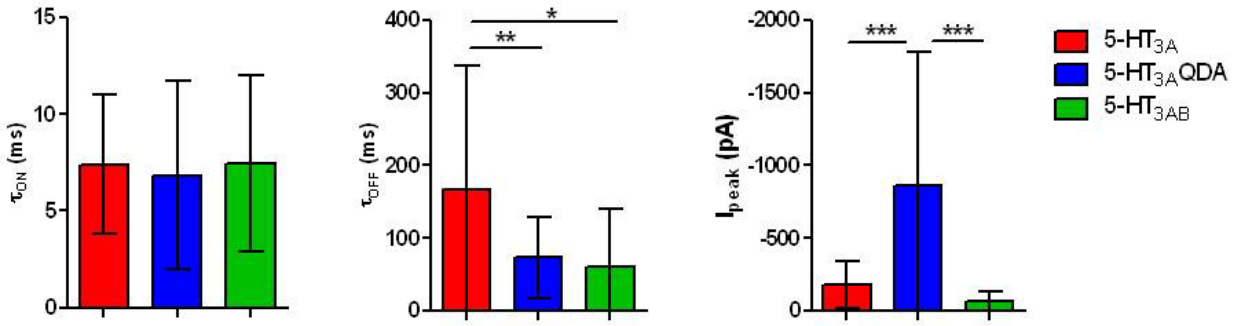

Figure 35: Comparing macroscopic current characteristics of 5-HT_{3A}, 5-HT_{3A}QDA and 5-HT_{3AB} channels.
Shown are means of all patches and their SD. One Way ANOVA tests with following Tukey Tests were performed. Indicated statistical significance: * $p < 0.05$, ** $p < 0.01$, *** $p < 0.001$.

5-HT Concentration Response

At -100 mV, 5-HT_{3A}QDA transfected cell patches were exposed to different serotonin concentrations.

Figure 36 shows an example of currents over the same patch, induced by 100, 30, 3 and 1 µM 5-HT. The peak current amplitudes depend on agonist concentration.

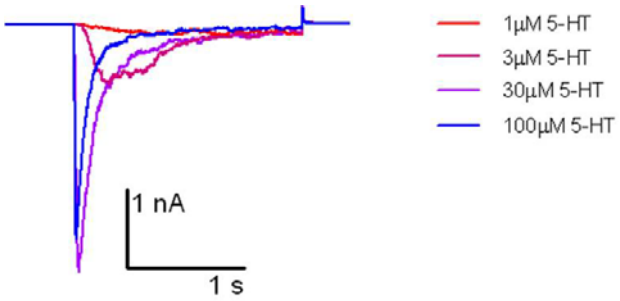

Figure 36: Example of currents over the same 5-HT_{3A}QDA transfected patch, induced by 100, 30, 3 and 1 µM 5-HT at -100 mV

Figure 37 shows the dose response curve for 5-HT on 5-HT_{3A}QDA channels (blue), which has a slope of 1.6 and reaches its half maximal point (EC_{50}) at 5.9 µM 5-HT. This is very similar to the EC_{50} for serotonin on 5-HT channels (4.49 µM), which is plotted in red in the same figure. The wild type data are pooled data from previous projects as published in (Brünker, 2010).

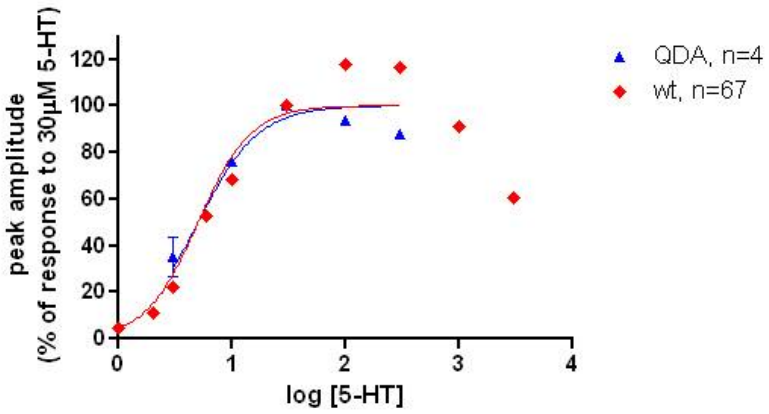

Figure 37: Dose response curves for serotonin on 5-HT_{3A} wt channels (from previous studies, as published in Brünker 2010) and on 5-HT_{3A}QDA channels.
They were fitted with formula 13, Hill slopes of 1.9 and 1.6 and EC_{50} of 4.4 µM and 5.9 µM respectively.

Voltage dependence

At 30 µM serotonin 5-HT_{3A}QDA transfected cell patches were exposed to different voltages.

Figure 38 shows an example of currents from the same patch, induced at a voltage range of -100 mV to +100 mV, in steps of 25 mV.

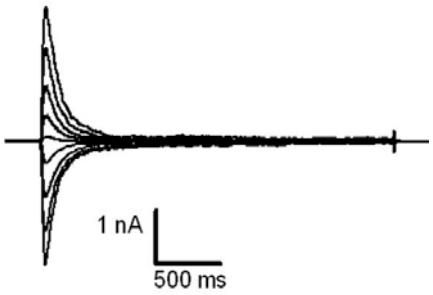

Figure 38: Macroscopic currents from the same 5-HT_{3A}QDA transfected cell patch, induced by 30 µM 5-HT in a voltage range of -100 mV to +100 mV, in steps of 25 mV.

Figure 39 plots the peak current amplitudes of each trace against the respective voltage. Four patches are shown, where the complete voltage range could be applied.

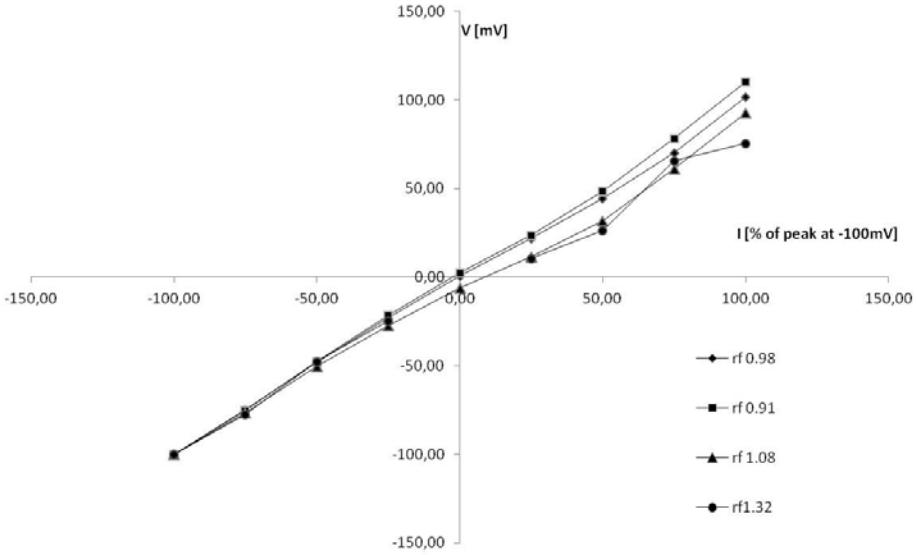

Figure 39: I-V curves for four individual patches.
Peak amplitudes of macroscopic currents evoked by 30 µM 5-HT on transiently 5-HT$_{3A}$QDA transfected HEK cells.

The reversal potentials of all curves are close to zero and show little rectification: the rectification factors vary from 0.91 to 1.32.

As shown in Figure 39 and Table 3, 5-HT$_{3A}$QDA is not rectifying. Figure 40 shows the average of the same four I-V curves for 5-HT$_{3A}$QDA (blue), in comparison with the average of six wild type I-V curves (red).

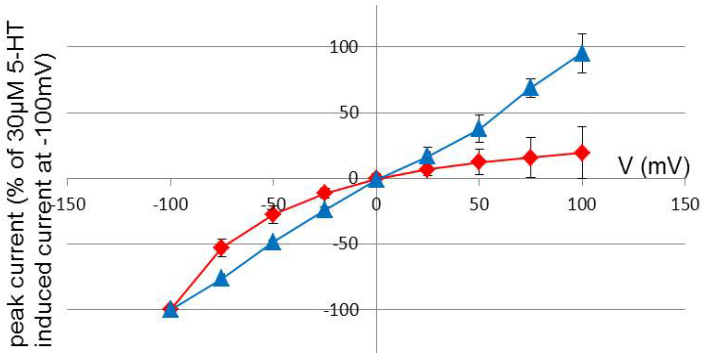

Figure 40: IV curves for 5-HT$_{3A}$ and 5-HT$_{3A}$QDA transfected cell membrane patches in comparison.
Red: wt 5-HT$_{3A}$ (n=6), rf = 7.8 ± 1.3 (SD, n=6)
Blue: 5-HT$_{3A}$ QDA (n=4), rf = 1.1 ± 0.2 (SD, n=4)

Both I-V curves show a reversal potential around zero, but when applying positive voltages, the channels' current responses differ. While 5-HT$_{3A}$ is clearly outward rectifying with a rectification factor of 7.8 ± 1.3, 5-HT$_{3A}$QDA does not show such rectification. The respective rectification factor is close to one (1.1 ± 0.2). This resembles more the I-V of heteromeric 5-HT$_{3AB}$ channels (page 48: Voltage Dependence).

Rectifying factor

The rectifying factor is calculated with formula (14). It needs fewer experiments per patch and therefore could be done at more patches than the complete I-V.

Table 3 lists rectifying factors of nine patches of 5-HT_{3A}QDA transfected HEK cells. All nine I-V relations show close to no rectification. The average rectifying factor was -1.2 ± 0.2 SD.

Table 3: Rectifying factors of nine individual patches and their average.
The larger rf (formula 14), the more outward rectification.

patch	1	2	3	4	5	6	7	8	9	**avg**	SD
rf	-0.98	-0.91	-1.08	-1.32	-1.31	-1.29	-1.17	-1.22	-1.26	**-1.2**	0.2

5-HT_{3A}QDA - Cell-attached Patches

To be able to analyze single channel properties, many single channel events per patch are needed. As excised patches are more fragile, the less invasive cell-attached conformation is chosen for single channel recordings. For the same reason, the standard holding potential is reduced to -80 mV. The following chapters describe amplitudes and kinetics of single channel events recorded with such patch configurations. Control and substance or different agonist concentrations were applied to different patches.

Typical Current Traces

Figure 41 shows one cell-attached recording of a 5-HT_{3A}QDA transiently transfected HEK cell. The recording pipette was filled with 0.1 µM 5-HT, channel openings are indicated downwards.

Single channel events are identified by fast changes in the membrane current, which gives them the rectangular appearance of steps or stair cases. A loss of channel activity over time can be seen with nearly every patch. Despite the presence of fewer events towards the end of the recording, these often seem to appear in groups, even as multiple channel openings.

Stretches ‘A’ and ‘B’ are magnified and shown in Figure 42. Stretch ‘A’ shows a series a quick channel openings, stretch ‘B’ shows a stretch of slower channel openings that partially overlap.

The magnified stretch ‘C’ in Figure 43 marks a stretch in the recording that is too noisy to be analyzed properly. The amplitudes of the here seen events don’t open to certain level nor do they show a typical stair case shape. Such a stretch will be deleted and its duration subtracted from the total duration of the recording before any further analysis

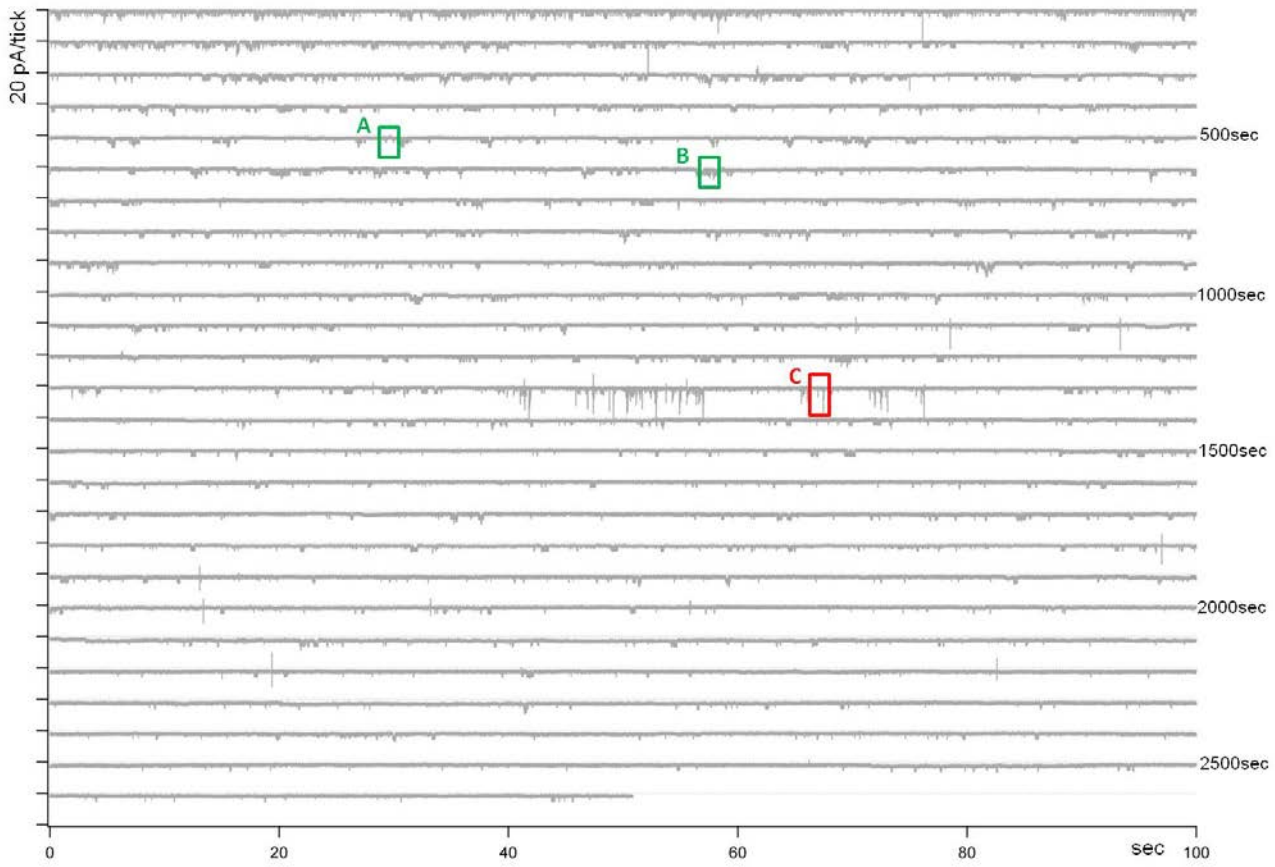

Figure 41: Representative recording of a cell attached patch transiently transfected with 5-HT_{3A}QDA.
Conditions: 0.1 µM 5-HT, - 80 mV. Channel openings indicated downwards. Green and red marked stretches are magnified in Figure 42 and Figure 43.

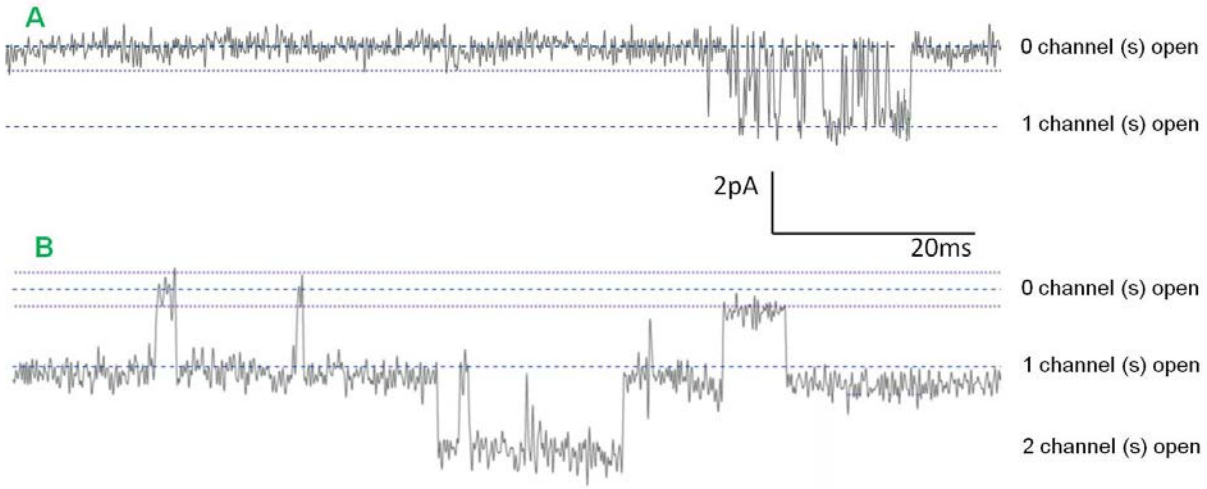

Figure 42: Magnified stretches from the recording shown in Figure 41.
A: Series of quick channel openings. B: Longer channel openings, which partially overlap. The blue dotted lines show amplitude levels of different channel numbers. The purple dotted lines show the membrane noise level, which is calculated by a IGOR routine.

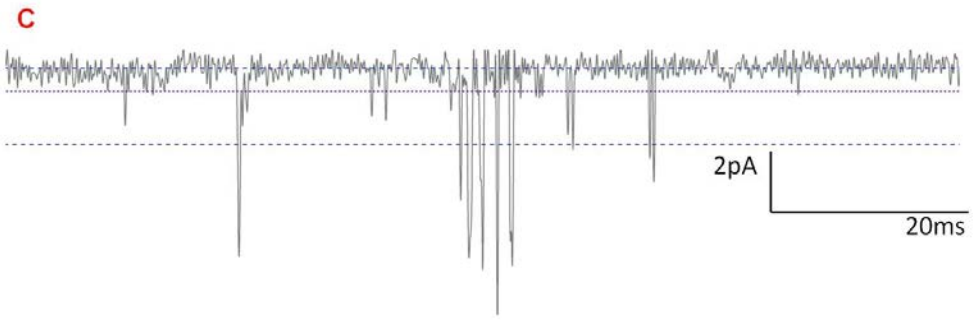

Figure 43: Magnified stretches from the recording shown in Figure 41.
Brief events don't show distinguished steps at one certain level. The blue dotted lines show amplitude levels of different channel numbers. The purple dotted line shows the membrane noise level, which is calculated by a IGOR routine.

Amplitudes

Each recording is first analyzed by the idealization tool in the program QuB before those data, together with the original trace are uploaded into IGOR routines. Personalized IGOR routines determine the amplitude and duration of each event that was identified as channel opening by QuB and then plot respective durations into histograms for further analysis. Figure 44 shows an enlarged segment of a recording that includes three channel openings, the red superimposed line represents the idealization into channel openings and closings by QuB.

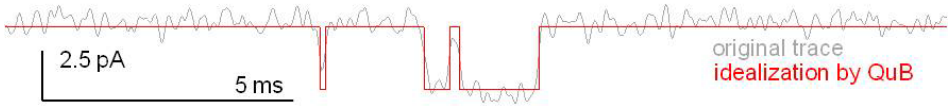

Figure 44: Example of a trace recorded at -80 mV induced by 30 nM 5-HT that includes three channel openings (indicated downwards).
The red lines represent the idealization by QuB.

The first opening in Figure 44 is very short and appears to have a smaller current amplitude than the other two events. As it is very short, it may have become truncated by filtering.

When event amplitudes are plotted against their duration (Figure 45, left), there appears a shift of short events towards smaller amplitudes. This is a phenomenon which can be explained by filtering: Due to recording limitation and filtering, short events can appear smaller in their amplitudes than long events, the peak gets cut off. This group of short events explains the second peak that the amplitude histogram (Figure 45, right) of the same patch shows on the right. The amplitude histogram is fitted by a Gaussian curve and the peak of this fit is used to assess the mean peak of

single channel current amplitudes. Open times and amplitudes are shown of a patch that was recorded at 30 nM 5-HT and shows a mean peak current of -2.58 pA for single channel openings.

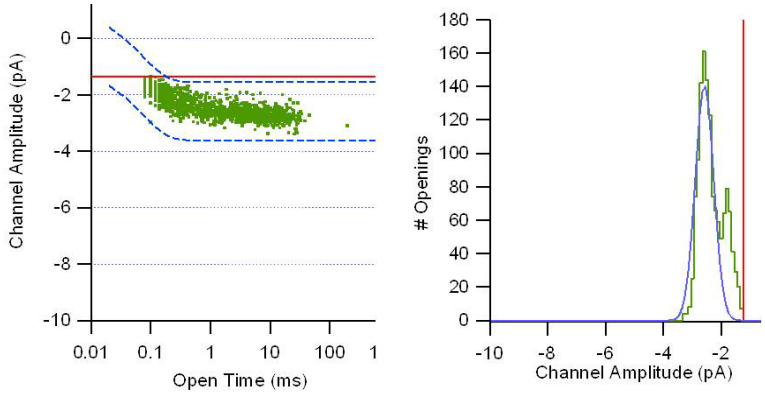

Figure 45: Example of single channel amplitude analysis of one cell attached patch of a 5-HT_{3A}QDA transiently transfected cell.
Conditions: -80 mV, 30 nM 5-HT. **Left:** Every green dot represents one single channel event (n=1334), scattered blue lines mark resolution limits introduced by the used filter setting (3 kHz), red line represents the half maximal amplitude used by QuB to identify events. **Right:** Histogram of individual events and their amplitudes, blue line represents a Gaussian fit of the histogram (peak at -2.58 pA), red line represents the half maximal amplitude used by QuB to identify events.

Truncated single channel amplitudes do appear as a right shoulder, sometimes even as an additional peak within amplitude histograms, but by using the peak of the Gaussian fit of those histograms, those truncated single channel amplitudes are not taken in account.

Mean peaks of the Gaussian fits of amplitude histograms for 27 patches are listed in Table 4. The patches were all clamped to -80 mV and exposed to different 5-HT concentrations. The sum of 36,853 single channel openings showed a mean amplitude of -2.63 ± 0.04 pA (± SD). This corresponds to a conductance of 33 pS. The current amplitudes did not differ depending on agonist concentration (one way ANOVA, p = 0.975), as shown in Table 4.

Table 4: Current amplitudes (pA) of single 5-HT_{3A}QDA channel events.

Induced by different serotonin concentrations at -80 mV. The amplitudes are not concentration dependent (one way ANOVA, p = 0.975).

[5-HT] (µM)	n (patches)	n (events)	I (pA)	SD
3	7	4469	-2.67	0.2
0.3	6	16291	-2.67	0.18
0.1	4	12687	-2.61	0.18
0.03	10	3406	-2.59	0.2
total / mean	27	36853	-2.63	0.04

As reported previously (Corradi et al., 2009), a low proportion of low conductance events occurred in some recordings. Those were discarded for all analysis.

Duration Histograms

The analysis program plots histograms of the duration of open, closed and cluster events within a recording. These duration histograms are fitted with multiple exponential functions (formula 6) to assess time constants of channel kinetics. Figure 46 shows examples of these histograms for the combined results of ten 30 nM 5-HT patches.

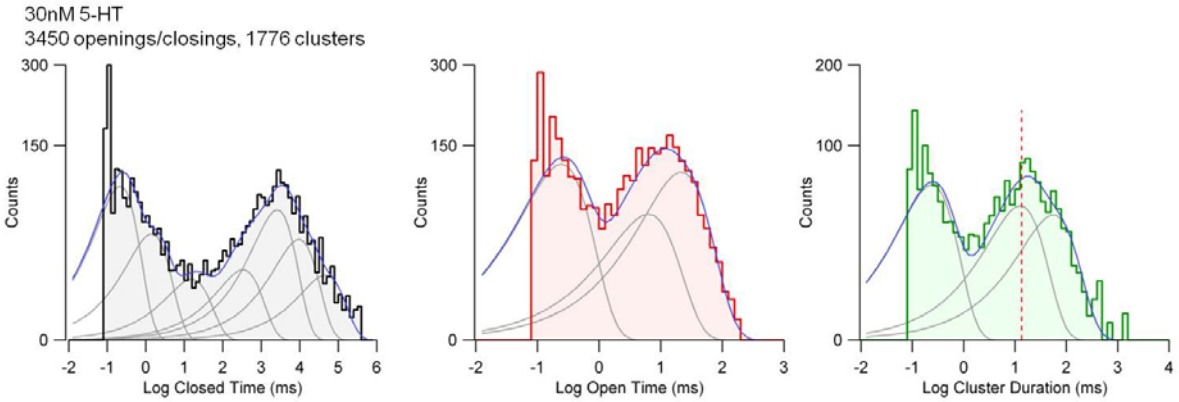

Figure 46: Duration histograms for combined events of ten patches from *human* 5-HT_{3A}QDA receptors, activated by 30 nM 5-HT, with superimposed fits (blue solid lines).
Closed duration histograms are fitted with seven, **open** and **cluster** duration histograms with three exponential components (grey solid lines).

Data from duration histograms are used to quantify the channel activity and how the activity changes with changes in recording conditions. To make this quantification comparable between patches that include different numbers of channels, opening and closing series of individual channels are extracted from the mixture of activity of several channels. This is achieved by the selection of clusters. One cluster is assumed to represent openings and closings by an individual channel protein (Figure 3 and Figure 4).

Clusters

Experimentally a series of transitions of one channel results in a cluster, a series of single channel openings, interrupted by closings that do not exceed a certain duration (= critical time t_{crit}). Figure 47 shows an example for such a cluster.

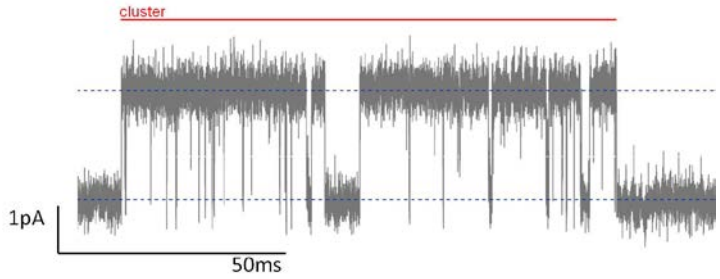

Figure 47: Current trace over a 5-HT_{3A}QDA transfected cell patch to depict a cluster.
Channel opening is indicated upwards, recorded at -80 mV and 0.1 µM 5-HT. Red line: one cluster duration.

Critical Time Between Clusters (t_{crit})

The section on “Cluster Determination” (page 37) explains how we arrived at a critical gap duration of 30 ms for standard conditions. At 30 nM 5-HT, the combined closed duration histogram shows a dip between the third and fourth components (Fig 48). This supports the decision to choose a critical closed duration of 30 ms. The histogram was fitted with formula 6 to seven components and values are listed in the table under the figure. Durations for the third and the fourth components are highlighted blue.

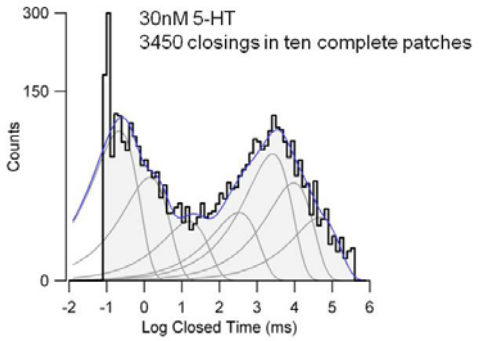

τ 1	fr.amp 1	τ 2	fr.amp 2	τ 3	fr.amp 3	τ 4	fr.amp 4	τ 5	fr.amp 5	τ 6	fr.amp 6	τ 7	fr.amp 7
0.19	0.29	0.97	0.16	7.08	0.05	131.96	0.06	1309.30	0.30	6009.04	0.12	35404.60	0.02

Figure 48: Combined duration histogram for closings of 5-HT_{3A}QDA channels at 30 nM 5-HT.
Blue line: fit of the histogram (formula 6), grey lines: individual components of the fit, 10 patches). The table below shows the according values for the individual components (time constants in ms, fractional amplitude fr.amp..

Closed duration histograms after cluster selection can be fit to three components. Figure 49 shows the resulting closed duration histogram for the data in Figure 48. The time constants and their fractional amplitudes resemble the first three components of the closed duration histogram before cluster selection. This further supports the use of 30 ms as the critical time between clusters.

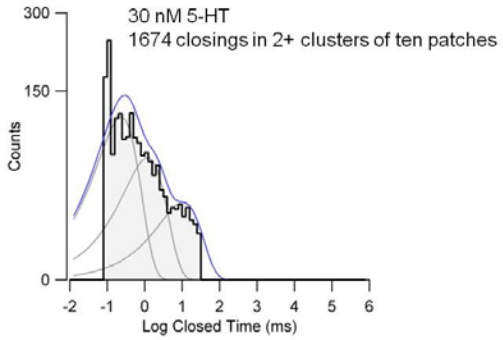

τ 1	fr.amp 1	τ 2	fr.amp 2	τ 3	fr.amp 3
0.19	0.55	0.95	0.31	8.32	0.13

Figure 49: Combined duration histogram for closings in 2+ clusters of 5-HT_{3A}QDA channels at 30 nM 5-HT
Blue line: fit of the histogram (formula 6), grey lines: individual components of the fit, 10 patches). The table below shows the according values for the individual components (time constants in ms, fractional amplitude fr.amp.).

Fraction of individual events

Not all channel openings turn into clusters that include multiple events. Sometimes individual channel openings are directly followed by a closure longer than $t_{crit.}$ Figure 50 depicts the fractions of such individual openings at different agonist concentrations.

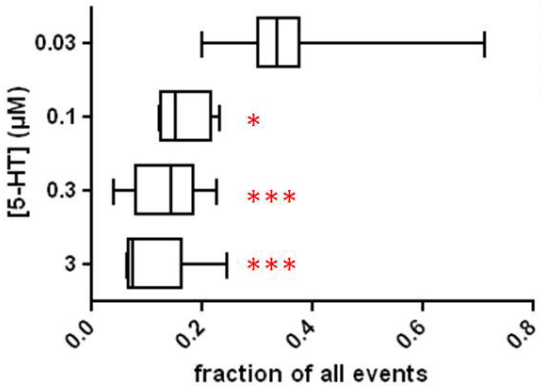

[5-HT] (µM)	3	0.3	0.1	0.03
n patches	7	6	4	10
median	0.08	0.15	0.15	0.34

Figure 50: Fraction of individual channel openings that do not turn into a 2+ cluster for events from human 5-HT_{3A}QDA receptors at different 5-HT concentrations.
One way ANOVA test indicates significant differences of fractions between different [5-HT] ($p = 0.0001$), followed Tukey's Multiple Comparison Test shows significant difference of fractions at 0.03 µM 5-HT to all other concentrations, p values are indicated *** $p < 0.0001$, * $p < 0.005$.

Although a trend can be seen towards a higher fraction of individual events at lower serotonin concentrations, at 3 µM to 0.1 µM 5-HT, the fractions of individual events are statistically similar (12 % - 17 %, respectively). Only at the lowest agonist concentration of 30 nM, does the fraction increase to a statistically significant value of 36 %.

Distinguishing Different Types of Clusters

Clusters don't always look alike. Those that do contain more than one opening can be of different length and contain different numbers of openings. One question is rather certain clusters are composed by certain openings and closings. Therefore clusters can be distinguished by the following criteria:

Independent from how many components are used to fit a cluster duration histogram, a critical time ($t_{crit\ long}$) can be found, which marks the point of least overlap between the second to shortest and the shortest cluster duration component. Clusters that last longer than $t_{crit\ long}$ are defined long clusters, clusters that are shorter are defined brief clusters. Later within this theses, this definition will be used to form quasi macroscopic currents (page 75: Quasi Macroscopic Currents).

As shown above, not all clusters display multiple openings. If a cluster contains at least two openings, it is called a 2+ cluster.

As the Corradi model (page 11: Kinetic Models for 5-HT3A QDA Receptor Channels) is based on clusters that contain at least five openings, this group of clusters will be worth looking at separately as well. If it contains at least five openings, it is called a 5+ cluster.

Cluster Durations

Individual Patches

Cluster durations are exponentially distributed. Thus, the SD of the distribution is equal to the mean value. Some patches have few clusters (as few as 20). One sample may have predominantly very short or very long clusters. This makes a very high number of long patches necessary to be able to provide proper statistics.

In addition to the comparison of the exponential fit components of cluster duration histograms the medians of all cluster durations for each recording are compared. A wide variation in cluster duration from patch-to-patch may be evidence for more than one mode of cluster behavior.

Variability between patches

To get a first overview over cluster durations, the duration distributions within the individual recordings were determined. Table 5 shows the median cluster durations for ten cell-attached recordings obtained at 30 nM 5-HT.

The cluster durations of all cluster types of patch 9 and patch 4 differ from the ones of the other eight patches. These patches are not especially short or have especially few clusters.

When comparing 2+ and 5+ cluster durations of the 30 nM patches, patches 1 and 8 particularly stick out. Although they were recorded under the exact same conditions as the other patches, they seem dominated by short clusters, which leads to significant differences in 2+ and 5+ cluster duration medians to several other recordings. This difference probably does not turn out statistically significant for patch 8, because it does contain very few events.

Some other significant differences in cluster durations between recordings were found. Those differences are not only due to a wide variety of cluster durations, but indicate a non-normal distribution of cluster durations, possible different groups of distribution and thus different cluster modes.

Table 5: The medians of cluster durations within ten recordings at 30 nM 5-HT.
The medians are given for different groups of clusters. All clusters include all events in a recording, including individual openings. Red arrows indicate significant differences between recordings as results of non-parametric tests. The level of significance is determined by Dunn's post tests and indicated by red stars.

cluster durations at 30 nM 5-HT										
patch	13-03-15 E3	13-03-14 E2	13-02-18 E2	13-03-01 E4	13-03-01 E5	13-03-07 E1	13-03-14 E1	13-01-15 E6	13-03-18 E1	13-03-18 E3
patch #	1	2	3	4	5	6	7	8	9	10
# of all clusters (incl. indiv. events)	743	59	129	95	118	225	112	66	118	111
median all clusters (incl. indiv. events) **(ms)**	3.2	6.3	9.5	1.3	3.4	2.3	4.6	3.2	12.6	3.5
				*		***			***	
		***								
# of 2+ clusters	274	15	52	31	42	72	34	14	54	37
median 2+ clusters (ms)	13.5	64.7	43.7	12.3	21.4	30.8	39.3	16.4	36.4	29.7
					*					
		***		**					**	
		*								
					***					
						*				
								*		
										***
# of 5+ clusters	39	5	12	8	9	20	10	3	16	11
median 5+ clusters (ms)	30.1	329.3	67.5	30.8	62.7	152.4	84.3	35.8	77.6	147.9
									**	
***p ≤ 0.001		*								
** p ≤ 0.01						***				
* p ≤ 0.05							*			
								*		
										***
patch duration (s)	1090	1203	265	1327	1025	996	986	1893	970	825

Variability over Time

Similarly to the rundown that is observed at macroscopic currents over time, single channel activity does change over time within a patch as well. This is not a steady process. Figure 51 shows the number of channel openings over time for five individual patches. Stretches of very low activity can be followed by a sudden increase of channel openings.

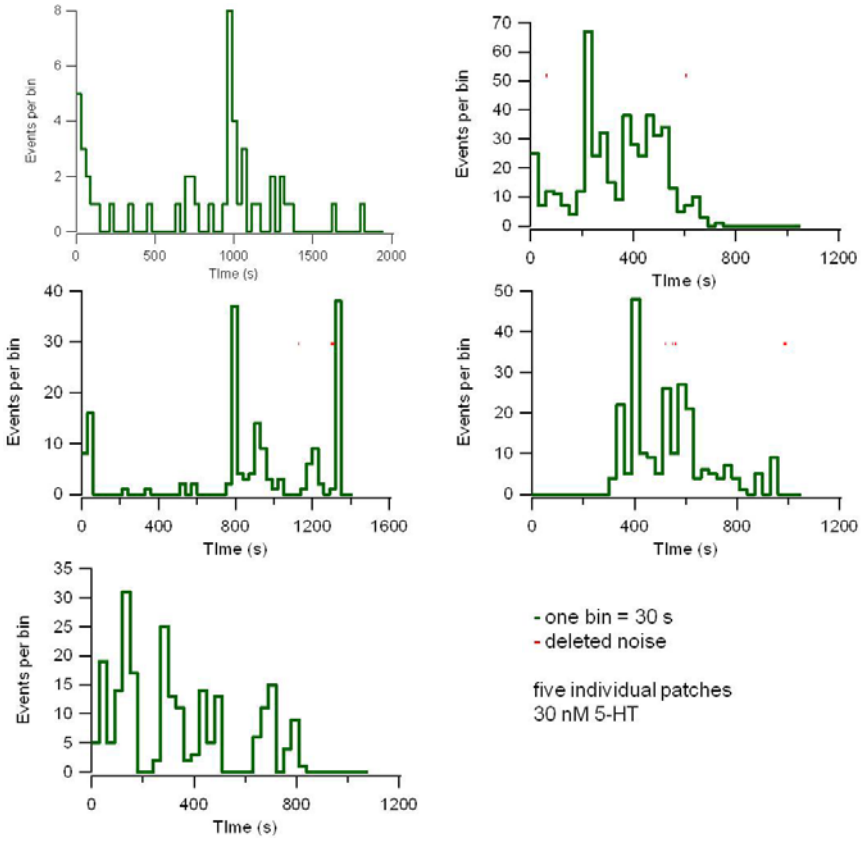

Figure 51: The number of openings in five individual recordings over time.
5-HT$_{3A}$QDA transfected cells were patched, clamped to -80 mV and their currents recorded in cell attached configuration. The patch pipette was filled with 30 nM 5-HT. Time scales differ because of different patch durations. Red marks represent stretches that were deleted because they were too noisy to be analyzed and therefore include no events.

Stretches of very low activity can be followed by a sudden increase of channel openings. Does the change of activity level also change cluster characteristics over time? To investigate the differences in median durations of events within 2+ clusters, all dwell times of the first halves of recordings of the same serotonin concentration were pooled and compared with the pooled dwell times of the respecting second halves. Table 6 shows the resulting medians of open, closed and cluster durations for the used serotonin concentrations.

When comparing the 1st with the 2nd halves of recordings at 0.1 µM, 0.3 µM and 3 µM 5-HT, all event durations (openings, closings, clusters) within 2+ clusters differ. Openings are longer during 2nd halves, closings are shorter during 2nd halves, clusters are longer during 2nd halves. Often those differences are marginal (i.e. the medians for closed durations at 0.3 µM), nevertheless does the multiple comparison test result in statistical differences. Only at 30 nM, the recordings were consistent over time. No event durations differ significantly between the 1st and 2nd halves of 30 nM recordings, suggesting that this should be the serotonin concentration of choice for control experiments.

Table 6: Event durations in 2+ clusters for 1st halves, 2nd halves and complete cell attached recordings of 5-HT$_{3A}$QDA channel activity induced by different serotonin concentrations. Medians of 1st and 2nd halves were compared by Dunn's Multiple Comparison Test (***p < 0.001, **p < 0.01, *p < 0.05).

25% percentile **event duration median (ms)** 75% percentile	open durations			closed durations			cluster durations		
	1st half	2nd half	complete	1st half	2nd half	complete	1st half	2nd half	complete
number of events	1860	438	2299	1369	304	1674	490	134	625
0.03µM 5-HT	0.28 **2.92** 12.41	ns 0.36 **2.41** 9.26	*** 0.30 **2.78** 11.68	0.12 **0.34** 1.14	ns 0.14 **0.42** 1.25	*** 0.14 **0.34** 1.14	8.86 **20.25** 46.01	ns 3.80 **15.81** 39.65	*** 7.66 **19.78** 44.60
0.1µM 5-HT	0.38 **4.88** 16.97	*** 0.71 **6.61** 18.68	0.50 **5.58** 18.04 ns	0.16 **0.42** 1.59	* 0.16 **0.36** 1.06	0.16 **0.40** 1.36 ns	18.63 **44.07** 103.80	* 20.68 **57.70** 128.10	18.99 **51.52** 121.90 ns
0.3µM 5-HT	0.38 **1.60** 12.30	*** 1.00 **2.58** 6.72	0.70 **2.22** 7.84	0.20 **1.20** 5.28	*** 0.20 **1.14** 3.69	0.20 **1.16** 4.14	14.48 **38.74** 107.70	*** 32.76 **83.90** 164.70	19.52 **54.60** 140.70
3µM 5-HT	0.50 **3.60** 11.31	*** 1.04 **5.18** 15.85	0.58 **3.96** 12.10	0.12 **0.37** 1.33	*** 0.10 **0.24** 0.80	0.12 **0.34** 1.16	15.20 **28.34** 61.28	ns 10.38 **27.08** 57.74	14.34 **28.16** 60.96

Cluster Duration Components for Individual Patches

Cluster duration histograms of individual recordings for events in 2+ clusters were fitted with two exponential components. Figure 52 shows one example of a 2+ cluster duration histogram for an individual recording that was fitted with exponential components with the time constants 1.96 ms and 73 ms.

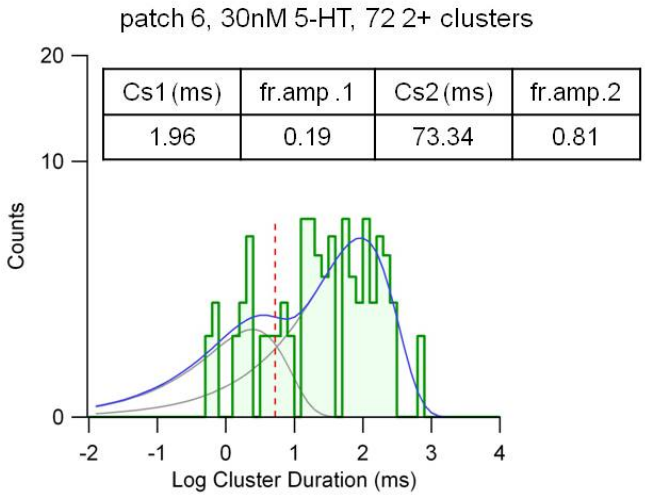

Figure 52: Example of a 2+ cluster duration histogram for one out of ten 30 nM 5-HT recordings. Values of the two exponential fits (grey lines) are listed above. Red dotted line represents $t_{crit\ long}$.

Figure 53 shows the resulting time constants for the cluster duration components at different serotonin concentrations. Histograms of some recordings could only be fitted with one component. Respective time constants are depicted red. When two cluster components could be fitted, they are separated by the according medians (20 – 55 ms). Clusters of one component fits show intermediate time constants (16 - 112 ms). They are very close to the median of the respective serotonin concentration and probably represent a mixture of events of both components.

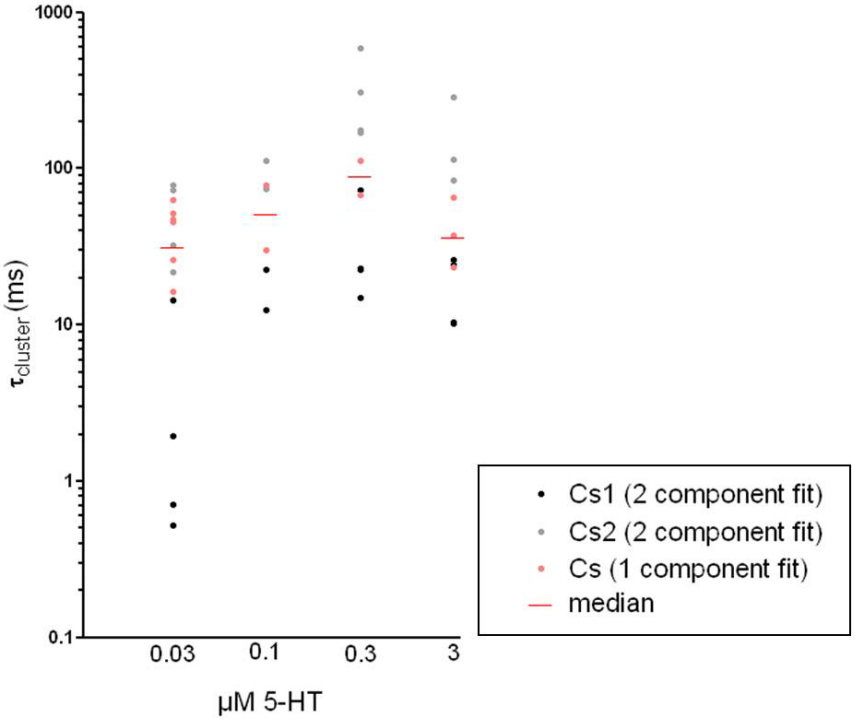

Figure 53: Plotting time constants (ms) of fitting 2+ cluster duration histograms of individual patches at different serotonin concentrations.
Fitting cluster duration histograms with one (red) or two (black and grey) components.

Cluster Duration Components at Different Serotonin Concentrations

Cluster duration histograms for combined dwell times of one serotonin concentration were fitted with three duration components, when all clusters were included. Figure 54 shows fitted cluster duration histograms for ten combined 30 nM 5-HT recordings. When all clusters are plotted, the histogram can be fitted to three exponential components with the time constants 0.19, 10 and 44 ms. The larger the number of events in the selected clusters, the fewer components were used for fitting the respective duration histograms.

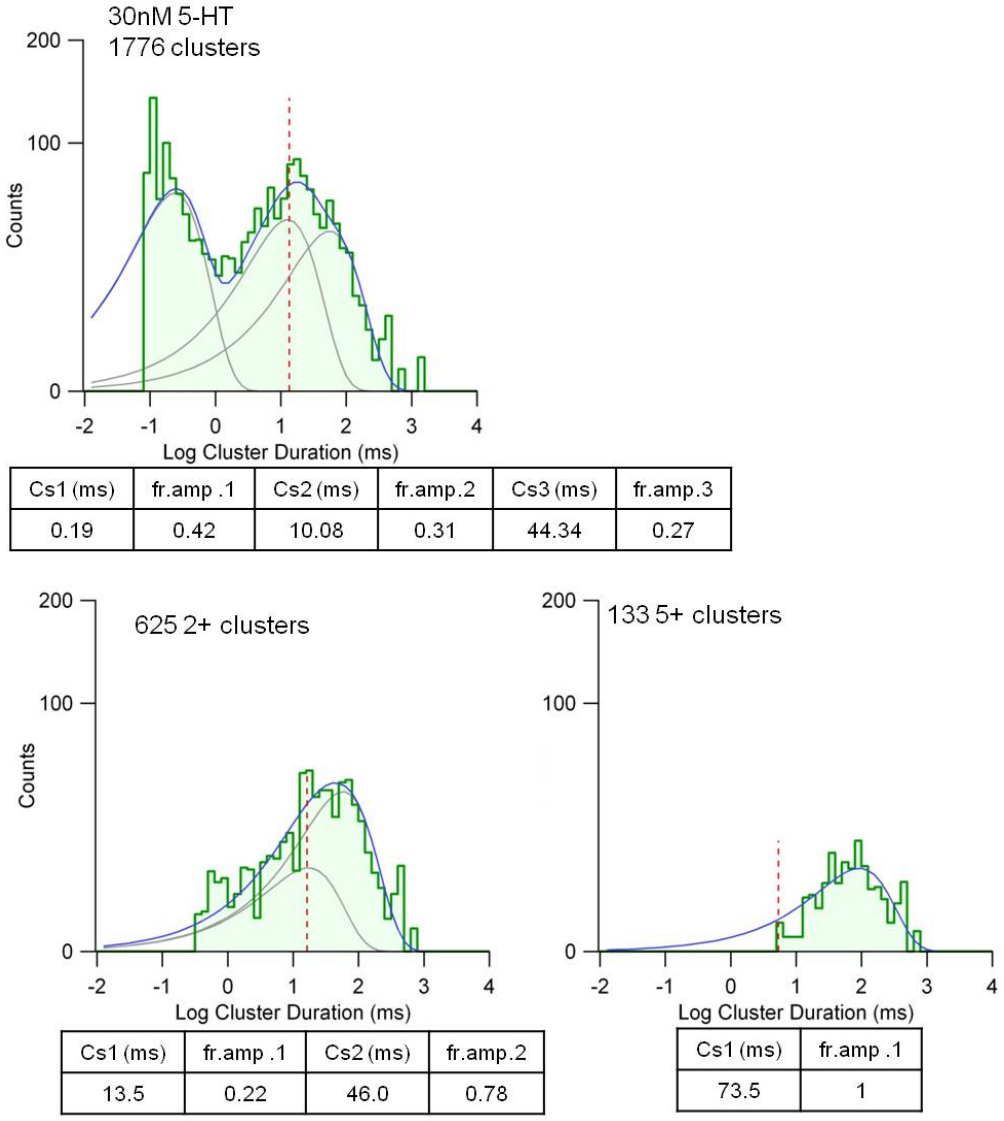

Cs1 (ms)	fr.amp .1	Cs2 (ms)	fr.amp.2	Cs3 (ms)	fr.amp.3
0.19	0.42	10.08	0.31	44.34	0.27

Cs1 (ms)	fr.amp .1	Cs2 (ms)	fr.amp.2
13.5	0.22	46.0	0.78

Cs1 (ms)	fr.amp .1
73.5	1

Figure 54: Cluster duration histograms for ten combined patches, events were recorded at 30 nM 5-HT and -80 mV.
Plotted are the counts of events and their durations including all clusters of the recording (top), 2+ clusters (bottom left) and 5+ clusters (bottom right).Tables list the values of the exponential fits (grey lines). Events were normalized so that each recording gains the same weight.

Table 21 - Table 23 in the attachment list time constants and fractional amplitudes of cluster duration components for single channel events induced by different 5-HT concentrations. These values are plotted in Figure 55, where fractional amplitudes and time constants for the fit components are plotted for each of the applied serotonin concentrations. The lines that cross the time line represent weighted averages of cluster durations calculated by the formula

$$Cs(avg) = \frac{fr.amp._1 * Cs_1 + fr.amp._2 * Cs_2 + fr.amp._3 * Cs_3}{n\ (Cs)} \quad (18).$$

These weighted averages summarize all cluster components of one condition.

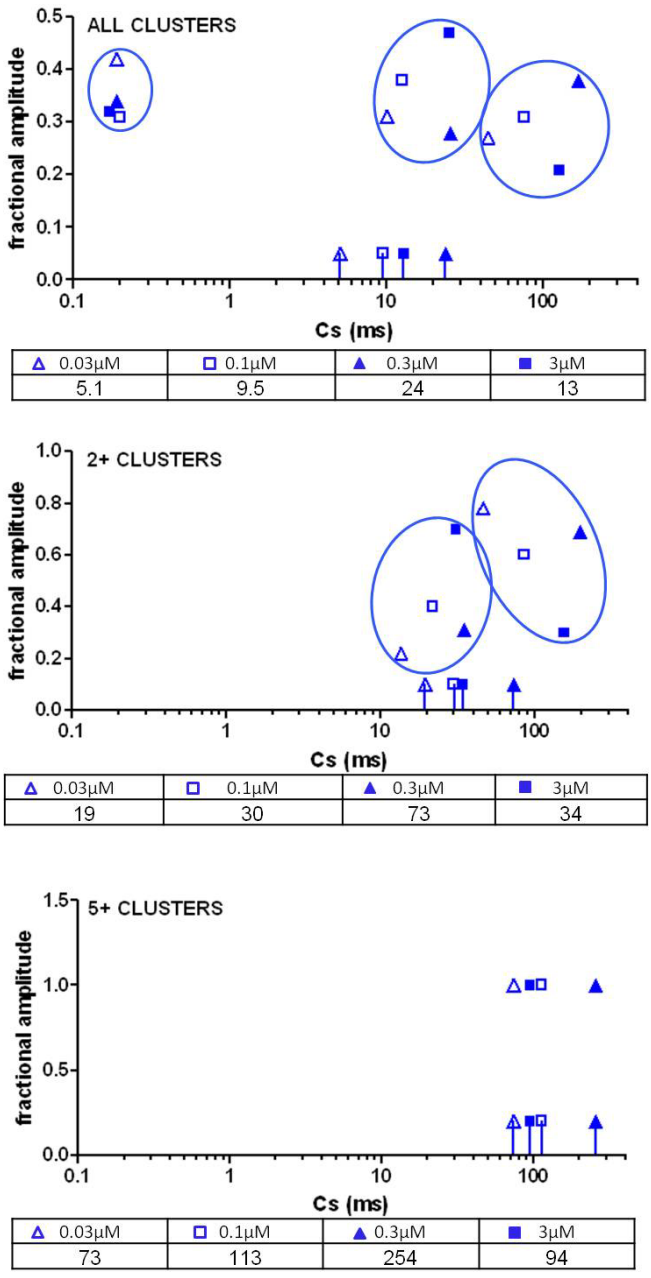

Figure 55: Cluster duration time constants (ms) and their fractional amplitudes at different 5-HT concentrations. Circles mark the different components, symbols connected to the time axis represent the weighted average durations (ms) of clusters, which are listed under each figure.
t_{crit} = 30 ms
Fractional amplitudes and cluster components can be found in Table 21 - Table 23 in the attachment.

Cluster duration increased with serotonin concentration. At 0.3 µM the longest clusters are evoked. They did last 24 ms in average, 73 ms when excluding one opening clusters. Interestingly, application of the highest serotonin concentration leads to the smallest fraction of longest clusters. Single channel activity here tends to happen in intermediate cluster durations.

In recordings of the lowest agonist concentration the fraction of the briefest clusters is higher than in other recordings.

Quasi Macroscopic Currents

If each cluster represents the activity of a channel until it desensitizes, the macroscopic decay should be shaped by the duration of clusters. Alignment of all clusters of one recording and summing their amplitudes produces a quasi macroscopic current (QMC). If cluster duration represents desensitization, one expects to find the same number of decay constants as number of cluster components. Figure 56 shows the alignment of all clusters in one 3 µM recording and one 30 nM recording. Exponential decays predicted from the fit of the cluster histogram are superimposed (red).

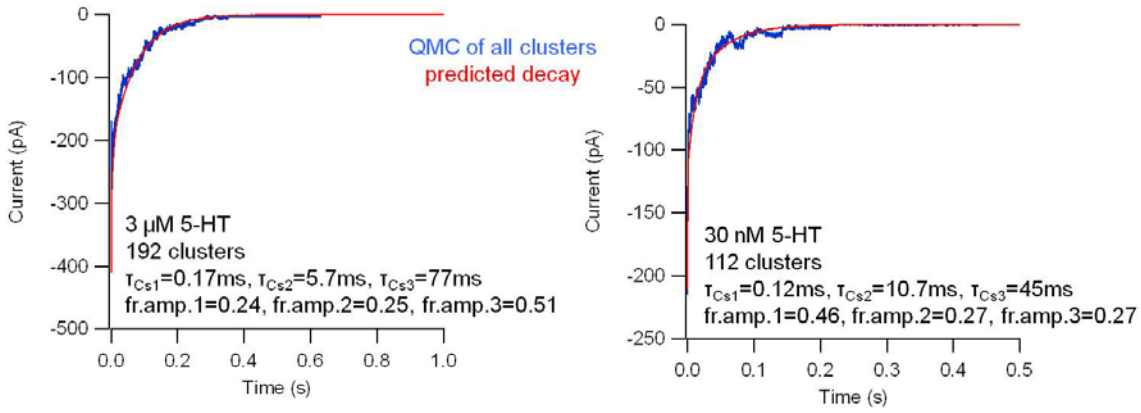

Figure 56: Predicted macroscopic decay based on cluster components.
Quasi macroscopic currents were formed by aligning and summing all clusters of one patch (blue). Predicted decay was calculated by three exponential curve with the three cluster components of respective patch (red).

Time constants of brief clusters are around 0.2 ms (Table 23), thus brief clusters contribute only to the very first few milliseconds of the net current of the QMC. In an actual macroscopic current, the contribution of brief clusters would be obscured by the onset of the current. Figure 57 shows the same two patches in which only the

clusters longer than $tau_{crit\ long}$ are used to form the QMC (blue). Respective one exponential fits (τ_{macro}) of the QMC are superimposed (red).

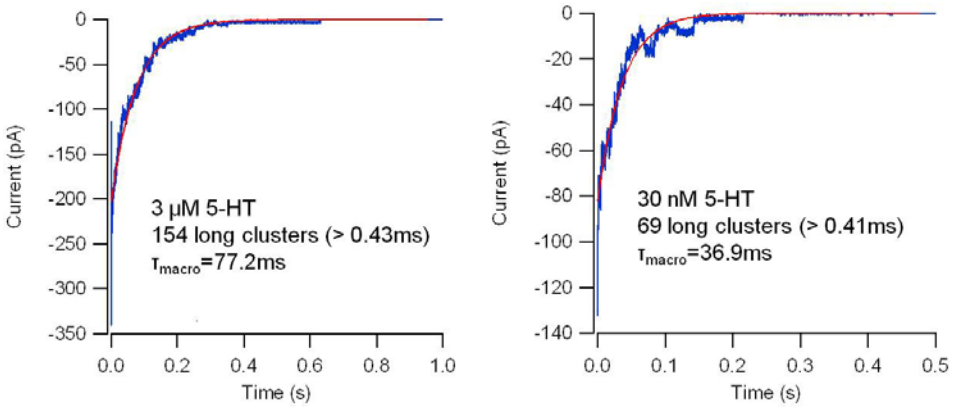

Figure 57: Examples of macroscopic currents obtained by aligning and summing up clusters (blue) and their exponential fits (red).

To evaluate whether QMCs resemble macroscopic currents recorded from outside-out patches, the respective decay constants were compared. Table 7 shows the median decay constants of QMCs based on single channel recordings of 5-HT_{3A}QDA currents induced by different serotonin concentrations. The far right column shows the average decay constant of 37 macroscopic recorded patches exposed to 30 µM serotonin.

Table 7: Decay time constants of quasi macroscopic currents built by aligning and summing long clusters of single channel events in cell attached patches compared with decay time constants of recorded macroscopic currents in outside-out patches.
QMCs of different [5-HT] were compared by Dunn's Multiple Comparison tests (**p ≤ 0.005). They were pooled and compared to recorded macroscopic decay constants, which did not show significant differences (t-test).

	cell-attached patches				outside-out patches
[5-HT] (µM)	0.03	0.1	0.3	3	30
25%percentile **median** 75%percentile	16.5 **33.0** 48.8	25.6 **74.5** 107	145 **193** 449	26.3 **47.2** 77.2	
	**		ns		
25%percentile **median** 75%percentile	28.8 **47.2** 108				29.0 **63.5** 90.8
n (patches)	10	4	6	7	37

QMCs under 30 nM show the fastest (τ_{macro}=33 ms), QMCs under 0.3µM the slowest (τ_{macro}=193 ms) decay, which results in a statistically significant difference between the two. This correlates with the concentration dependent slowing of weighted averages of cluster components (Figure 54).

Decay constants of the one exponential fits of quasi macroscopic currents are similar to real macroscopic currents of 5-HT_{3A}QDA transfected outside out patches.

This supports the applied method to select clusters (page 37: Cluster) because it allows us to generate macroscopic currents from single channel properties.

Openings in Clusters

Variability between patches

Median open durations for individual recordings were determined. Resulting medians for ten patches that were exposed to 30 nM 5-HT are listed in Table 8. Statistical tests reveal several significant differences between patches, which indicates that the channel can open in more then one open mode.

Table 8: Median open durations (ms) of 10 individual patches, exposed to 30 nM 5-HT.
Statistical significance tested by one way ANOVA, Kruskal-Wallis (nonparametric test), post test: Dunns. Significance level: $p \leq 0.05$, indicated by red arrows

open durations at 30 nM 5-HT										
patch	13-03-15 E3	13-03-14 E2	13-02-18 E2	13-03-01 E4	13-03-01 E5	13-03-07 E1	13-03-14 E1	13-01-15 E6	13-03-18 E1	13-03-18 E3
patch #	1	2	3	4	5	6	7	8	9	10
# of all openings	1334	116	263	167	225	457	232	94	320	242
patch duration (s)	1090	1203	265	1327	1025	996	986	1893	970	825
median all clusters (ms)	**0.98**	**7.40**	**4.22**	**0.60**	**2.40**	**2.50**	**3.63**	**3.04**	**1.60**	**4.42**
# of 2+ clusters	865	72	186	103	149	304	154	42	256	168
median 2+ clusters (ms)	**1.12**	**11.24**	**5.93**	**2.04**	**3.72**	**5.58**	**5.76**	**5.32**	**1.64**	**7.79**
# of 5+ clusters	252	46	76	46	65	180	81	17	153	102
median 5+ clusters (ms)	**6.64**	**50.28**	**16.02**	**5.67**	**10.48**	**22.73**	**21.35**	**15.04**	**7.32**	**21.81**

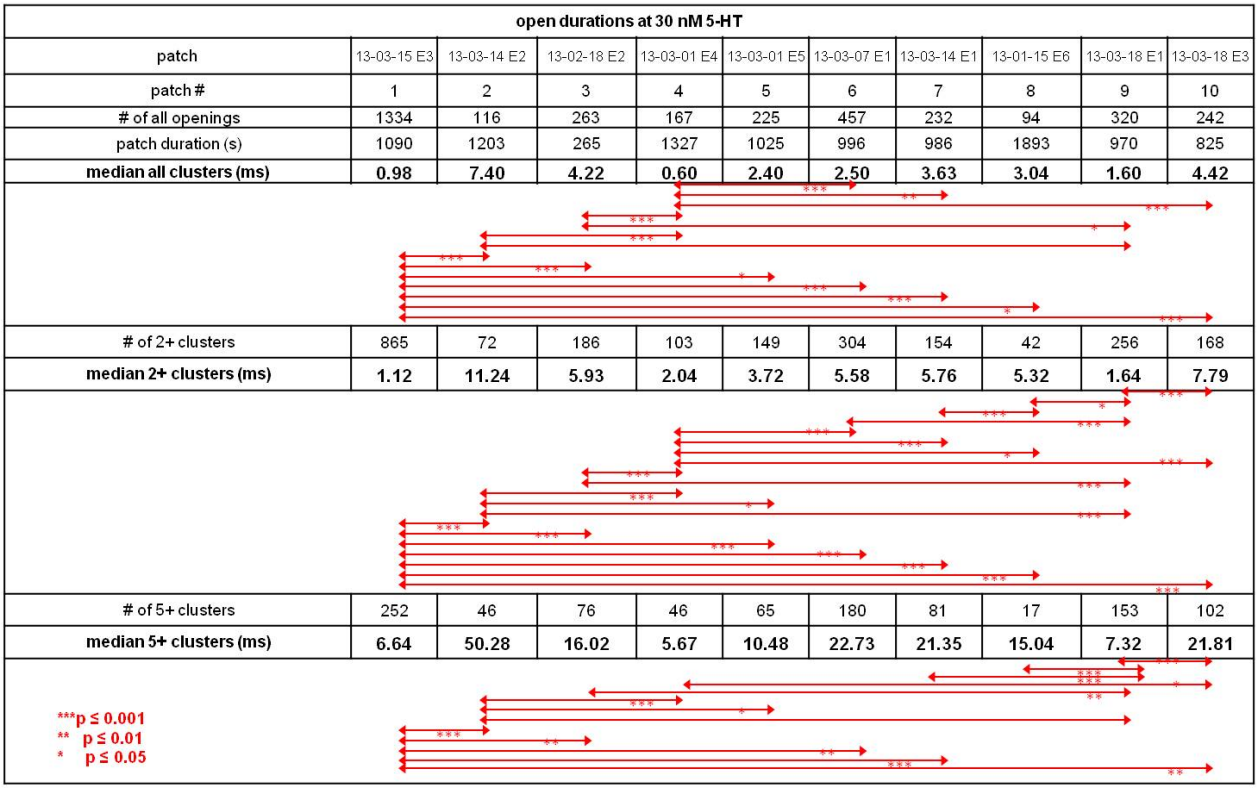

Especially for open durations in 2+ clusters, many significant differences are found. Just like when comparing median cluster durations patch 1 sticks out. But also patch 4 appears to be different to other patches.

Median open durations are always longer in 2+ clusters than in all clusters, which could be a hint that individual openings are mainly brief openings. Open durations in 5+ clusters are even longer.

Figure 58 plots the relation of the number of openings in all clusters to the 2+ cluster duration under 30 nM 5-HT. Each point resembles one patch.

The Spearmann correlation test results in a correlation coefficient r of 0.68, which indicates a positive correlation of cluster and open durations in a patch. The p value of 0.035 is significant (*), which rejects the hypothesis that random sampling could result in seemingly correlating data sets. The linear regression shows a significant slope of 0.14 ms open duration per ms cluster duration.

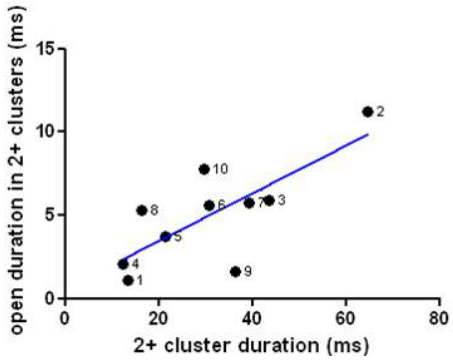

Figure 58: Cluster durations of ten 30 nM recordings in relation to open durations.
Blue line shows the linear regression with a slope of 0.14. Each number represents one patch.

Open Duration Components in 2+ Clusters for Individual Patches

Open duration histograms of individual recordings were fitted with two exponential components (formula 6). Figure 59 shows one example of an open duration histogram for 2+ clusters of an individual recording that was fitted with exponential components with the time constants 0.26 ms and 19 ms.

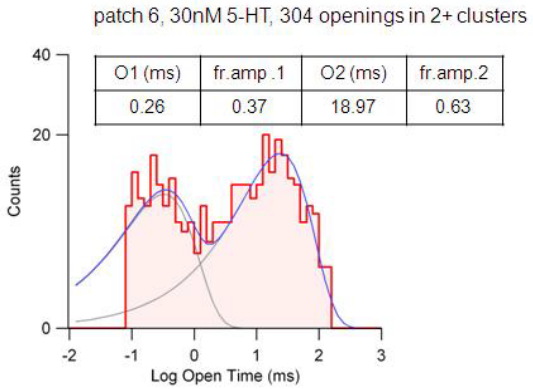

Figure 59: An example of an open duration histogram for one out of ten 30 nM 5-HT recordings.
Values of the two exponential fits (grey lines) are listed above the figure.

Figure 60 shows the resulting time constants for two component fits of open duration histograms of individual recordings at different serotonin concentrations. For all recordings, the two open duration components were clearly separated.

There are only two open states for one channel, and only two open components for histograms of individual patches. Open components are variable between patches. When pooling open durations of several patches into one histogram, the varieties get pooled as well, and more components are necessary to fit the according histogram (Figure 61).

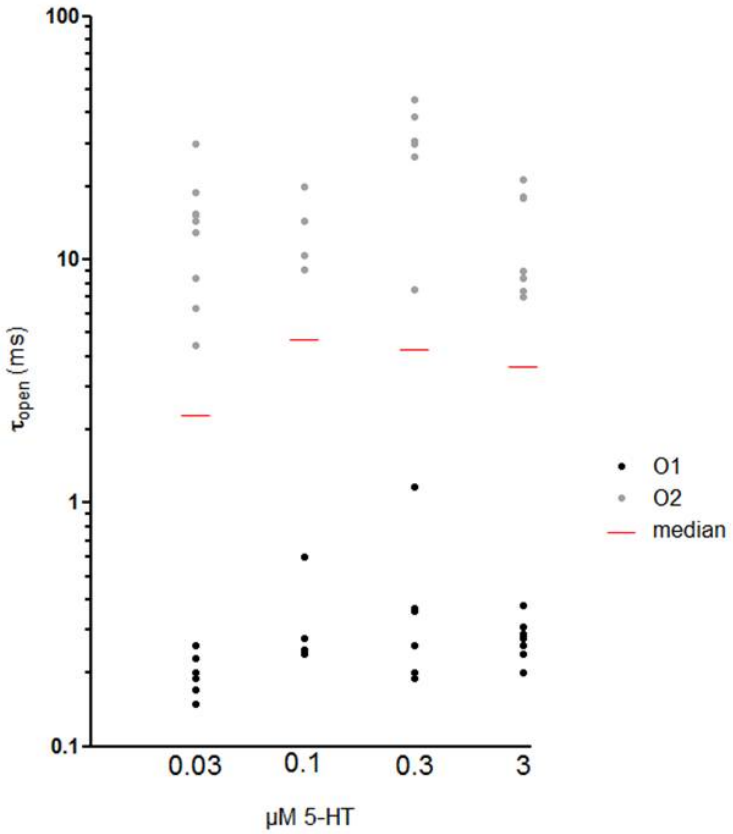

Figure 60: Resulting time constants (ms) of individual patches at different serotonin concentrations.
Duration histograms for openings in individual patches were fitted with two exponential components (formula 6).

Open Duration Components at Different Serotonin Concentrations

Combined open time histograms of experiments under different 5-HT concentrations suggest three open components with the time constants. Figure 61 demonstrates on the example of 10 combined 30 nM recordings, that by introducing a third exponential component as well the left as the right shoulder of the right peak

of the histogram are captured better. This improvement can also be quantified by a smaller chi².

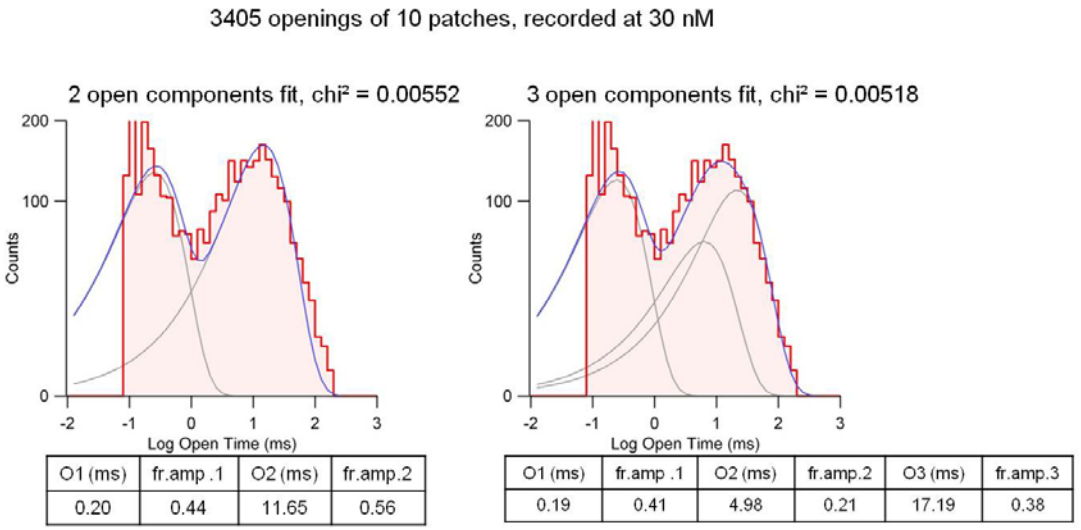

O1 (ms)	fr.amp .1	O2 (ms)	fr.amp.2
0.20	0.44	11.65	0.56

O1 (ms)	fr.amp .1	O2 (ms)	fr.amp.2	O3 (ms)	fr.amp.3
0.19	0.41	4.98	0.21	17.19	0.38

Figure 61: Open duration histograms and their fits (formula 6) for ten combined patches
Events were recorded at 30 nM 5-HT and -80 mV. Plotted are the counts of openings and their durations all clusters. **Left**: Fit with two exponential components. **Right**: Fit with three exponential components. Chi² improves slightly when applying three components and the left as well as the right shoulder of the right peak of the histogram are covered better. Events were normalized so that each recording has the same weight.

Figure 62 and Figure 61 show fitted open duration histograms for ten combined 30 nM 5-HT recordings. When openings of 2+ clusters are included, the histogram can be fitted to three exponential components with the time constants 0.21, 4.3 and 16 ms. The duration histogram for events in 5+ clusters was fitted with only two components of 0.26 and 12 ms. Values and Duration histograms for the other applied serotonin concentrations can be found in the supporting material (Table 21 - Table 23).

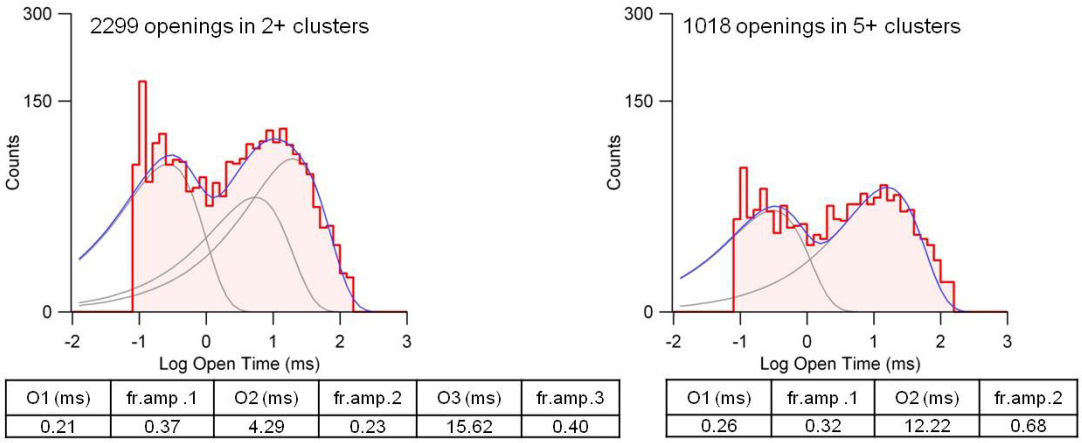

O1 (ms)	fr.amp .1	O2 (ms)	fr.amp.2	O3 (ms)	fr.amp.3
0.21	0.37	4.29	0.23	15.62	0.40

O1 (ms)	fr.amp .1	O2 (ms)	fr.amp.2
0.26	0.32	12.22	0.68

Figure 62: Open duration histograms for different types of clusters of ten combined patches.
Events were recorded at 30 nM 5-HT and -80 mV. Plotted are the counts of openings and their durations in 2+ clusters (left) and in 5+ clusters (right).Tables list the values of the exponential fits (grey lines). Events were normalized so that each recording has the same weight.

Figure 63 plots the fractions of the three open components at different 5-HT concentrations to their durations. The tables under each plot list weighted averages of duration components for each applied serotonin concentration, which were calculated with the formula

$$O(avg) = \frac{fr.amp._1 * O_1 + fr.amp._2 * O_2 + fr.amp._3 * O_3}{n(O)} \quad (19).$$

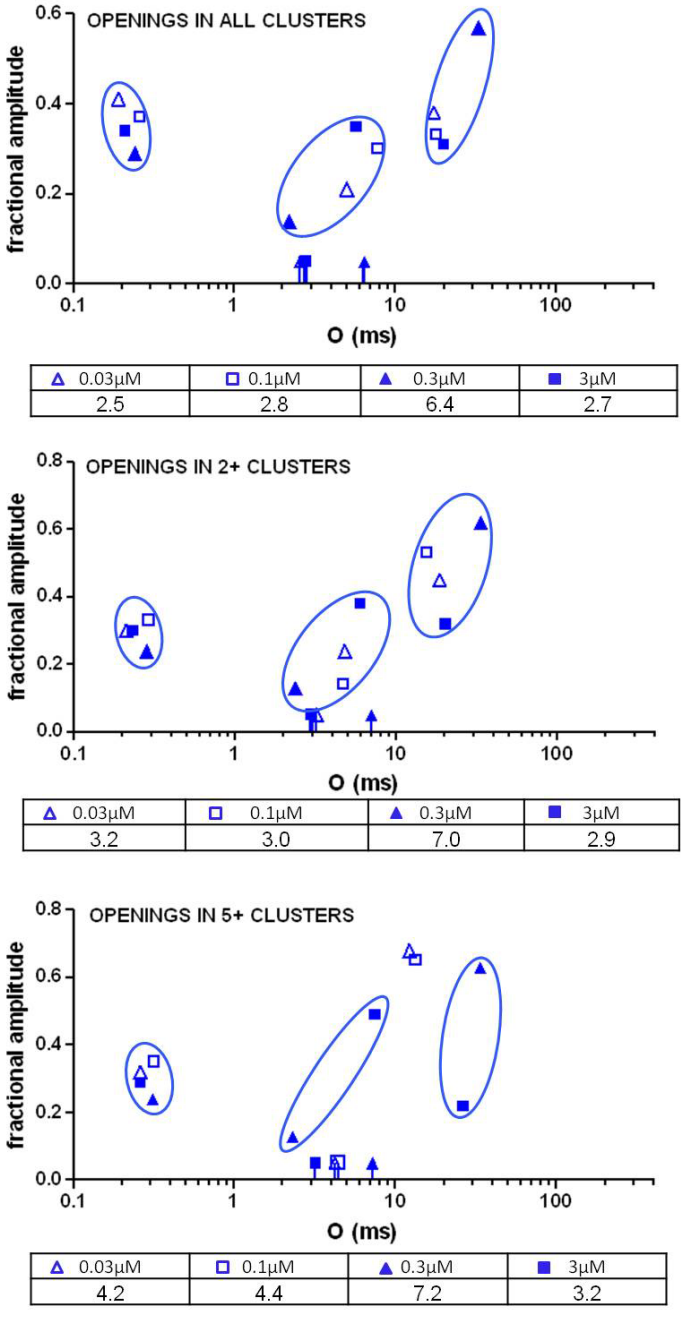

Figure 63: Open durations and their relative amplitudes for different types of clusters at different 5-HT concentrations.
Circles mark the different components, symbols connected to the time axis represent the weighted average durations (ms) of clusters, which are listed under each figure.
t_{crit} = 30 ms
Fractional amplitudes and cluster components can be found in Table 21 - Table 23 in the attachment.

The fraction of short openings with 30 nM 5-HT decreases when individual openings are excluded. With 100 nM 5-HT the fraction of intermediate openings

decreases. Thus one can assume that at the lowest serotonin concentration individual openings are mostly short, at 100 nM serotonin they are mostly of the intermediate component. For higher concentrations there doesn't seem to be a certain component that is represented in individual openings.

Interestingly, at the low serotonin concentrations intermediate open durations within 5+ clusters became so sparse, that the respective component is not included into the istogram fits anymore. Open duration histograms for combined patches of 30 nM and 100 nM recordings are fit with only two exponential components.

Weighted averages of open durations are very similar between different serotonin concentrations. Only at 0.3 µM, the overall open duration is longer (6.4 ms for all openings). Between the different types of clusters a tendency can be seen that clusters with more openings contain slightly longer openings.

Open Probability and Number of Openings within Clusters

The number of openings before a channel closes and leaves the flickering mode into a more stable closed mode was also determined. Table 9 lists the number of openings in all clusters and in clusters longer then $t_{crit\ long}$ under different serotonin concentrations.

The number of openings within clusters induced by 0.03 µM 5-HT is significantly lower (1.96 ± 0.39) than at higher concentrations. In clusters longer than critical time between the shortest and the second to shortest component a median of 3.17 ± 1.13 clusters are found under 30 nM 5-HT, which is not statistically significant, but shows a clear tendency towards fewer openings as well. This is due to the appearance of a very short cluster component at 30 nM 5-HT. Because $t_{crit\ long}$ is not a fixed number, but is adjusted with every recording, the long cluster component in 30 nM recordings corresponds to the brief cluster component in recordings of higher serotonin concentrations.

Table 9: Number of openings within clusters for the human 5-HT_{3A}QDA channels at different 5-HT concentrations.
Listed are medians with their standard deviations. One way ANOVA test implies significant differences ($p = 0.0004$), following Tukey's Multiple Comparison Test implies significant differences, which are indicated ** $p < 0.005$.

[5-HT] (µM)	3	0.3	0.1	0.03	mean	SD
n patches (n events)	7 (4469)	6 (16291)	4 (12687)	9 (3406)		
# openings in all clusters	4.0	4.1	3.3	2.0	3.3	1.0
SD	1.4	1.7	0.6	0.4		
			* *			
		* *				
openings in clusters > $t_{crit\ long}$	7.5	6.9	5.9	3.2	5.8	1.9
SD	4.6	3.4	2.0	1.1		

Figure 64 plots the relation of the number of openings in clusters to the median cluster duration under 30 nM 5-HT. Each point resembles one patch.

The Spearman correlation test indicates weak correlation between number of openings in a cluster and cluster duration ($r = 0.32$) and the linear regression shows no significant slope.

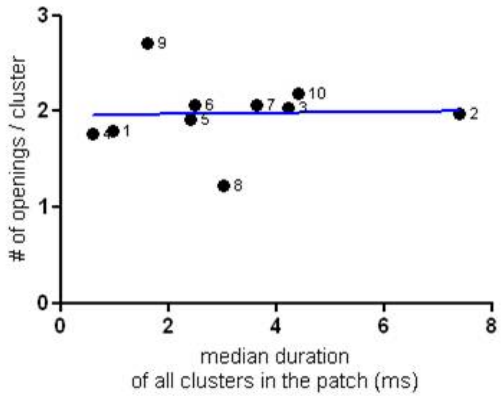

Figure 64: Cluster durations of ten 30 nM recordings in relation to the number of openings in all clusters.
Blue line shows the linear regression, with a non significant slope of 0.006. Spearman correlation coefficient r=0.32.

Do changes in open and closed durations in clusters result in changes in open probability in these clusters? The open probability (p_{open}) was determined by calculating the mean fraction of time that the channel is open within a cluster. As can be seen in the plots of the frequency of open probabilities in clusters for eight individual 30 nM recordings in Figure 65, brief clusters as well as long clusters mostly had a high open probability > 80 %. Only in one out of the shown eight patches, frequent clusters of lower open probabilities were recorded.

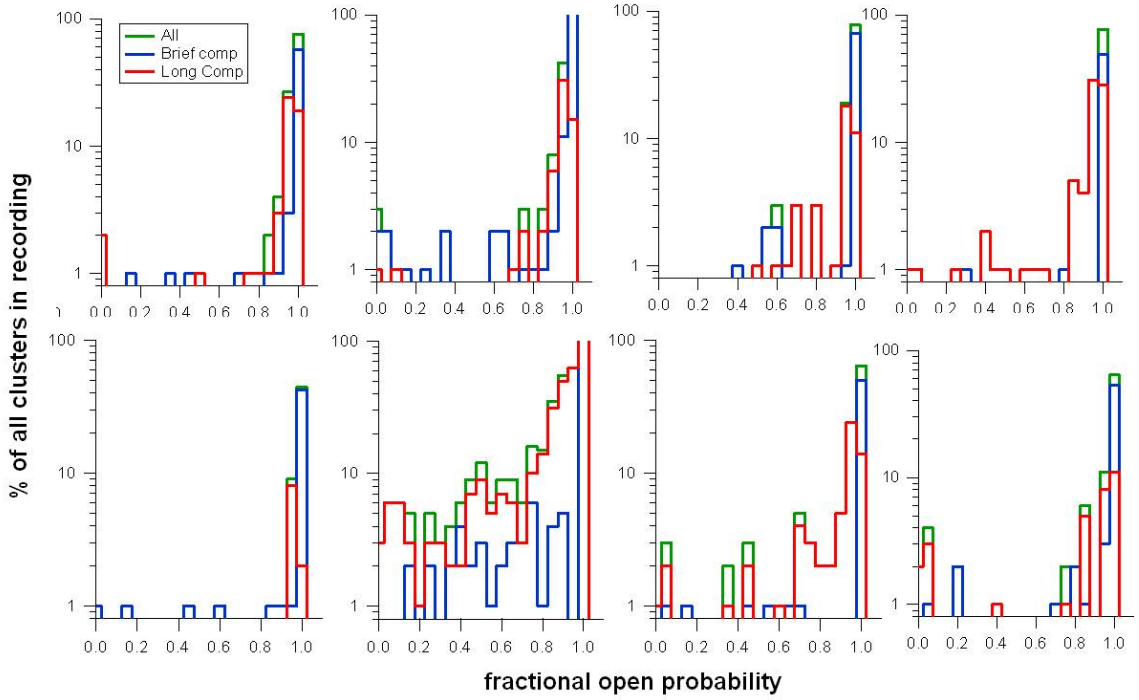

Figure 65: Fractional open probabilities within clusters for eight individual patches of 5-HT_{3A}QDA transfected cells.
Patch pipettes were filled with 30 nM 5-HT. Long cluster components were longer than $t_{crit\ long.}$, brief cluster components shorter than $t_{crit\ long}$.

Table 10 lists the median open probabilities and median number of openings in clusters at different serotonin concentrations including their 25 % and 75 % percentiles. Indicated statistically significant differences are results of Dunn's Multiple Comparison Tests.

Table 10: Medians of open probabilities and number of openings in clusters under different serotonin concentrations.
Smaller numbers before and after the median are 25% and 75% percentiles.
[x] n = 6 patches, * p < 0.05, ** p < 0.01 (Dunn's Multiple Comparison Tests)

[5-HT]	30nM	100nM	300nM	3µM
n patches	10	4	6	7
p_{open} total (%)	0.170 0.257 0.555	0.550 2.225 5.006	0.571 0.844 3.250	0.380 0.675 [x] 0.924
p_{open} all clusters	0.908 0.940 0.950	0.878 0.907 0.925	0.822 0.902 0.949	0.860 0.876 0.907
# openings in all clusters	1.8 2.0 2.1	2.7 2.9 3.8	3.1 3.7 4.8	2.9 4.5 5.2
p_{open} long clusters	0.870 0.930 0.950	0.836 0.882 0.906	0.597 0.918 0.964	0.809 0.873 0.894
# openings in long clusters	2.9 4.1 5.3	5.5 7.9 8.6	5.1 11.2 11.4	6.2 8.9 11.0

Open probabilities in complete recordings (p_{open} total) tend to be lower with lower serotonin concentrations, but due to wide ranges of 25% and 75% percentiles do not result in statistical significance. Interestingly open probability within clusters shows

opposite tendencies: it becomes larger with lower serotonin concentrations. For clusters obtained at 30 nM and 3 µM serotonin, this results in a statistical difference.

The number of openings in clusters increases with concentration, although only the lowest number of openings at 30 nM is statistically significant. The 25% percentiles for the number of openings show a small range (2.7-3.1 in all clusters), but the high percentile increases with concentration. At higher 5-HT concentrations, more events per cluster are possible. Clusters with only a few – or even one – opening become rare, but still infrequently occur.

The significant differences between serotonin concentrations that can be found for the number of openings and the open probability in all clusters can be explained by the high fraction of individual openings at 30nM (Figure 50). Many individual openings decrease the median numbers of openings in clusters. Since the open probability for each individual openings cluster is 100 %, the open probability in clusters at 30 nM 5-HT is even higher (94 %) than at the other concentrations (88-91%).

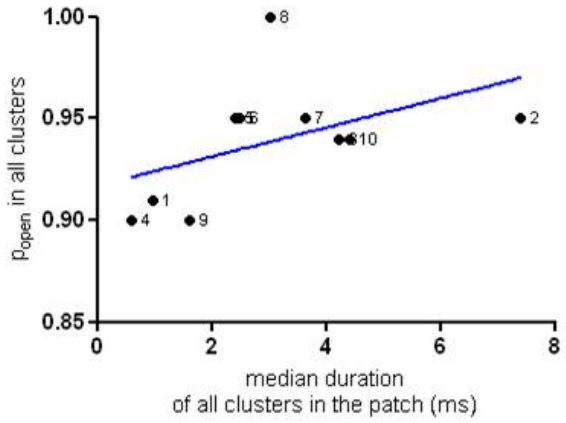

Figure 66: Cluster durations of ten 30 nM recordings in relation to the fractional open probability in clusters.
Blue line shows the linear regression with a slope of 0.007. Spearman correlation coefficient r=0.52. Each number represents one patch.

Figure 66 plots the relation of open probability in 2+ clusters to the cluster duration under 30 nM 5-HT. Each point resembles one patch. The Spearman correlation test results in a tendency towards positive correlation (r = 0.52) and the linear regression shows a non significant slope of 0.7% per ms cluster duration.

Beginning and Ending of a Cluster

To evaluate if clusters are preferably started or ended by a certain component of open durations, the fractions of the first and last openings in clusters were compared with the fractions of all events of clusters. Figure 67 displays the composition of clusters by the fractions of the three different open components. Grey bars represent 1st and last openings in clusters, black bars represent all openings in clusters. The fractions for none of the three components did differ between the positions of openings. Complete clusters as well as the first and last events in clusters are composed by 41 % to 58 % long openings.

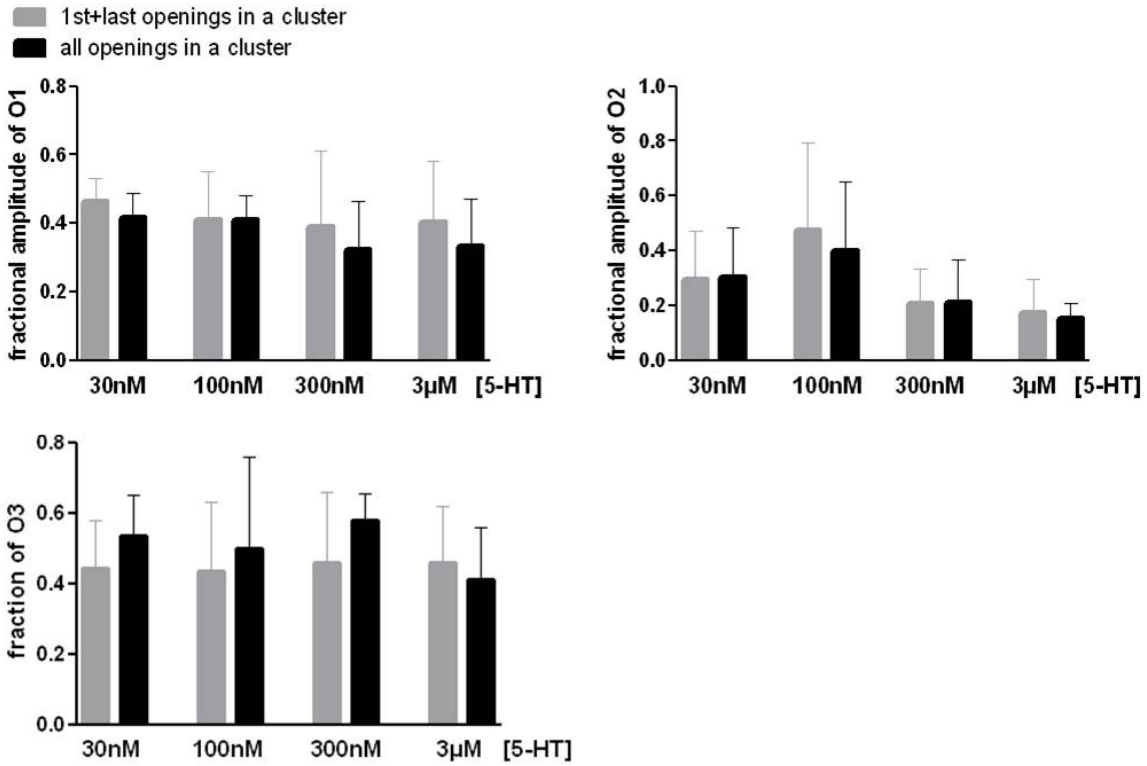

[5-HT]	30nM (10 patches)		100nM (4 patches)		300nM (6 patches)		3µM (7 patches)	
	1st+last	all	1st+last	all	1st+last	all	1st+last	all
O1	0.46 ± 0.07	0.42 ± 0.07	0.41 ± 0.14	0.41 ± 0.07	0.39 ± 0.22	0.33 ± 0.14	0.40 ± 0.18	0.34 ± 0.13
O2	0.30 ± 0.17	0.30 ± 0.18	0.48 ± 0.32	0.40 ± 0.25	0.21 ± 0.12	0.21 ± 0.15	0.18 ± 0.12	0.15 ± 0.05
O3	0.41 ± 0.15	0.46 ± 0.16	0.46 ± 0.20	0.58 ± 0.08	0.44 ± 0.19	0.50 ± 0.26	0.44 ± 0.14	0.53 ± 0.12

Figure 67: Fractions of the three open components that start or end clusters (first + last) vs. fractions of longest open components of all events in all clusters at different 5-HT concentrations.
5-HT_{3A}QDA transfected HEK293 cells were patched and clamped to -80 mV. n patches = 4-10 per concentration. The fractions were evaluated for each patch and then averaged. Bars represent SD. There were no significant differences found between any fractions of 1st + last openings of a cluster and all openings of clusters.

Closings within Clusters

Combined closed time histograms of experiments under different 5-HT concentrations suggest three closed components within clusters. Figure 68 shows fitted closed duration histograms for ten combined 30 nM 5-HT recordings. When all clusters are plotted, the histogram can be fitted to seven exponential components, the first three with the time constants 0.17, 0.99 and 5.80 ms. The three components within 2+ and 5+ clusters had similar time constants. Values and Duration histograms for the other applied serotonin concentrations can be found in the attachment (Table 21 - Table 23).

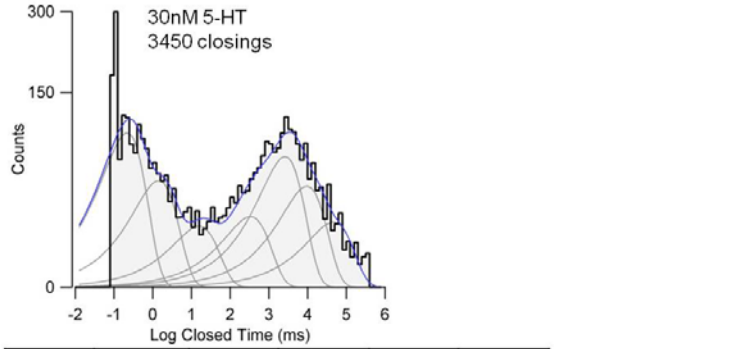

C1 (ms)	fr.amp .1	C2 (ms)	fr.amp.2	C3 (ms)	fr.amp.3
0.17	0.31	0.99	0.14	5.80	0.05

C4 (ms)	fr.amp .4	C5 (ms)	fr.amp.5	C6 (ms)	fr.amp.6	C7 (ms)	fr.amp.7
57.37	0.03	456.46	0.07	2802.33	0.27	18338.10	0.12

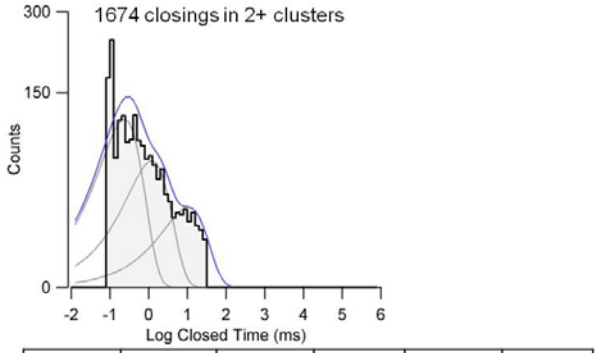

C1 (ms)	fr.amp .1	C2 (ms)	fr.amp.2	C3 (ms)	fr.amp.3
0.17	0.61	0.98	0.27	7.77	0.12

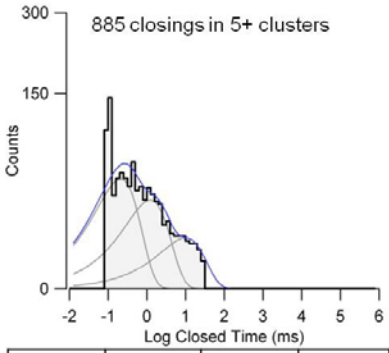

C1 (ms)	fr.amp .1	C2 (ms)	fr.amp.2	C3 (ms)	fr.amp.3
0.16	0.58	0.95	0.32	7.46	0.10

Figure 68: Closed duration histograms for ten combined patches
Events were recorded at 30 nM 5-HT and -80 mV. Plotted are the counts of events and their durations including all clusters of the recording (top), 2+ clusters (bottom left) and 5+ clusters (bottom right).Tables list the values of the exponential fits (grey lines). Events were normalized so that each recording has the same weight.

Figure 69 plots the fractions of the three closed components at different 5-HT concentrations against their durations. The tables under each plot list weighted averages of duration components for each applied serotonin concentration, which were calculated with the formula

$$C(avg) = \frac{fr.amp._1 * C_1 + fr.amp._2 * C_2 + fr.amp._3 * C_3}{n\,(C)} \quad (20).$$

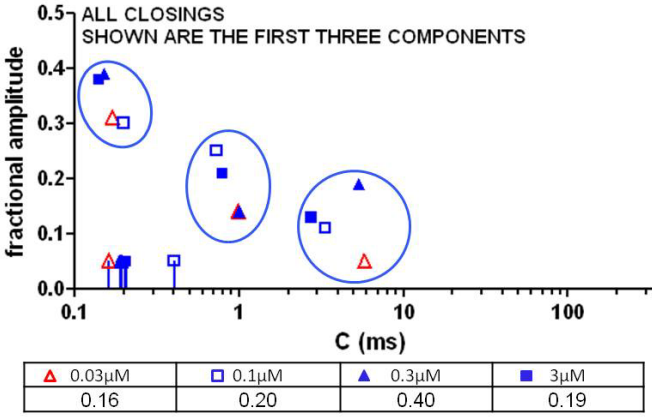

0.03µM	0.1µM	0.3µM	3µM
0.16	0.20	0.40	0.19

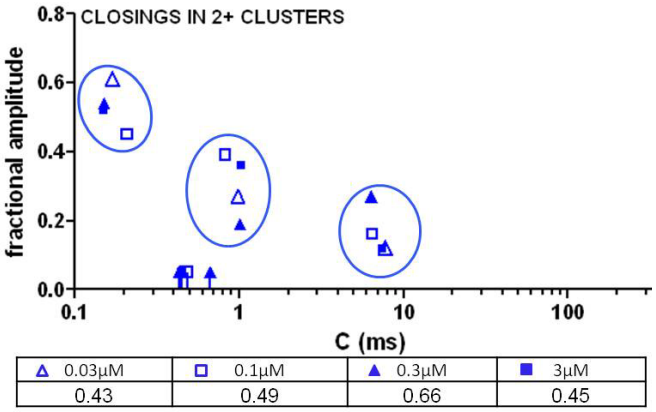

0.03µM	0.1µM	0.3µM	3µM
0.43	0.49	0.66	0.45

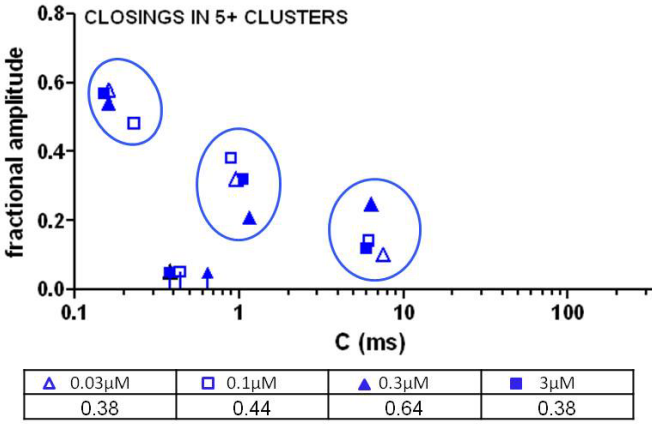

0.03µM	0.1µM	0.3µM	3µM
0.38	0.44	0.64	0.38

Averaged closed time durations at most different 5-HT concentrations did not differ. Only for 0.3 µM 5-HT, closings are longer with a weighted average for closed durations of 0.4 ms in the complete recording and 0.66 and 0.64 ms in 2+ and 5+

clusters. Also between different types of clusters neither time constants nor fractions of components do change. Different cluster types at different agonist concentrations are composed of similar closings.

To evaluate how strongly closed duration in clusters influences the overall ion flux during a cluster, fractional open probabilities in 2+ clusters of individual 30 nM recordings were plotted to the respective closed durations (Figure 70).

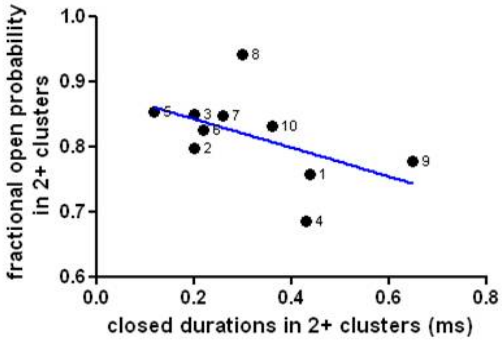

Figure 70: Fractional open probabilities in 2+ clusters of ten 30 nM recordings in relation to the closed durations (ms) in 2+ clusters.
Blue line shows the linear regression with a slope of -0.22, which is not significant. Spearman correlation coefficient r=-0.61. Each number represents one patch.

A tendency towards lower open probabilities at longer closed durations is notable, which results in a negative correlation and a Spearman correlation coefficient r of -0.61. The linear regression is not significant.

Closings Out of Clusters

When closings out of clusters depend only on serotonin concentration and on the number of channels in the patch, the distribution of the closings longer than the ones in the third component should be random. Surprisingly, these long closing components are very reproducible between the combined histograms for different serotonin concentrations. Table 11 lists the closed components and their amplitudes for combined closed-duration histograms at 30nM – 3µM serotonin.

The combined histogram for 300 nM seems to miss the 5^{th} component. But components six and seven can be aligned with respective components for the other concentrations again.

Table 11: Closed components (ms) and their fractions for different serotonin concentrations. Components and fractions result from combined closed duration histograms and their fits for each serotonin concentration before selecting clusters.

	tau comp1	fr.amp comp1	tau comp2	fr.amp comp 2	tau comp3	fr.amp comp 3	tau comp4	fr.amp comp 4	tau comp5	fr.amp comp 5	tau comp6	fr.amp comp 6	tau comp7	fr.amp comp 7	tau comp8	fr.amp comp 8	# events
30nM	0.17	0.31	0.99	0.14	5.8	0.05	57	0.03	456	0.07	2802	0.27	18338	0.12			3450
100nM	0.20	0.30	0.73	0.25	3.4	0.11	25	0.04	276	0.09	1674	0.14	14162	0.07			12627
300nM	0.15	0.39	1.0	0.14	5.3	0.19	74	0.08			1638	0.09	14214	0.08	109826	0.02	16294
3µM	0.14	0.38	0.79	0.21	2.7	0.13	44	0.05	252	0.07	1991	0.09	10529	0.14			4644

5-HT$_{3A}$ QDA – With Propofol

Propofol (2,6-diisopropylphenol) is the most commonly used intravenous anesthetic. Because of its simple symmetric structure (Figure 71), it is a good model molecule to study mechanisms on ligand gated ion channels. Propofol has been used in extended previous macroscopic studies on 5-HT$_{3A}$ (Barann et al., 2008), so that its effects on the wild type channel are well known. This makes propofol an appropriate substance for a first pharmacological study with 5-HT$_{3A}$QDA. When applied using the equilibrium application (++) protocol, 18µM propofol inhibited peak 5-HT$_{3A}$ currents by 50% and accelerated current decay. Propofol was less effective at inhibiting current in the open channel application (-+) protocol. We used 18µM propofol throughout this thesis.

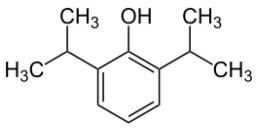

Figure 71: chemical structure of propofol

Excised Outside-Out Patches

Figure 72 shows current traces obtained using two different propofol application protocols on two patches with 5-HT$_{3A}$QDA receptors. During open channel (-+) experiments, 18µM propofol was applied simultaneously with 5-HT. Equilibrium (++) experiments were conducted by exposing the patch to propofol for one minute before a 5-HT pulse is added. Average values from control and wash out trace were used as control reference to compensate for rundown.

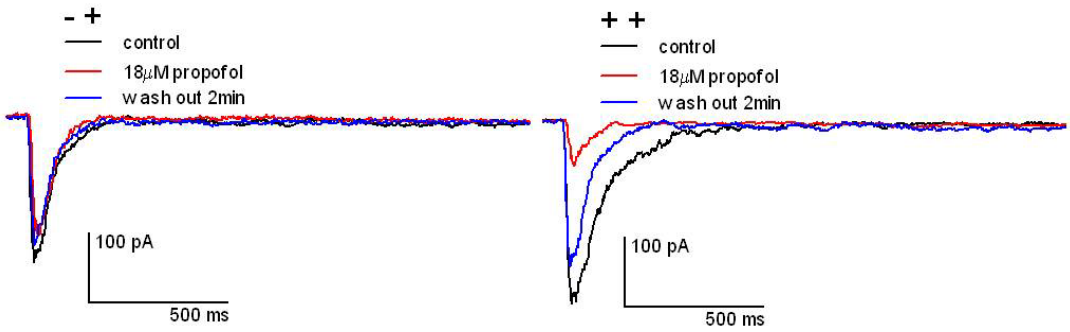

Figure 72: Example of macroscopic 5-HT$_{3A}$QDA currents exposed to 18 µM propofol. Left: open channel application. Right: equilibrium application. V=-100 mV.

Equilibrium and open channel propofol application was performed on four individual patches. Averaged effects on peak amplitude and kinetics ± SD are listed in Table 12. The effects are similar to those seen with 5-HT_{3A} receptors. There was a significant reduction in the peak current in both the -+ (to 84.3%, p=0.004) and ++ (to 45.4%, p=0.001) application protocols. Inhibition was significantly greater in the ++ application protocol (p=0.004). The decay phase of 5-HT induced currents gets faster when propofol is applied, τ_{OFF} is reduced by 56 % (-+, p=0.02) or 50.5 % (++, p=0.02). The onset phase does not change significantly, although a trend to longer onsets can be seen. These changes in macroscopic kinetics correlate with a prolongation of the onset currents and a speeding up of decay of macroscopic 5-HT_{3A} currents that was reported previously (Barann et al., 2008).

Table 12: effects of open channel (-+) and equilibrium (++) application of 18 µM propofol on macroscopic currents of 5-HT_{3A}QDA channels.
Paired two tailed t-tests. Indicated significance: ** p ≤ 0.001, * p ≤ 0.005

condition		% of control	SD	n (=patches)
peak (pA)	-+	84.3 **	3.8	4
	++	45.5 **	8.7	4
τ_{ON}	-+	130.3	51.8	4
	++	111.8	19.4	4
τ_{OFF}	-+	56.0 *	19.6	4
	++	50.5 *	21.0	4

While the effect of 18 µM propofol on the kinetics 5-HT_{3A}QDA currents is similarly strong for both application protocols, equilibrium application induced a stronger peak amplitude reduction than open channel application did.

Cell-Attached Patches

Cell attached patches of 5-HT_{3A}QDA transfected cells were made with patch pipettes filled with 18 µM propofol and 100 nM 5-HT and were clamped to -80 mV. The concentration of propofol used here resembles the IC_{50} of propofol at equilibrium application to outside out patches of expressing 5-HT_{3A} receptors (Barann et al., 2008) and to outside out patches of expressing 5-HT_{3A}QDA receptors (above).

The total open probability in complete recordings did not differ significantly, but did show tendencies towards lower open probabiloities when propofol was applied.

Table 13: Total open probability in cell attached recordings with 100 nM 5-HT with and without 18 µM propofol.
Student's t-test does show no statistical significance.

25%percentile median 75%percentile	p_{open} total %	n (patches)
100nM 5-HT	0.55 2.2 5.0	4
100nM 5-HT + 18µM propofol	0.12 1.8 3.8	4

Durations of single channel events were analyzed by fitting duration histograms as described before. The resulting time constants and frequencies are summarized in the following sections. Table 21 to Table 23 with the results can be found in the Supporting Material.

Current Amplitudes

The mean single channel current amplitude when both 18 µM propofol and 100 nM 5-HT were present in the patch pipettes was -2.68 pA ± 0.21 pA (SD). This is not significantly different from that found for 100 nM 5-HT alone (Table 12). This corresponds to a conductance of 33.5 pS.

Table 14: mean single channel amplitudes (pA) of channel openings in 5-HT_{3A}QDA transfected cell patches.
Patch pipettes were filled with 100 nM 5-HT ± 18 µM propofol. Patches were clamped to -80 mV.

condition	**100nM 5-HT**	**+ 18 µM propofol**
n patches (n events)	4 (12687)	4 (8390)
channel amplitude (pA)	-2.58	-2.82
	-2.70	-2.81
	-2.79	-2.68
	-2.38	-2.38
average	-2.61	-2.68
± SD	0.18	0.21

Duration Histograms

Closed duration histograms for all events in the combined four patches with propofol were fitted with five components, open and cluster duration histograms (selected by t_{crit} 30ms) with three components. Figure 73 shows the respective histograms, time constants (ms) and their fractional amplitudes are listed for each component under the figure.

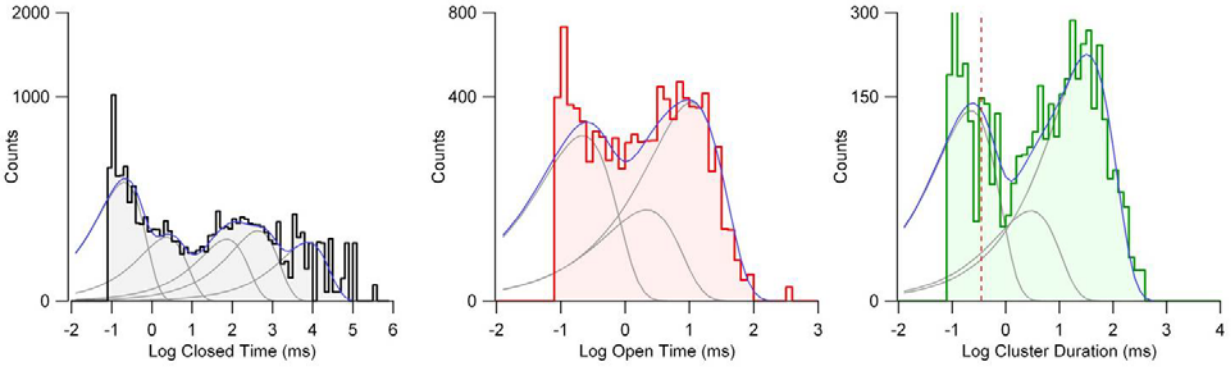

100 nM 5-HT + 18 µM propofol (4 patches)

	tau comp1	fr.amp comp1	tau comp2	fr.amp comp2	tau comp3	fr.amp comp3	tau comp4	fr.amp comp4	tau comp5	fr.amp comp5	tau comp6	fr.amp comp6	tau comp7	fr.amp comp7	# events
C	0.16	0.47	1.9	0.13	59	0.13	344	0.04	5927	0.03					8390
O	0.17	0.37	1.7	0.11	8.5	0.52									8390
Cs	0.18	0.34	2.3	0.08	26	0.58									4410

Figure 73 : Closed, open and cluster duration histograms of complete recordings with 100 nM 5-HT and 18 µM propofol.
t_{crit} was 30 ms, time constants and fractional amplitudes of component fits (formula 6) are listed in the table under the figure.

Closed time histograms for propofol differed from controls in several ways. With propfofol, there were only five closed components compared to seven under control conditions. The time constants of these components are further apart than in the controls (Figure 46). These changes, especially in the third closed component, suggest that the critical closed time for cluster selection may differ from the control value.

Critical Time Between Clusters

Figure 74 shows the aligned time constants of the closed components for individual patches with and without propofol along the averaged closed components of all combined control histograms (colored dotted lines). The time constant of the fastest component is nearly the same as the control average of 0.17 ms (black). The second component has a somewhat longer duration than the one under control conditions (green). With propofol, there is no component that corresponds to the 5 ms control closed time (blue). The time constant of the next component seen with propofol resembles the fourth one in control experiments (pink, average 50 ms) and therefore will be classified as ‘fourth’ component in the following discussion.

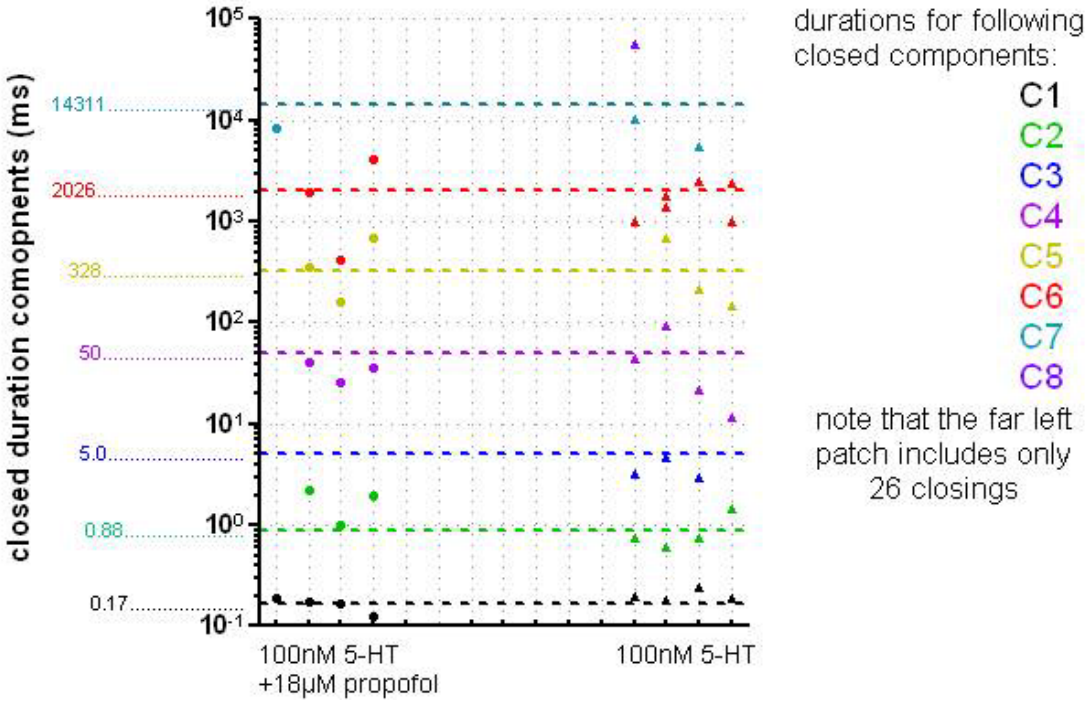

Figure 74: Aligning closed components (ms) for complete individual patches with and without propofol.
Closed components for individual patches under 100 nM control and under 100 nM 5-HT + 18 µM propofol were aligned along the averaged closed components of all combined control histograms (colored dotted lines).

In the absence of additional data, the most parsimonious choice for critical time is 30 ms, the same as with control. This choice does not truncate the two fastest closed components and it produces QMCs that are consistent with the effect of propofol on the desensitization of macroscopic currents (page 98: Quasi Macroscopic Currents).

Event Durations

Figure 75 shows scattergram displays of the results of fitting event duration histograms. Each point shows the amplitude (y-axis) and time constant (x-axis) of each histogram component. The blue squares correspond to patches with 100 nM 5-HT alone; the red squares correspond to patches with 100 nM 5-HT and 18 µM propofol. A line is drawn between the corresponding blue and red squares to indicate clearly the effects of propofol. The symbols at the bottom of each scattergram indicate the weighted averages and the table below each scattergram presents these averages. The weighted average durations were compared using Dunn's Multiple Comparison Tests, which always resulted in highly (*** $P < 0.001$) significant differences between control and propofol.

Closed time duration histograms within 2+ clusters of channels exposed to 18 µM propofol were fitted with two components, the second one having an intermediate duration between the second and third control components. Propofol increased the fraction of short closings. Overall, this results in a small decrease in the weighted average of closed durations. This effect is more pronounced within 2+ and 5+ clusters.

Propofol did not significantly change the fraction or duration of the briefest open component. Propofol reduced the intermediate and long open durations by a factor of 2.9 and 2.0 respectively and increased the fraction of long openings. The net result was to decrease the weighted average of open components to 57 %. Changes in open kinetics result in a decrease of the weighted average open durations to 60 % of control in 2+ clusters and to 39 % of control in 5+ clusters.

Cluster duration histograms of patches exposed to 100 nM 5-HT and 18 µM propofol were fitted with three components, just as histograms of patches without any propofol. Median cluster durations are significantly reduced to about a third. Additionally, the fraction of the intermediate cluster component is reduced to less than 0.1, and thus is below the threshold we set for considering a component to be significant.

Figure 75: Event durations and their fractional amplitudes at different [5-HT] ± 18 µM propofol. The symbols connected to the time axis indicate the weighted averages and the table below each scattergram presents these averages. Comparing the control with the respective propofol duration medians by Dunn's Multiple Comparison test always resulted in highly significant differences (*** $p < 0.001$). Time constants and their fractions that the plots are based on can be found in Table 21 - Table 23 in the attachment. t_{crit} was 30 ms.

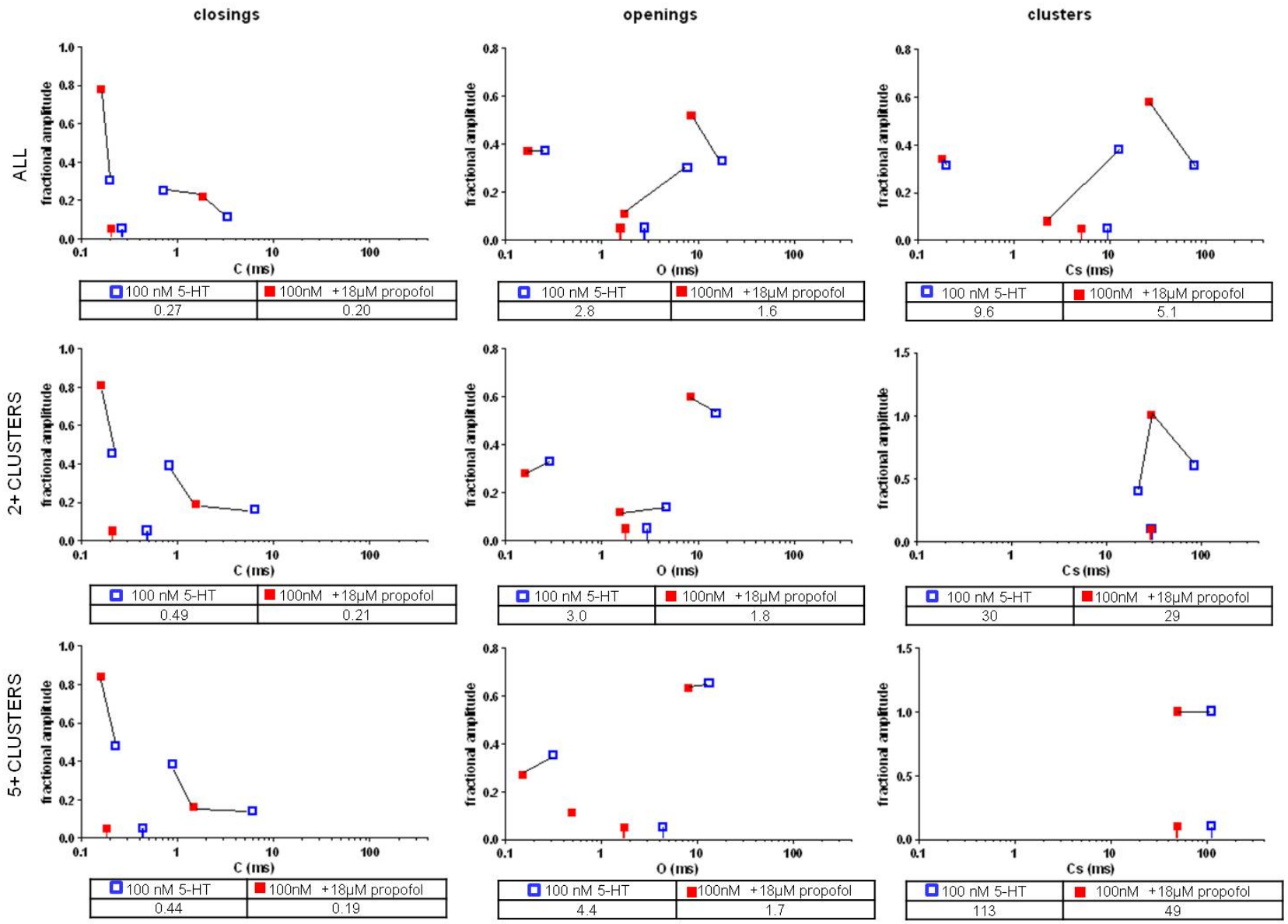
closings
openings
clusters
ALL
2+ CLUSTERS
5+ CLUSTERS
fractional amplitude
C (ms)
O (ms)
Cs (ms)
100 nM 5-HT
100nM +18µM propofol
0.27
0.20
2.8
1.6
9.6
5.1
0.49
0.21
3.0
1.8
30
29
0.44
0.19
4.4
1.7
113
49

Number of Openings and Open Probability within Clusters

Neither the open probabilities nor the number of openings within clusters were influenced significantly by adding 18 µM propofol to patch pipettes. Clusters recorded including propofol in the recording pipette contain 2.9 openings on average; the longest ones contain 4.4 openings on average. The open probability within clusters remains high with an average of 0.87 in all and 0.82 in the longest clusters.

Table 15: number of openings and open probabilities within clusters of 5-HT_{3A}QDA single channel recordings with and without 18 µM propofol.
Student's *t*-tests showed no significant differences. 'Clusters' excludes individual openings. 'Long clusters' are longer than the critical time between the second and the third cluster component.

	openings per cluster		openings per cluster longer than t_{crit} to longest comp	
	0.1 µM 5-HT	+ 18 µM propofol	0.1 µM 5-HT	+ 18 µM propofol
n patches	4	3	4	3
mean	3.3	2.9	5.9	4.4
SD	0.6	1.1	2.0	1.9

	open probability in clusters		open probability in clusters longer than t_{crit} to longest comp	
	0.1 µM 5-HT	+ 18 µM propofol	0.1 µM 5-HT	+ 18 µM propofol
n patches	4	3	4	3
mean	0.90	0.87	0.87	0.82
SD	0.03	0.01	0.04	0.01

This means that dispite the many effects of propofol on single channel kinetics (Figure 75), the net ion flux does within clusters not seem to change.

Quasi Macroscopic Currents

Quasi macroscopic currents show how the changes in single channel kinetics (Figure 75) are predicted to effect macroscopic current. Figure 76 shows the QMC formed by summing and aligning all clusters longer than tcrit long (left) and the QMC formed by summing and aligning all clusters (right) of one measurement recorded with 100 nM 5-HT and 18 µM propofol in the recording pipette. The predicted decay (red), which is superimposed to the QMC of all clusters, is calculated from a three exponential decay function, using the three cluster components that result from the corresponding cluster histogram fit. In this case these components were 0.15, 4.8 and 26 ms.

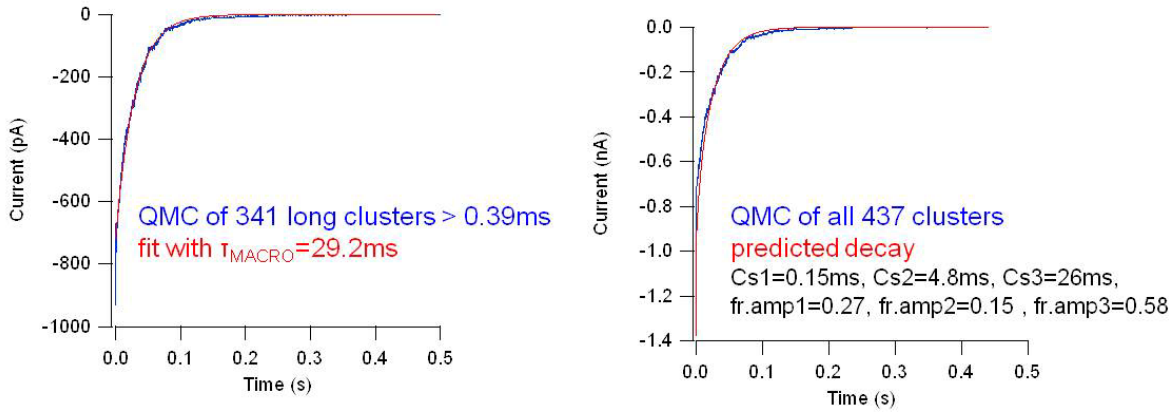

	100nM 5-HT	100nM 5-HT + 18µM propofol
# patches	4	3
25% percentile median 75% percentile	25.6 74.6 106	11.0 28.8 29.2

Figure 76: Quasi Macroscopic Currents of recordings at 100 nM 5-HT + 18 µM propofol.
Left figure: Aligning and summing clusters of one recording longer than the critical time between the first and the second cluster component (blue) results in a QMC that can be fitted by a single exponential with a time constant of 29.2 ms (red). Right figure: Aligning and summing up all clusters (blue) resembles the predicted decay (red).

The table beneath the figure compares the median of fitted QMC decays of three propofol recordings with the median of fitted QMC decays of four control recordings. The magnitude of the effect of propofol on the QMC decay is similar to the magnitude of the effect on 5+ cluster durations. In both cases time constants shorten to 39 % of control. This correlates with the shortening of the decay of macroscopic currents of 5-HT_{3A}QDA channels to half, shown in Table 12.

Being able to reproduce macroscopic currents supports the choice of critical time of 30 ms between clusters.

5-HT_{3A}QDA - With Phenol

Phenol (Figure 77) has the structure of propofol with the two isopropyl groups removed. Thus, it might be expected to exhibit some, but not all, of the effects of propofol itself on 5-HT_{3A} receptors. Previous studies on wild type human 5-HT_{3A} receptors showed that the effects of phenol on macroscopic currents were dependent on the agonist concentration (Barann et al., 2008). Phenol applied at equilibrium, inhibited the peak currents elicited by 30 µM 5-HT with an IC_{50} of 1.6 mM. However, when phenol and 5-HT were applied simultaneously, 1 mM phenol enhanced currents elicited by application of 3 µM 5-HT but did not affect the amplitude of currents elicited by 30 µM 5-HT. 3 mM phenol also slowed current decay. Therefore, different 5-HT concentrations were used in this study as well. Based on the previous studies, the concentration of phenol used here, 3 mM, might be expected to show evidence for both the inhibitory and potentiating effects of phenol.

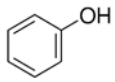

Figure 77: chemical structure of phenol

Cell Attached Patches

Cell attached patches were formed of 5-HT_{3A}QDA transfected cells with patch pipettes containing either 30 nM 5-HT (4 patches) or 3 µM 5-HT (6 patches) with 3 mM phenol. These data were compared to the data previously obtained for 30 nM and 3 µM 5-HT in the absence of any substances.

It was immediately apparent that phenol had a potentiating effect on the channel. Table 16 lists open probabilities for combined recordings with and without phenol. Recordings obtained in the presence of 3 mM phenol showed higher activity levels. Compared to control recordings, the total open probability increased 9 fold (30 nM 5-HT) and 15 fold (3 µM 5-HT).

Table 16: Open probabilities of complete recordings including their 25 % and 75 % percentiles for combined recordings with 30 nM and 3 µM with and without 3 mM phenol.
Student's t-tests result in statistically significant differences between phenol recordings and their respective controls. * $p \leq 0.05$, *** $p \leq 0.001$.

condition	3 µM 5-HT	3 µM 5-HT + 3 mM phenol	30 nM 5-HT + 3 mM phenol	30 nM 5-HT
n patches (n events)	7 (4469)	6 (23059)	4 (2349)	10 (3406)
25% percentile median 75% percentile	0.38 0.68 0.92	1.9 10.4 29.5 *	1.5 2.4 4.3 ***	0.17 0.26 0.56

As a result of this high activity, many segments of single channel recordings had to be deleted due to the presence of double and triple events. Figure 78 illustrates the high activity level of one representative phenol recording by plotting open times, amplitudes and occurrence of all events over time. Before clusters with multiple channel openings were deleted for further analysis (top row), the recording contained 22101 single channel openings and 27488 multiple (double + triple) channel openings. Most of them occurred during the first 400 s of the 1400 s recording. The peaks that indicate different number of open channel levels are clearly separated in the amplitude versus duration plot as well as in the amplitude histogram.

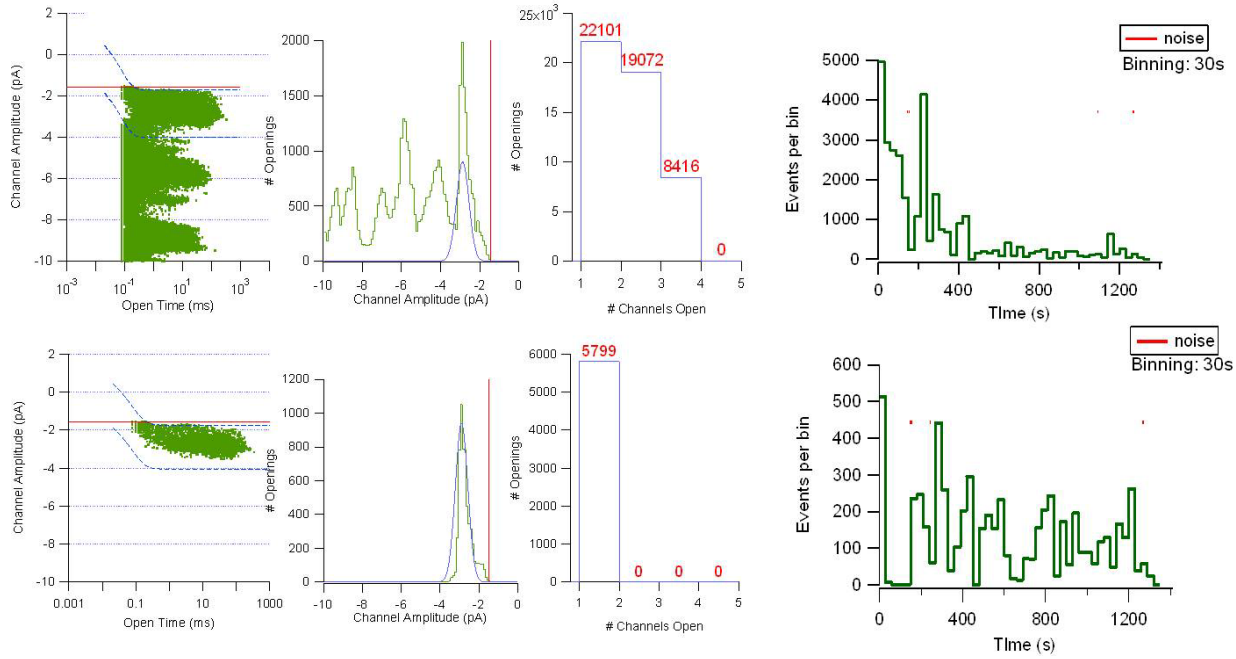

Figure 78: Activity of one complete cell attached recording with 3 µM 5-HT + 3 mM phenol in the recording pipette.
Graphs as they are depicted by different IGOR routines. Top: before, Bottom: after deleting clusters with multiple channel openings. Plotted are (from left to right) open durations and amplitudes for every individual opening with indicated resolution threshold (red line) and amplitude distortion (blue dotted line) due to filtering, amplitude histogram with resolution threshold (red line) and Gaussian fit (blue line), number of single, double and triple events in the patch, number of events over complete duration of the recording including indication of deleted noisy stretches (red lines).

The lower row of Figure 78 shows the data after clusters containing multiple conductance levels are deleted. Deleting these multiple events, however, biases the data towards shorter open and cluster durations. In addition, the high frequency of channel openings increases the risk that the activity of more than one channel is included in a cluster. Thus, the resulting histograms should be considered to be first approximations to the distributions of events that would be seen with patches containing fewer active channels.

Current Amplitudes

In the presence of 3 mM phenol the single channel amplitude of 5-HT_{3A}QDA receptors is increased. At 3 µM 5-HT, a tendency is visible (increase from -2.67 ± 0.19 pA to -2.80 ± 0.12 pA), but at lower agonist concentrations this effect is significant (increase from -2.59 ± 0.19 pA to -2.90 ± 0.19 pA). Thus, with 30 nM 5-HT, single channel amplitudes increase by 12 % when 3 mM phenol is present.

Table 17: Single channel amplitudes in recordings with and without 3 mM phenol.
Mean of fits of Gaussian amplitude distributions. Unpaired Student's t-tests show significant differences in single channel amplitudes at 30 nM 5-HT ± 3 mM phenol, * $p < 0.05$.

condition	3 µM 5-HT	3 µM 5-HT + 3 mM phenol	30 nM 5-HT + 3 mM phenol	30 nM 5-HT
n patches (n events)	7 (4469)	6 (23059)	4 (2349)	10 (3406)
avg channel amplitude (pA)	-2.67	-2.80	-2.90	-2.59
SD	0.19	0.12	0.19	0.19
			*	

Critical Time Between Clusters

Closed duration histograms of phenol experiments revealed a shift towards shorter events. Figure 79 shows the closed duration histograms for the combined patches of measurements with 3 µM 5-HT plus 3 mM phenol (left) and for those with 30 nM 5-HT plus 3 mM phenol (right). The corresponding time constants and their fractional amplitudes of the closed components are listed in the table under the figure.

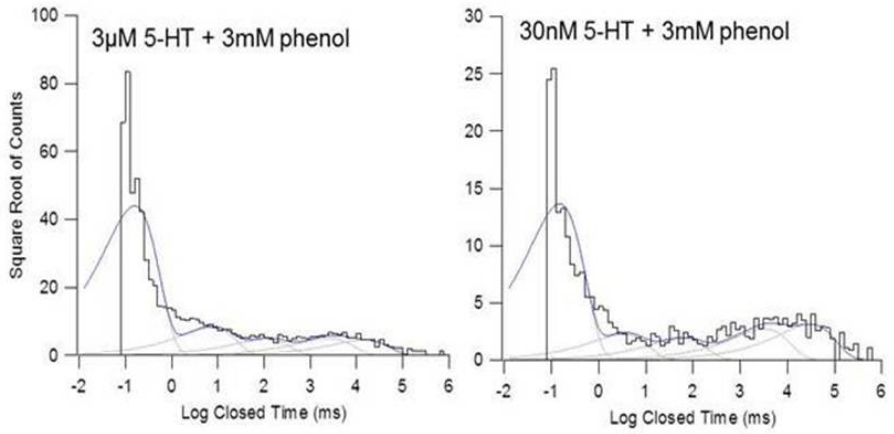

5-HT + 3 mM phenol												
	τ1	fr.amp 1	τ2	fr.amp 2	τ3	fr.amp 3	τ4	fr.amp 4	τ5	fr.amp 5	# patches	# events
30nM 5-HT	0.12	0.88	2.2	0.03	42	0.02	2614	0.03	24188	0.05	4	2349
3µM 5-HT	0.13	0.93	5.8	0.03	85	0.01	2044	0.01	11887	0.01	6	23059

Figure 79: Closed duration histograms for complete combined patches under 3 µM and 30 nM 5-HT + 3 mM phenol and their fits (formula 6, black line).
Individual exponential components are indicated (grey lines) and their time constants and fractions are given in the table under the figure.

Closings of the shortest component comprised the majority of closed events. The time constants of the second and third components were prolonged. At 3 µM 5-HT with phenol, the third time constant was 84.94 ms, under 30 nM 5-HT + 3 mM phenol the third time constant was 44.53 ms (Figure 79).

Alignment of the closed duration components indicate a possible difference in the critical closed time between clusters between control and phenol. To determine an adjusted critical time between clusters for single channel activity induced by 5-HT and phenol, the closed components were compared to the ones at control conditions. Figure 80 shows the closed components for individual patches recorded with 3 µM and 30 nM 5-HT with and without phenol. The colored dotted lines indicate the averaged closed components of all combined histograms for different serotonin concentrations.

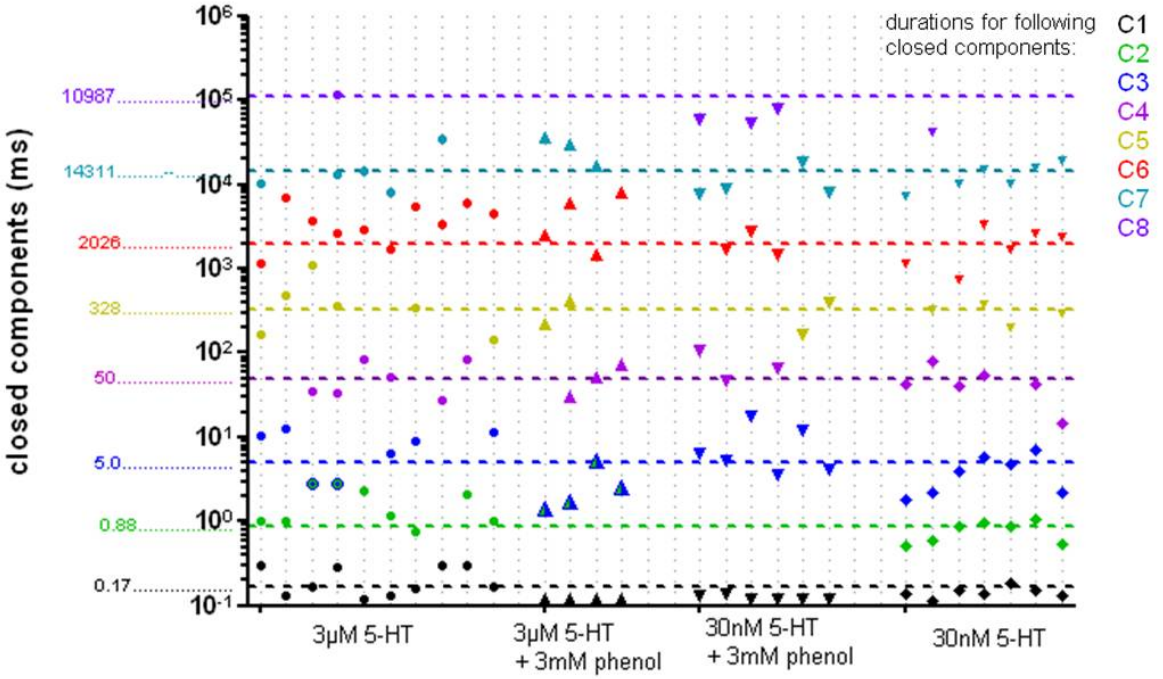

Figure 80: Aligning closed components (ms) for complete individual patches with and without phenol at different [5-HT].
Closed components for individual patches at 3 µM and 30 nM control and at 3 µM and 30 nM 5-HT + 3 mM phenol were aligned along the averaged closed components of all combined control histograms (colored dotted lines).

In phenol experiments, the first closed component is faster (0.12 and 0.13 ms) than in control measurements (black). The second closed component is larger and can possibly be classified together with the third component in control measurements (blue). This might suggest that as with propofol, the same t_{crit} as for control recordings (30 ms) can be used. However, with 30 nM 5-HT and 3 mM phenol, the second closed component tends to be even longer than the third control component. So in order to introduce a critical time for clusters comparable to the one at control and at the same time prevent a distortion of the second closed component in phenol measurements, a slightly longer (100 ms) t_{crit} might be needed.

The time constant of the third closed component for phenol experiments resembles the fourth closed components for control measurements (purple). If one wants to include the same number of closed states within clusters as we did for control analysis, t_{crit} must be between this fourth and the fifth component (300 ms).

Figure 81 shows closed duration histograms and respective fit components (table under the figure) for combined phenol experiments at different 5-HT concentrations. The histograms were plotted after selecting 2+ clusters with the three possible critical times 30, 100 and 300 ms that were described above. Only the choice of t_{crit} =

300 ms avoids distortion or even omission the third closed components (bold values in the table under the figure). The reproducibility of the three closed components before and after cluster selection suggests that this closed duration is appropriate as t_{crit} for clusters. Thus the following analysis of single channel events under phenol was performed with clusters separated by a critical closed time of 300 ms.

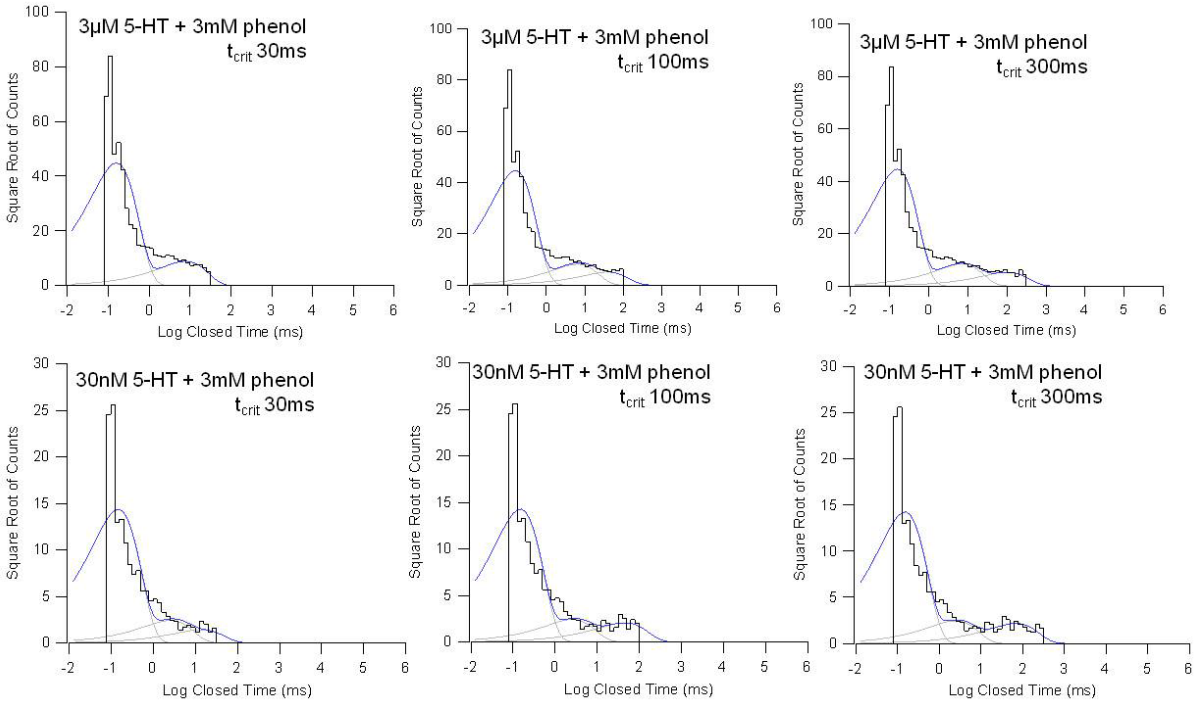

[5_HT]	tcrit (ms)	C1 (ms)	fr. amp1	C2 (ms)	fr. amp2	C3 (ms)	fr. amp3
3µM	30	0.13	0.96	6.20	0.04	X	X
3µM	100	0.13	0.96	5.12	0.03	**30.93**	0.01
3µM	300	0.13	0.95	5.63	0.03	**82.51**	0.01
30nM	30	0.12	0.96	2.21	0.03	**14.29**	0.01
30nM	100	0.12	0.95	2.04	0.03	**35.95**	0.02
30nM	300	0.12	0.95	1.95	0.03	**54.73**	0.02

Figure 81: Closed duration histograms for different 2+ clusters of combined patches under 3 µM and 30 nM 5-HT + 3 mM phenol and their fits (black line).
Individual exponential components are indicated (grey lines) and their values given in the table beneath.

The fits of the closed duration histograms (before as well as after cluster selection) are not ideal. For example, the fits underestimate the number of closings around 1 ms duration. This together with the fact that all components longer than the first one have extremely low fractions (down to 0.003, Figure 79) make any quantitative interpretation of the fits and their respective time constants and fractions very speculative. This may be due to the need to exclude the large number of multiple openings from the analysis.

Event Durations

Duration histograms of single channel events were fitted as described previously with formula 6. The resulting time constants and fractions of the components are plotted in Figure 82 . Results for individual patches can be found in Table 21 - Table 23 in the attachment. The symbols at the bottom of each scattergram indicate the weighted averages and the table below each scattergram presents these averages.

When 3 mM phenol is present, most of the closings are very short (0.12 and 0.13 ms). Nearly all closed events (about 96%) belong to the shortest component for both agonist concentrations. Weighted averages for closed durations are not given in Figure 82, because a quantitative description of any closed component longer than the first one is not reliable.

Open duration histograms were fit with three components. The duration of the shortest openings increases and the respective fraction of openings decreases in the presence of phenol. Additionally, the fraction of longest open components increase. In 5+ clusters, open duration histograms for phenol measurements at both serotonin concentrations were fit with three components, whereas at 30 nM control the intermediate component is missing. This results in a reduction of the second and the third fractional amplitude in comparison to the fraction of the long openings in 30 nM control recordings. All weighted averages of open durations are longer when 3 mM phenol is applied in addition to 5-HT. At the lower serotonin concentration (30 nM), open duration increases by 4.8 fold. At the higher concentration (3 µM) the effect is smaller – open duration only increase by 1.8 fold. Within clusters, the prolongation of openings is less apparent. Adding phenol to 30 nM and 3 µM 5-HT increases the open durations by 2.9 and 1.5 fold, respectively.

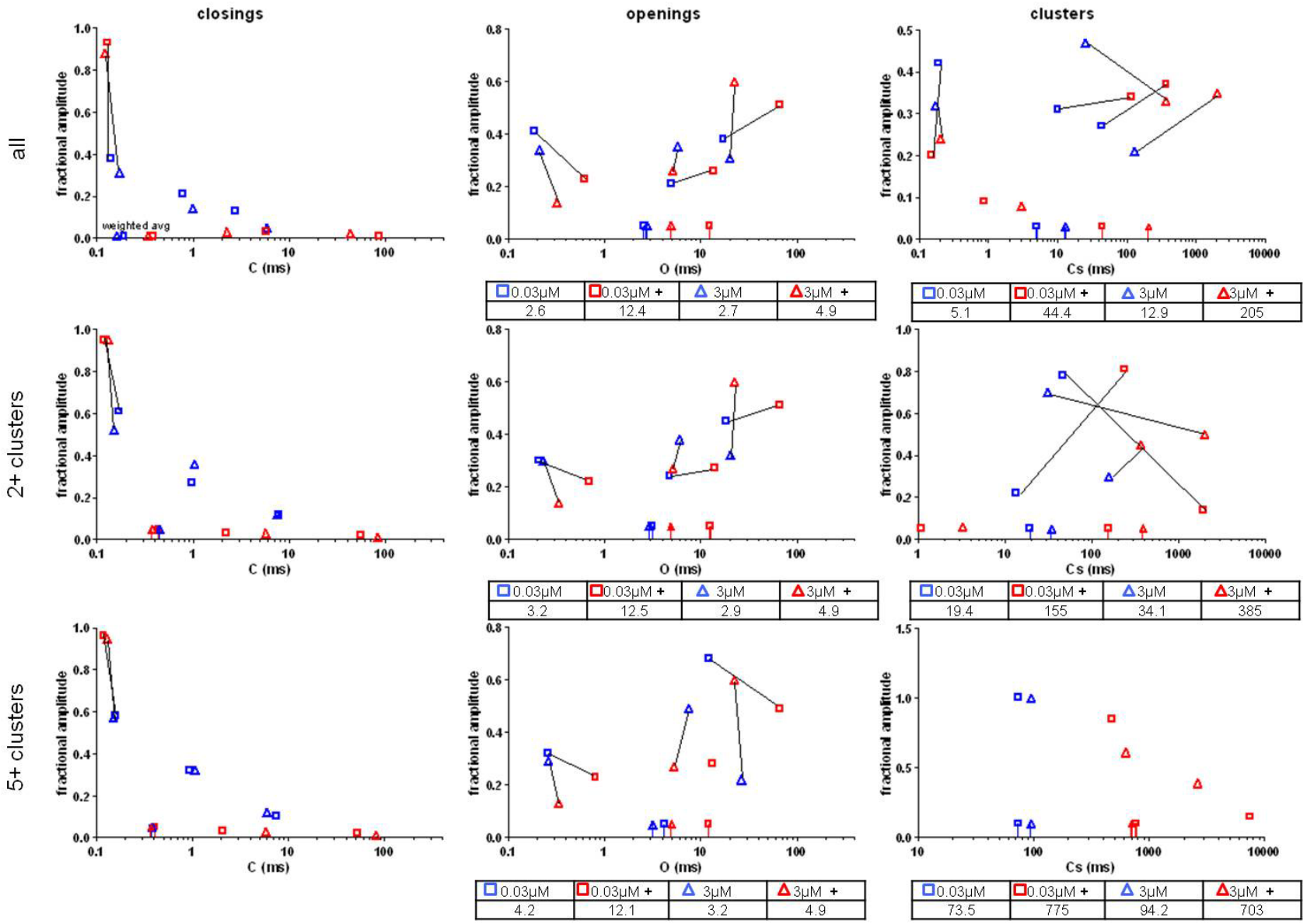
closings
openings
clusters
all
2+ clusters
5+ clusters
fractional amplitude
C (ms)
O (ms)
Cs (ms)
weighted avg
0.03µM
0.03µM +
3µM
3µM +
2.6
12.4
2.7
4.9
5.1
44.4
12.9
205
3.2
12.5
2.9
4.9
19.4
155
34.1
385
4.2
12.1
3.2
4.9
73.5
775
94.2
703

Figure 82: Event durations and their fractional amplitudes at different [5-HT] ± 3 mM phenol.
The symbols at the bottom connected to the time axis (lollypops ☺) of each scattergram indicate the weighted averages and the table below each scattergram presents these averages. Comparing the control with the respective phenol duration medians by Dunn's Multiple Comparison test always resulted in highly significant differences (*** $p < 0.001$). Values of time constants and their fractions that the plots are based on can be found in Table 21 - Table 23 in the attachment. t_{crit} for phenol durations is 300 ms, t_{crit} for control durations 30 ms.

Number of Openings and Open Probability within Clusters

The open probabilities (p_{open}) in all and in long clusters (formula 7) at different serotonin concentrations with and without phenol are listed in Table 18.

Despite the multitudes of effects of phenol on closed and open durations within clusters (Figure 82), the open probabilities within clusters did not change. However, clusters include more open events when phenol is added to 3 µM or 30 nM 5-HT in the recording pipette. The number of openings in all clusters is increased by 9 fold, the number of openings in long clusters is increased by 5 fold.

Table 18: Open probabilities (%) and number of openings within clusters for the human 5-HT_{3A}QDA channels at different 5-HT concentrations ± 3 mM phenol.
Indicated significances by Mann-Whitney tests: ** $p \leq 0.01$. For this table, long clusters are defined as all clusters longer than the critical gap time between the second and the third cluster component. All clusters excludes individual openings.

25% percentile **median** 75% percentile	3µM 5-HT	3µM 5-HT + 3mM phenol	30nM 5-HT + 3mM phenol	30nM 5-HT
# patches	7	6	4	10
p open (all clusters)	86 **86** 90	86 **88** 91	86 **93** 94	91 **95** 95
p open (long clusters)	82 **87** 89	80 **85** 91	82 **87** 89	80 **85** 91
# openings in all clusters	3.0 **4.3** 4.8	22.9 **40.4** 121 **	7.3 **9.2** 18.0 **	1.8 **2.0** 2.1
# openings in long clusters	5.3 **6.2** 7.9	35.9 **59.7** 218 **	10.9 **15.4** 33.4 **	2.6 **3.0** 3.9

Quasi Macroscopic Currents

The strong prolongation of cluster duration that is demonstrated in Figure 82 indicates a longer decay phase for 5-HT_{3A}QDA channels with phenol than in control recordings. To further investigate this, quasi macroscopic currents (QMCs) were formed by aligning and summing up all long clusters of a recording. With phenol, QMCs were calculated with a $t_{crit\ long}$ defined as the critical gap time between the second and third cluster components. The QMCs were fitted with one exponential curves, as shown in Figure 83 on the left for two recording. Resulting decay

constants and the number of clusters that were summed up are listed in the table on the right.

Control QMCs with 3 µM or 30 nM 5-HT showed decay constants of 82 ± 87 ms and 123 ± 247 ms respectively (Figure 57). When phenol was applied simultaneously with 3 µM or 30 nM 5-HT, the decay constants were 1691 ± 1069 ms and 863 ± 622 ms respectively. The decay of QMCs with 3 mM phenol are prolonged by 7fold at lower and by 20fold at higher 5-HT concentration.

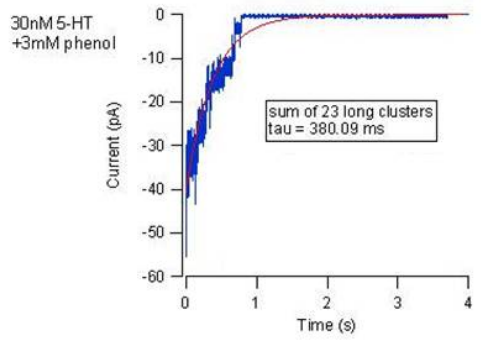

patch	# cluster comp	t_{crit} (ms)	t_{crit} long (ms)	# all clusters	# long clusters	decay QMC (ms)
30+ph_1	3	300	69.16	41	23	380
30+ph_2	3	300	249.4	64	20	1138
30+ph_3	2	300	0.82	36	26	322
30+ph_4	3	300	255.29	77	14	1611
avg						863
std						622

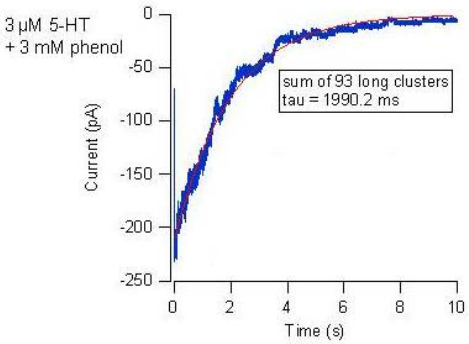

patch	# cluster comp	t_{crit} (ms)	t_{crit} long (ms)	# all clusters	# long clusters	decay QMC (ms)
3+ph_1	4	300	6.2	27	15	2006
3+ph_2	3	300	188.4	134	93	1990
3+ph_3	3	300	8.6	49	32	774
3+ph_4	3	300	164.7	139	69	1441
3+ph_5	3	300	401.8	16	8	3461
3+ph_6	2	300	1.43	70	65	471
avg						1691
std						1069

Figure 83: Quasi macroscopic currents for individual phenol experiments at different serotonin concentrations.

For QMCs with phenol, $t_{crit\ long}$ is defined as the critical time between the second and the third cluster component. Tables give the types of clusters that are found in the recording and the resulting decay constants when fitting QMCs with one exponential curves. Left: Two examples of QMCs of individual phenol recordings at different serotonin concentrations (blue) and their respective fits (red).

Discussion

Previous macroscopic studies on 5-HT_{3A} receptor channels have shown that actions of anesthetics on excitatory ligand gated channels are diverse and complex (Belelli et al., 1996; Stevens, 2005; Urban et al., 2006; Barann et al., 2008). To gain a more detailed insight into molecular mechanisms responsible for anesthetic actions, these effects need to be interpreted in terms of single channel kinetics.

First, the search for a single channel model will be discussed. After a brief characterization of the 5-HT_{3A} receptor channel, two high conductance variants of the receptor – a native one and a mutant one – were characterized and evaluated with the aim of finding a suitable model for single channel studies (see: Comparing Three 5-HT3R Variants to Find a Model for Single Channel Studies).

Next, having found such a model in the *human* 5-HT_{3A}QDA receptor, its kinetics will be discussed. A detailed analysis of its single channel kinetics was necessary to serve as control for future substance studies (see: *h*5-HT_{3A}QDA as a Model for Studying Single Channel Kinetics in wt *h*5-HT_{3A}).

Lastly, substance studies with this kinetic model will be discussed, starting with the widely-used intravenous anesthetic propofol. In order to associate substance effects with functional groups, additional studies were begun with phenol (and n-hexanol, see supporting material). These studies confirmed the suitability of the *human* 5-HT_{3A}QDA receptor channel as a model for single channel substance studies (see: Effects of Substances on 5-HT_{3A}QDA Channels).

Comparing Three 5-HT_3R Variants to Find a Model for Single Channel Studies

The major aim of this study was to find and evaluate a single channel kinetic model for 5-HT_3 receptor channels, which can be used to study the effects of anesthetic related substances on these channels.

The effects of anesthetics on the homomeric 5-HT_{3A} channel have been well characterized. Some experiments were performed to confirm the stability of the properties of wild-type 5-HT_{3A} receptors. However, this channel has a single channel conductance too small to be resolved (M. Barann, Meder, et al. 2000; M. Barann,

Dilger, et al. 2000; Urban, Bleckwenn, and Barann 2006; Martin Barann et al. 2008). (see: 5-HT_{3A}).

The native 5-HT_{3AB} channel (Niesler et al. 2007) could be a potential alternative, as the introduction of B subunits increases the single channel conductance significantly (Hapfelmeier et al., 2003; Stewart et al., 2003). I found that expression of receptors with both A and B subunits was too inconsistent to be used as a model system for single channel 5-HT_3 kinetics (see: 5-HT_{3AB}).

Thus, another homomeric 5-HT_{3A} version was considered. Mutation of three arginine residues in the A subunit of 5-HT_{3A} receptor channels to the corresponding amino acids of the B subunit have been shown to create a high conductance mutant, 5-HT_{3A}QDA (Livesey et al. 2011). 5-HT_{3A}QDA channels do not occur naturally, but are the least modified homomeric channels that show single channel conductances large enough to be resolved. These channels had reproducible kinetic and conductance properties. However, there were some differences in macroscopic kinetics between wild-type 5-HT_{3A} and 5-HT_{3A}QDA channels in the absence and presence of substances. Thus, we conclude that 5-HT_{3A}QDA channels are suitable for studying the effects of substances on single channels provided that macroscopic current measurements are also performed on this mutant channel (see: 5-HT_{3A}QDA).

5-HT_{3A}

Representative samples of macroscopic currents through 5-HT_{3A} channels have been characterized to serve as controls. Having obtained the expected results they ensure that experimenter and setup can be excluded as being responsible for several unexpected findings when other 5-HT_3 subunit compositions were used in subsequent experiments. These included differences in channel parameters that had not been previously reported and unexpected variabilities in the results that were obtained with heteromeric 5-HT_{3AB} receptors.

In these control experiments, macroscopic currents induced by applying 30 µM 5-HT to outside out patches from 5-HT_{3A} stably transfected cells showed a fast onset of 7.6 ± 3.7 ms and a slower offset of 156.6 ± 154.1 ms (Figure 16). They reached 50 % recovery from desensitization after 17.4 ± 1.7 ms (Figure 17). Applying different concentrations of 5-HT revealed an EC_{50} of 6.8 µM (Figure 18), applying different voltages revealed an inward rectification. These values are in line with those

previously found (M. Barann, Meder, et al. 2000; M. Barann, Dilger, et al. 2000) and did not reveal any unexpected surprises.

5-HT$_{3AB}$

A first evaluation of the occurrence of single channel events in currents from 5-HT$_{3AB}$ stably transfected cell patches could be obtained just by looking at the noise level of individual macroscopic traces during the current offset phase. At one extreme, the noise level of 5-HT evoked current traces did not differ much from that of background current without 5-HT (Figure 20), at the other extreme single channel events could be detected either singly or in staircases (Figure 19). As patches without resolvable single channel openings still did show a typical macroscopic 5-HT$_3$ channel response to 5-HT, there still are functional serotonin gated channels present.

Detecting single channel events was not always as clear as shown in Figure 19, although the traces would often be nosier and spikier (Figure 84, C) than is characteristic for a patch expressing purely 5-HT$_{3A}$ homomers. However, traces that looked like pure 5-HT$_{3A}$ were also seen (Figure 20).

When characterizing stably transfected 5-HT$_{3AB}$ cells that had been passaged only a few times after clone selection, many patches showed channels with properties that were distinct from those of pure 5-HT$_{3A}$ as previously described (Davies et al., 1999; Brady et al., 2001). They were less sensitive to serotonin (EC_{50} = 42 µM), had a close to linear instead of a strongly rectifying current-voltage characteristic (rf around 2), recovered faster from desensitization ($\tau_{recovery}$ = 5.5 s, see Figure 20) and showed large single channel conductances (13.4 ± 1.6 pS, page 46: Current Amplitudes).

Macroscopic currents from these patches showed a fast onset with a τ_{ON} of 7.5 ± 4.5 ms and a decay phase with a τ_{OFF} of 61.2 ± 78 ms (n=13 patches ±SD).

Although the reversal potential for all patches was close to zero mV, some patches of stably transfected 5-HT$_{3AB}$ cells showed macroscopic currents that varied in their voltage dependence. Patches with clearly distinguishable single channel events showed very little rectification (rf close to 2, Figure 28). Others showed higher values of rectification 4 ≤ rf ≤ 9. As rectification is a characteristic of homopentameric 5-HT$_{3A}$ channels (Barann et al., 2000b), this heterogenic group may contain a mixture of 5-HT$_{3AB}$ heteromers and 5-HT$_{3A}$ homomers, which is more (higher rf, closer to 9) or less (smaller rf, closer to 4) dominated by homomers.

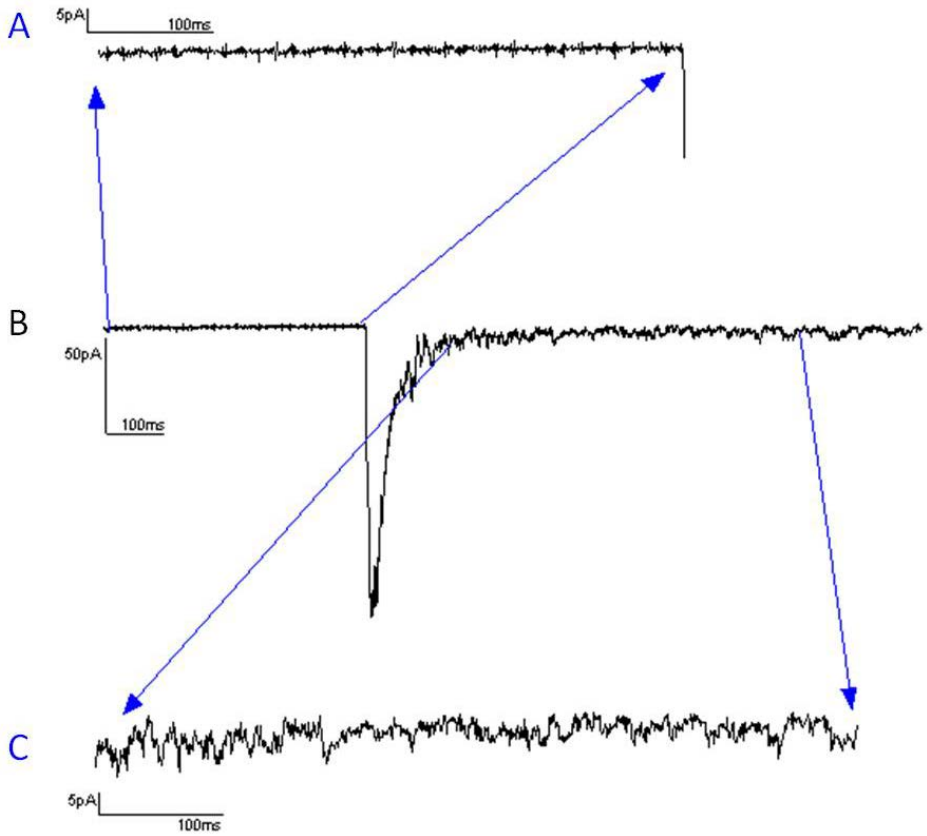

Figure 84: Representative trace of an outside out patch of a stable 5-HT_{3AB} transfected HEK cell. **A**: Magnification of a baseline section, **B**: Complete trace, **C**: Magnification of steady state current, to emphasize irregular noise with events/spikes emerging from the background.

Concentration response curves based on outside out patch recordings from 5-HT_{3AB} transfected cells exhibited a range of EC_{50} values as well. These can be grouped into two populations. The concentration response of a patch resembles either the response one would expect of 5-HT_{3A} channels, or has a lower slope and a higher EC_{50} (Figure 30). The latter population had resolvable single channel events. Our data suggests that both 5-HT_{3A} and 5-HT_{3AB} receptors are formed when both subunits are present and that the relative number of 5-HT_{3AB} receptors is highly variable.

This may be a common situation. Different EC_{50} values for activation of 5-HT_3 receptors by 5-HT have been reported in the literature (Table 19). Due to experimental differences, variations in the EC_{50} can be expected. But the shift of EC_{50} towards higher concentrations that is induced by introducing B subunits should be similar between publications. The last column in Table 19 shows the ratio of EC_{50} values for 5-HT_{3AB} receptors compared to 5-HT_{3A} receptors in each study. The EC_{50} ratios that were determined by electrophysiological methods varied considerably: 2.07 – 11.11 fold. Variability in the relative expression of 5-HT_{3AB} receptors is a

plausible explanation for inconsistency in published results. In addition, almost all of the published EC_{50}s for 5-HT_{3AB} receptors are lower than those found for the supposedly heteromeric group in the present study (Table 19, EC_{50} = 42 µM). The exception to this is the study of Walstab et al. 2008 in which the presence of two populations was noted and the concentration-response curves were fit to two components. They deduced that the 5-HT_{3AB} population had an EC_{50} of 83 µM when HEK cells were transfected with cDNA at an A:B ratio of 1:4. Furthermore, Cheng and group showed that the chaperone hRIC-3 promotes expression of homopentameric 5-HT_{3A} receptors and suppresses heteromeric 5-HT_{3AB} receptors in Simian COS7 cells (Cheng et al., 2007). Similar effects were reported by Walstab et al, who reported that RIC-3 can interact with 5-HT3A, -C, -D, and -E subunits and predominantly enhances the surface expression of homomeric 5-HT_{3A} receptors in HEK293 cells (Walstab et al., 2008). Although it has not been reported that HEK cells express RIC-3 naturally, it is conceivable that other chaperon proteins fulfill similar functions in HEK cells and thus influence the expression rate of individual channel subunits on the cell surface.

The fact that groups tend to stop working on the heteromeric 5-HT_{3AB} after publishing only a few results might be a hint, that they have problems keeping a stable subunit expression as well.

Table 19: Concentration response characteristics of homomeric and heteromeric 5-HT_3 channels found by different groups.
[1]A:B transfection ratio 1:4; fit to 2 populations, [2]A:B transfection ratio 4:1; fit to 2 populations.

reference	prep./method	EC_{50} (µM)		ratio
		5-HT_{3A}	5-HT_{3AB}	5-HT_{3AB}/5-HT_{3A}
Brady et al. 2001	oocytes/V-clamp	1.3	5.2	4.00
Stevens 2005	oocytes/V-clamp	1.8	20	11.11
Davies et al. 1999	HEK/ whole cell	2.9	6	2.07
Baptista-Hon et al. 2012	HEK/ whole cell	5.1	16	3.14
Hapfelmeier et al. 2003	HEK/ whole cell	3	25	8.33
Walstab et al. 2008	HEK/ Ca^{2+}influx	1.7	3.4, 85.3[1] 2.4, 29.5[2]	2.00, 50.12 2.00, 18.35
present study	HEK/ outside-out	6.8	42	6.18

When evaluating existing studies of 5-HT_{3AB} channels, one has to be aware of the possibility that results are contaminated by coexisting 5-HT_{3A} homomeric channels. If

heteromeric channels dominated the expression pattern at the beginning of a study of a new clone, they would not have necessarily done so after many cell passages. Also, when a filter setting is used that does not allow resolution of 5-HT_{3AB} single channel events – as is often done in macroscopic recordings – 5-HT induced currents over heteromeric and homomeric channels can hardly be distinguished without a more detailed electrophysiological characterization. This is very likely for studies in whole cell patch clamp conformation, as those usually provide larger current peak amplitudes, so that a low resolution is chosen. If I-V curves are conducted by applying a voltage range up to only + 40 mV (Brady et al., 2001), differences in the channel conductance at positive voltages might not be as distinct as seen in the present study, where larger positive voltages (up to + 100 mV) were applied.

The idea of the importance of subunit expression levels is not new. Krzywkowski and group found that diversity within the human 5-HT_{3A} and 5-HT_{3B} subunit structure occurs through alternative splicing and polymorphisms, some of which impact upon receptor expression and function. They found that the expression of B subunits was suppressed more by small mutations in the respective DNA (Krzywkowski et al., 2008a, 2008b).

Heteromeric 5-HT_{3AB} channels might differ more from homomeric 5-HT_{3A} channels than thought, because previous results were confounded by unknowingly mixing HT_{3AB} characteristics with 5-HT_{3A} ones. This may be due to a mixture of different channels differing in stoichiometry of subunits, e.g. A2B3 (Barrera et al., 2005) or A3B2 (Miles et al., 2013) or any other combination, or due to different fractions of homomeric 5-HT_{3A} channels.

The appearance of homomeric 5-HT_{3A} like characteristics correlates with the absence of distinguishable single channel events (Figure 30) and with an increased number of cell passages (Figure 25, Figure 28). This leads to the conclusion that B subunit expression on the cell surfaces decreases and maybe even disappears from stably transfected 5-HT_{3AB} cells. The composition of expressed subunits after transient transfections cannot be verified either and could differ from transfection to transfection. The 5-HT_{3A} stably transfected HEK cell line used in the present study has been used for more than 15 years and has shown a stable protein expression as well as reproducible channel activity (Barann et al., 2000a, 2008; Decker, 2010; Meiboom et al., 2013). Finding that the stable transfection with 5-HT_{3A} and 5-HT_{3B} subunits is not stable over time was surprising, especially because heteromeric forms

of 5-HT_3 receptor channels are thought to be the dominant native species (Hapfelmeier et al. 2003; Niesler et al. 2003).

This lack of stability means that none of the currently available 5-HT_{3B} containing model systems are suitable for determining the effects of drugs on 5-HT receptors.

In summary the co-transfection of 5-HT_{3A} and 5-HT_{3B} subunits had to be discontinued and an alternative 5-HT_3 model for single channel kinetics and the effects of anesthetics related substances on them had to be found.

5-HT_{3A}QDA

In looking for an alternative model channel, a homomeric version is preferred to avoid any uncertainty in subunit composition. Mutating three arginine residues in the intracellular MA stretch of the A subunit of the 5-HT_3 receptor to the correlating amino acids of the B subunit creates a high conductance mutant, the 5-HT_{3A}QDA (Kelley et al., 2003a), (Peters et al., 2010). Just like the wild type, 5-HT_{3A}QDA forms functional homo pentameric ion channels. Transfections with this mutant will therefore not be receptive for eventual heterogeneous expression patterns. This and the fact that it is the least modulated mutant of 5-HT_{3A} that shows a high single channel conductance (Livesey et al., 2011) make 5-HT_{3A}QDA a good candidate for single channel studies.

One unanswered question is whether the QDA mutation changes the properties of the 5-HT_{3A} receptor macroscopic currents, suggesting perhaps that the single channel kinetics have been altered as well. To address this, the characteristics of macroscopic currents from the mutant channel were compared to those of the wild type (Barann, Dilger, et al. 2000; Barann et al. 2008; Meiboom et al. 2013; Decker 2010). Some significant differences were found (Figure 35).

Macroscopic currents from 5-HT_{3A}QDA had a similar onset, but a faster offset (Figure 35). Their peak amplitudes tend to be larger (Figure 35), which is influenced by the higher single channel conductance as well as by the number of channels and therewith by the expression rate on the cell surface.

The two concentration response curves of wild type and high conductance 5-HT_{3A} were similar (Figure 37). Previous studies reported similar EC_{50}s for serotonin for the two channels as well (Hussy et al., 1994). Although the data is sparse, there is a suggestion that 5-HT_{3A}QDA seems to reach the point of agonist block at slightly lower concentrations than 5-HT_{3A}.

5-HT_{3A}QDA has been used in several previous single channel studies and was assumed to be kinetically and pharmacologically similar to the wild type 5-HT_{3A} (Corradi et al., 2009, 2011). 5-HT_{3A}QDA channels show macroscopic currents with 5-HT_{3A}-like (agonist concentration dependence) as well as 5-HT_{3AB}-like (voltage dependence and kinetics) features.

Changing three arginine residues within the MA stretch of 5-HT_{3A} channels introduces additional electrophysiological changes other than just a higher single channel conductance. This has to be kept in mind when using 5-HT_{3A}QDA to build single channel kinetic models to interpret the behavior of wt 5-HT_3 channels. Thus, it is necessary to study the effects of subtances on macroscopic currents from 5-HT_{3A}QDA receptor channels.

h5-HT_{3A}QDA as a Model for Studying Single Channel Kinetics in wt h5-HT_{3A}

A detailed characterization of control single channel kinetics of 5-HT_{3A}QDA was necessary before single channel substance studies could be performed on human 5-HT_{3A}QDA receptor channels. To this aim, cell attached patches of 5-HT_{3A}QDA transiently transfected HEK cells were formed with pipettes containing 30, 100, 300 or 3000 nM 5-HT.

A crucial step when analyzing single channel activity is to define clusters. Clusters are assumed to represent the activity of one channel between long-lived non-conducting (either resting or desensitized) periods. Analysis of events within clusters provide information about the kinetics of single channels. The time between clusters depends on the unknown number of active channels in the patch and is difficult to interpret. (see: Determination of Clusters is a Crucial Step in Single Channel Analysis).

Patch-to-patch and time-dependent variability of 5-HT_{3A}QDA channel activity is observed. Different approaches are employed to analyze and interpret these variabilities. (see: Activity of *h*5-HT_{3A}QDA Channels Varies Between Patches and Over Time).

Macroscopic current kinetics depend on 5-HT concentration. The kinetics of 5-HT_{3A}QDA channels are more complex on single channel level then on macroscopic level. Therefore, single channel experiments must also be performed to determine

which single channel parameters depend on 5-HT concentration (see: Single Channel Kinetics Are 5-HT Concentration).

A comparison of human single 5-HT_{3A}QDA receptor channel data with a previous study on the mouse isoform will establish whether the complex kinetic model proposed by (Corradi et al., 2009) is applicable across species (see: Comparing the Kinetics of *Human* and *Mouse* 5-HT_{3A}QDA).

Quasi macroscopic currents were constructed from single channel data in order to compare macroscopic and single channel data (see: Quasi Macroscopic Currents Resemble Recorded Macroscopic Currents).

Finally, macroscopic and microscopic substance studies are performed, starting with the clinically most frequently used intravenous anesthetic propofol (see: Effects of Substances on 5-HT_{3A}QDA Channels).

Determination of Clusters is a Crucial Step in Single Channel Analysis

5-HT_{3A}QDA activity occurs in clusters (Figure 47). A cluster is considered to be formed from a series of openings and closings of one individual channel, while the time between clusters depends on the number of active channels that are present in the patch. Determination of clusters requires the introduction of a critical time t_{crit} that separates them. The closed time histograms for 5-HT_{3A}QDA channel activity contains multiple components, so determination of t_{crit} can be difficult. Closed components between clusters turned out to be more consistent from patch to patch than expected. Long closings were very reproducible even between different 5-HT concentrations.

Figure 85 illustrates this suprising consistency. In this figure, the time constants of the components were grouped according to their proximity to the components found in the combined, weighted average closed duration histograms. There is no obvious choice for the definition of a cluster. However, most of the patches studied contained more than one channel; the results may be distorted by the need to delete stretches of data containing multiple openings. In the future, an experimental protocol is needed to screen many patches. Only those patches with no multiple openings would form the basis for a consistent kinetic model. For now, we must compromise by choosing critical gap durations that produce QMCs that are consistent with measured macroscopic currents.

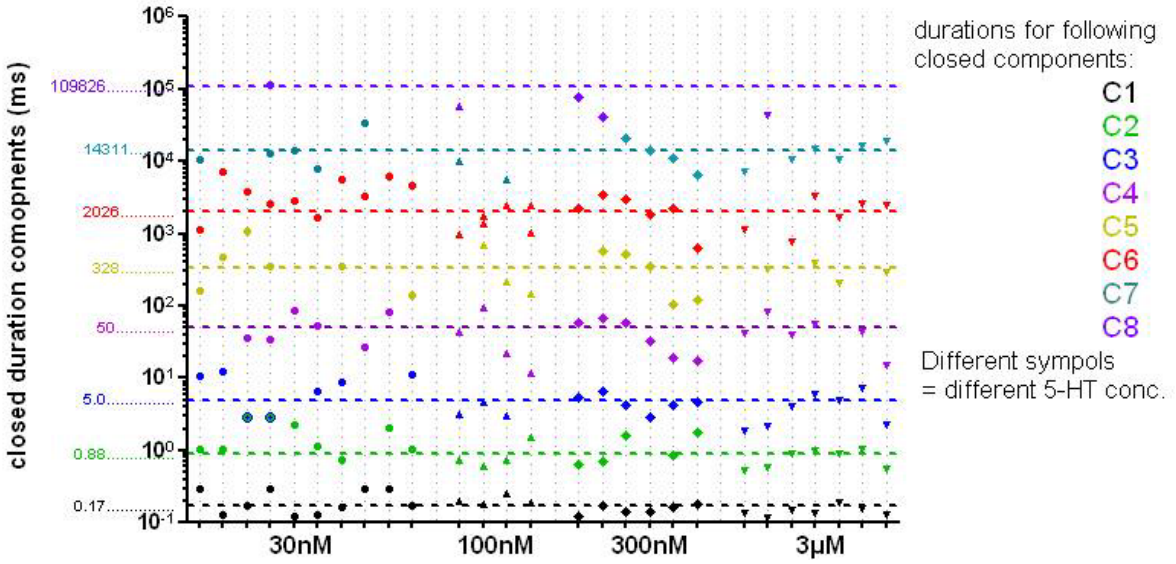

Figure 85: Duration components (ms) resulting from multiple exponential fits (formula 6) of closed duration histograms for individual patches at different serotonin concentrations.
Vertical grid lines: each line one patch. Horizontal grid lines: average components of all combined histograms at different [5-HT] (ms).

In the present study, we found that a critical time of 30 ms produced QMCs that resembled the macroscopic desensitization constant of control recordings (Table 7). In studies of single *mouse* 5-HT_{3A}QDA receptor channels, the critical time was chosen to be between 5 and 10 ms (Corradi et al., 2009, 2011).

Critical gap times over a range of serotonin concentrations were sufficiently reproducible (Figure 13) to assign one critical time for all control experiments. When substances are investigated, critical gap times between closed components can change (Figure 74 and Figure 80) and a new critical time may need to be determined. Based on these considerations, we chose a critical time of 30 ms for propofol experiments and 300 ms for phenol experiments.

Activity of h5-HT_{3A}QDA Channels Varies Between Patches and Over Time

Surprisingly, within a series of recordings at the same experimental conditions, individual patches were found that differed significantly in one or more single channel characteristic (30 nM 5-HT, -80 mV, Table 5). Such variability makes it difficult to compare substance influenced channel activity with control activity, when they are not recorded from the same patch. In the sum of patches, including or excluding exceptional recordings does not alter resulting kinetic values (Figure 12), as long as the histograms are normalized so that each patch is given the same weight.

Macroscopic currents from 5-HT_3 and other ligand-gated channels are known to undergo changes during the recording session. These include rundown, a decrease in the number of active channels (Figure 32); and acceleration, a speeding up of the onset (Figure 34) and/or offset of the current. The origins of these effects are not known but may be related to stress caused by the formation of a giga-ohm seal on the cell membrane (Suchyna et al., 2009).

Single channel recordings exhibited rundown: often the channel activity decreased over time (Table 6). In addition, for all except the lowest (30 nM) 5-HT concentration, event durations within clusters changed as well (Table 6). Open and cluster durations increased and closed durations decreased. This could be explained by the necessity to exclude clusters from the analysis that include multiple channel events. Long clusters and openings are more likely to overlap and create multiple channel events. Excluding these clusters and openings biases the data towards shorter events. Over time the channels open less frequently and therefore overlap less frequently. Fewer long events have to be excluded. When a minimum 5-HT concentration of 30 nM is applied, channel activity is very low over the complete recording time. Thus data are not biased and resulting event durations are more reproducible over time.

Due to the stability of channel activity over time and a reliable level of individual channel openings under 30 nM serotonin, the control analysis here focuses on 30 nM serotonin data. I was able to collect and pool 3450 individual channel openings in 10 patches. Other studies are based on data obtained at higher concentrations and usually pool fewer patches, the number of individual openings usually not given. Working at very low serotonin concentrations is very time consuming, because naturally respective patches have to last very long (here usually about 30 min) to provide a number of events that is high enough to be analyzed statistically. But it is needed in order to provide a solid control pool of data and analysis for future substance studies on single channel data.

Single Channel Kinetics Are 5-HT Concentration Dependent

The single channel conductance of 33 pS reported here (Table 4) agrees with the range of 22 – 36 pS for *human* 5-HT_{3A}QDA channels that was reported previously (Kelley et al., 2003; Deeb et al., 2006; Hales et al., 2006) and as expected does not change with agonist concentration.

One aim of this study was to relate single channel data to macroscopic data. Thus experiments encompassing a range of serotonin concentrations have to be performed that can produce sufficient macroscopic currents. On the other hand, in order to record individual channel activity, experiments at very low serotonin concentrations have to be performed. To meet these demands a range of 30 nM – 3 µM serotonin was used.

In microscopic currents, the fraction of open channels during the recorded steady state depends on the balance between activation and desensitization (Auerbach and Akk, 1998). Might the differences that one sees in microscopic recordings at different serotonin concentrations reveal changes in activation and desensitization rates? Duration components within clusters determined at different serotonin concentrations can still be grouped by their fractions and amplitudes. One can assume that the basic kinetic pattern of 5-HT_{3A}QDA doesn't change with serotonin concentration. This suggests that the multiple open and cluster components all arise from receptors of the same activatable closed state. Despite wide percentile ranges, Dunn's Multiple Comparison Tests mostly result in statistically significant differences within those clusters between open durations (Figure 63), closed durations (Figure 69) and cluster durations (Figure 55) at different serotonin concentrations. At serotonin concentrations between 30 nM and 300 nM, for 2+ clusters the duration of the longest open component (12 ms – 33 ms) as well as the duration of the longest cluster component (46 ms – 196 ms) increase with 5-HT concentration (values for the combined histograms of all recordings of respective serotonin concentrations, Table 22). The fraction of longest closings (12 % - 27 %) also does this. For the highest serotonin concentration of 3 µM though, these effects show reverse tendencies. The durations of the longest open (20 ms) and cluster (156 ms) components as well as the fraction of longest closings (12 %) decrease again. Block of the channel pore by serotonin at concentrations >5 µM has been described before (Bouzat et al., 2008; Corradi et al., 2009) and is a possible explanation for the cutoff of the increasing effects of serotonin on open duration. More long closings within clusters might not contribute to higher open probabilities, but they prolong a cluster and therewith the time that a channel spends in an activatable state; the duration until desensitization is prolonged. 5-HT_{3A}QDA channels are blocked by higher 5-HT concentrations (> 0.3 µM) but quantifying the blocking effect is difficult, because the above described bias towards shorter events at high agonist concentration and therewith high channel

activity can take part in the increasing effects as well. Channel desensitization also seems 5-HT concentration dependent and becomes faster at concentrations larger than 0.3 µM.

The probability to enter a 2+ cluster decreases at very low serotonin concentrations of 30 nM (Figure 50). This results in a high fraction of isolated openings and could be a hint that more than one bound agonist molecule is needed for the channel protein to undergo the conformational changes that are necessary to switch into the 2+ cluster mode.

Comparing the Kinetics of *Human* and *Mouse* 5-HT$_{3A}$QDA

A previous single channel study on the *mouse* 5-HT$_{3A}$QDA isoform proposed a kinetic model. This served as a guideline for considering an appropriate kinetic scheme for single channel activity of the *human* high conductance form. Like *mouse* 5-HT$_{3A}$QDA channels (Corradi et al., 2009), the *human* isoform shows complex channel kinetics. Table 20 lists the main results of the study conducted by Corradi and group and the corresponding results from the present study.

Despite some experimental differences between the studies, the numbers of components within clusters were the same. Corradi et al do not mention the possibility to fit open duration histograms of individual patches with only two components. We found briefer long open durations and cluster durations and smaller conductances, but these probably arise from the higher external calcium concentration in ECS that was used here. Calcium is known to inhibit 5-HT$_{3A}$ channel activity (Livesey et al., 2008; Noam et al., 2008).

Closed components for *mouse* 5-HT$_{3A}$QDA channels were shorter, with the briefest component having the largest frequency. This very short closed component (0.02 ms) would be too short to be resolved by recording and filter frequencies that were used during the present study. Our results show similar tendencies with the briefest closures having the highest frequency.

At low concentrations, the fractions of the three open components are comparable for both studies, but the two longer components have briefer time constants for the *human* channel (Table 20).

Table 20: Comparing the present with a previous study (Corradi et al., 2009).
All results are shown as values within clusters. Corradi et al did choose 0.5 µM, the present study did use 0.3 µM 5-HT as low agonist concentration. O = open duration, C = closed duration, Cs = cluster duration.

	Corradi et al.	present study
digitization interval	5 µs	20 µs
filter frequency	9 kHz	3 kHz
$[Ca^{2+}]$ in ECS	0.2 mM	1.8 mM
t_{crit} between clusters	crit.gap between 3rd/4th closed component (flexible)	crit.gap between 3rd/4th closed component (30 ms)
# of openings in analyzed clusters	5+	5+
single channel conductance	67 pS	32 pS
O (ms) 0.5/0.3 µM	0.20, 2.1, 110	0.31, 2.29, 33.52
respective fractions	0.31, 0.14, 0.55	0.24, 0.13, 0.63
O (ms) 3 µM	0.19, 7.1, 110	0.26, 7.45, 26.33
respective fractions	0.21, 0.16, 0.63	0.29, 0.49, 0.22
C (ms) 0.5/0.3 µM	0.02, 0.19, 1.5	0.16, 1.15, 6.36
respective fractions	0.78, 0.18, 0.04	0.54, 0.21, 0.25
C (ms) 3 µM	0.02, 0.18, 1.7	0.15, 1.06, 5.93
respective fractions	0.86, 0.10, 0.04	0.57, 0.32, 0.12
Cs (ms) 0.5/0.3 µM	1,420	254
Cs (ms) 3 µM	1,290	94

The table lists the values we obtain from combining all recordings on patches with the same serotonin concentration, thus three open components are assumed. But the fact that open duration histograms of individual recordings can be fitted with only two exponential components raises the question of where the third component originates. One possible interpretation would be a variability in the second component from patch to patch. This interpretation would require fewer open states in the predicted kinetic scheme, but different possible variations of the second open state. The appearance of an additional component when pooling data can also be interpreted as a statistical effect. The individual histograms are based on too few data points to resolve three components, instead this component shows a wide patch-to-patch range. Figure 86 shows a two component and a three component fit of the open duration histogram of one patch.

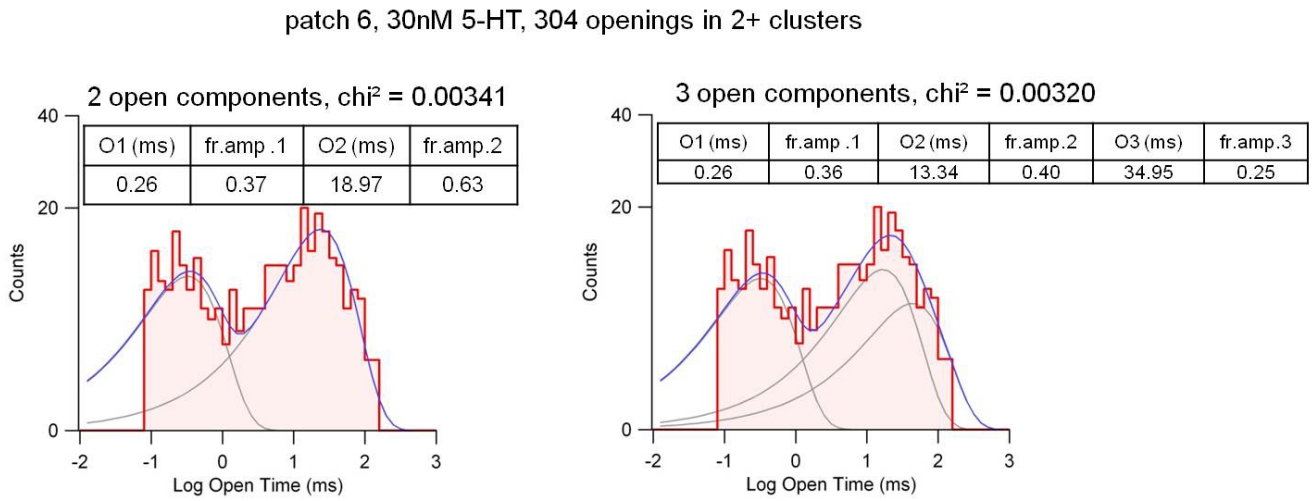

Figure 86: Open duration histograms for an individual recording of 30 nM induced single channel openings over human 5-HT_{3A}QDA, fitted with two (left) and three (right) exponential components.

Introducing a third component is possible, but does not improve the over all fit (chi² only decreases by 0.00021). The fact that median open durations in 2+ clusters of individual recordings can differ significantly from each other (Table 8) also supports the idea of one stable and one variable open state. A study on 5-HT_{3A} channels which contain different ratios of a subunit with a mutation that disables the agonist binding sites concludes that two binding sites at consecutive subunit interfaces enable brief individual openings, but two binding sites at nonconsecutive subunits are necessary to enable bursts of openings and longer open durations (Rayes et al., 2009). Different stochiometries of bound sites could be a possible explanation for different channel modes that lead to different open durations of longer openings.

When building a kinetic single channel model for the *mouse* 5-HT_{3A}QDA channel, Corradi and group assume that in the steady state, clusters are entered and ended by openings of the longest open component. This study could not confirm this finding in the *human* isoform. The fractions of open components are similar for all events within clusters and for the first and last events in clusters (Figure 67). In respect to the kinetic scheme this would mean that, in contrast to the Corradi model, a cluster can terminate via any of the three open states. Thus an additional transition is needed between the states C_2 and A3D, as indicated in the kinetic scheme in Figure 87.

The Corradi model predicts a very high open probability within clusters and thus does not allow for the possibility that substances such as phenol may increase the peak macroscopic currents obtained with high 5-HT concentrations. Inclusion of one or more additional closed states to the definition of a cluster may be necessary.

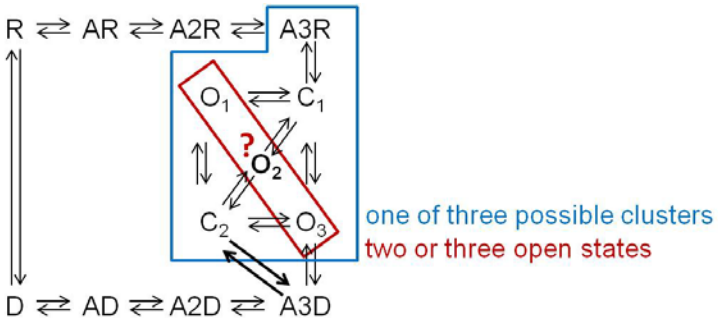

Figure 87: Extended kinetic scheme for human 5-HT$_{3A}$QDA receptor channel activity.
Based on the kinetic scheme for mouse 5-HT$_{3A}$QDA receptor channel activity predicted by Corradi et al, changed by introducing a transition between C2 and A3D. The number of open states is questionable. Data also suggest the possibility of three different clusters, which is not included here. Changes are indicated by bold font.

Corradi et al focused on 5+ clusters and thus include only one cluster component into their kinetic model. This might be a practical because less complicated way to present 5-HT$_{3A}$QDA channel kinetics, but probably does not account for all of the data. When cluster analysis includes all occurring clusters, the present study shows the presence of three cluster components. The longest component, which would be the one mainly composed of 5+ clusters, provides only 21-27% of them (at 30 nM-3 µM 5-HT, Table 21) Three pathways for terminating clusters would have to be included into the kinetic model to account for three cluster duration components. This increases the complexity of the kinetic scheme for single channel *human* 5-HT$_{3A}$QDA receptor channel activity even more.

To be able to predict a detailed kinetic single channel model for *human* 5-HT$_{3A}$QDA receptor channels, much more data - especially out of clusters - are needed. But I was able to confirm the high complexity of such model that was predicted based on data for another species variant. Data for the *human* variant even ask for additional transitions to be introduced into the model.

Quasi Macroscopic Currents Resemble Recorded Macroscopic Currents

Quasi macroscopic currents are similar to real macroscopic currents of 5-HT$_{3A}$QDA transfected outside out patches, which was quantified by comparing respective decay time constants (Table 7). Changes in cluster duration result in changes of decay constants of macroscopic currents (Figure 56).

Quasi macroscopic currents show that decay constants depend on cluster duration. Cluster duration depends on open duration and is influenced by closed

duration and the number of openings per cluster. Thus a change of the macroscopic decay constant can be due to many single channel effects.

Because QMCs resemble so well recorded macroscopic currents, they also serve as a confirmation for the determination of correct clusters.

Effects of Substances on 5-HT$_{3A}$QDA Channels

To verify the possibility to use 5-HT$_{3A}$QDA as a single channel model for 5-HT$_3$ receptor channels within future substance studies, representative anesthetic related drugs were applied and their effects on macroscopic as well as microscopic channel currents were observed. A comparison to former macroscopic studies on 5-HT$_{3A}$ will evaluate the reproducibility of these effects.

5-HT$_{3A}$ QDA – With Propofol

Macroscopic serotonin plus propofol induced currents were recorded. Propofol was applied in open channel (-+) and in equilibrium (++) mode. Figure 88 compares the results of those experiments with previous propofol studies on wt 5-HT$_{3A}$ channels (Witten, 2009). Witten found a reduction as well of peak amplitudes as of τ_{OFF} when applying propofol in either experimental mode, but no effects on τ_{ON}.

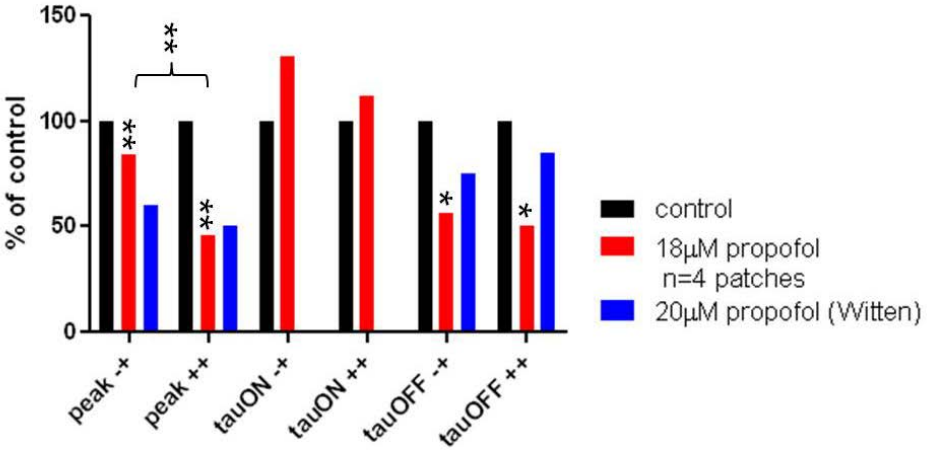

Figure 88: Comparing macroscopic effects of propofol on 5-HT$_{3A}$QDA and effects of propofol on 5-HT$_{3A}$ as found in (Witten, 2009).
* shows significant differences of present propofol study to its control. 5-HT$_{3A}$QDA data: Peak reduction by -+ application to 84.3 % and the peak reduction by ++ application to only 45.4 % was significant (P values of 0.004 and 0.001 respectively). Values of the inhibiting effects on peak amplitudes differed significantly between the application modes (P value 0.004). τ_{OFF} is reduced to 56 % (-+, P 0.02) or 50.5 % (++, P 0.02). The onset does not change significantly. Paired two tailed t-tests.

Propofol had similar effects on both channel variants. The peak amplitudes are reduced and the decay phase gets faster for 5-HT_{3A}QDA channels as well. In both application modes, the decay only takes half as long as under control condition, which can partially explain the peak reduction. Propofol effects on the current peak are significantly stronger in ++ application, thus there has to be an additional effect to the accelerated current decay. Possibly channels are already desensitized by propofol before the are opened by 5-HT application.

The only difference to the wild type is the less inhibiting effect on the 5-HT induced peak amplitude when applying propofol simultaneously with 5-HT (-+). The effect of propofol might be smaller on 5-HT_{3A}QDA channels because those desensitize faster and thus reach the equilibrium current faster than the wild type channels. The inhibiting effect can't reach the same impact as on slower wild type channels, because by the time the current peak is reached, desensitization already masks inhibiting effects of propofol.

Additionally the pharmacological similarity of the two channel variants could be confirmed by macroscopic outside-out recordings on 5-HT_{3A}QDA with n-hexanol. The according comparison with 5-HT_{3A} can be found in the supporting material (Figure 91 an Figure 90).

Single channel recordings were recorded with 100 nM 5-HT + 18 µM propofol filled patch pipettes and the resulting channel events were analyzed (Figure 75). Single channel amplitudes did not change and thus can be excluded as source for the reduction of macroscopic peak currents (Table 14). Propofol shows a high diversity of effects on 5-HT_{3A}QDA receptor channel activity. Except for the briefest open and the briefest cluster component, all event components, meaning their durations and their fractions are changed (Figure 89). This supports the previously predicted complexity of anesthetic induced effects, which superimpose in macroscopic recordings and thus mask each other and are not resolvable in macroscopic recordings.

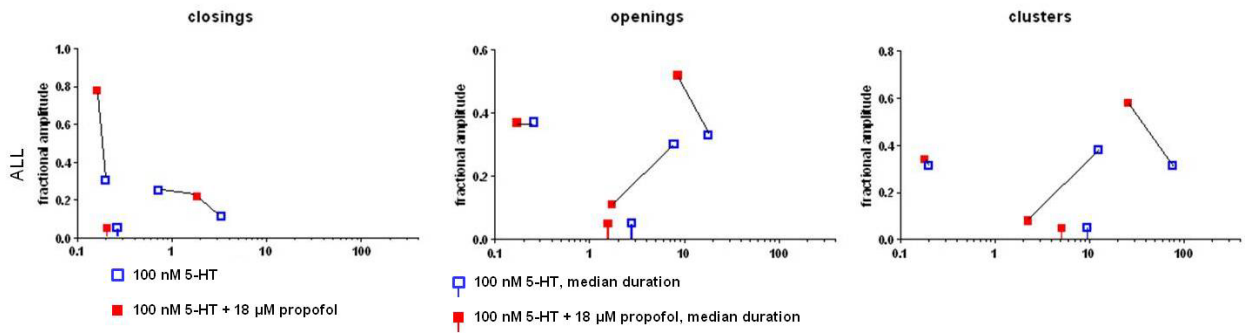

Figure 89: Event durations and their fractional amplitudes at 100 nM 5-HT ± 18 µM propofol. Lines that cross the time line represent the according weighted averages. Time constants and their fractions that the plots are based on can be found in Table 21 - Table 23 in the attachment.

Reduced cluster durations to about a third of their control reflect the reduced decay phase of macroscopic currents. The fractions of long open and cluster durations increased. This may reveal enhancing effects of propofol, which are masked in macroscopic experiments. Current enhancing and current inhibiting effects cancel out, so that over all the open probability within clusters and number of events within a cluster do not change (Table 18). This may indicate that more events are needed to enhance statistical differences. However, the main effects of propofol are to decrease cluster duration and possibly to increase the time between clusters. A reduced probability to enter a cluster, for example, can explain the larger effect of propofol on recorded macroscopic current peaks in ++ application mode compared to the -+ mode.

Overall, propofol seems to destabilize the channel protein. It tends to fluctuate faster between open and closed states, which results in shorter closings and openings. The number of openings in a cluster is unchanged. Thus the probability to end a cluster after an opening does not change, but shorter events sum up to shorter clusters. Shorter clusters sum up to shorter QMC decays, which resembles the acceleration of current decay in recorded macroscopic currents.

5-HT$_{3A}$ QDA – With Phenol

Applying 3 mM phenol to cell attached patches of 5-HT$_{3A}$QDA transfected cells caused a predominance of short closures and long openings in single channel recordings (Figure 82). Despite these enhancing effects of phenol on closed and open durations within clusters (Figure 82), the open probabilities within clusters did not change. However, clusters include more of the prolonged openings which results

in a strong prolongation of cluster duration. When aligning and summing up all long clusters of individual recordings, QMCs of patches exposed to 3 mM phenol showed much longer decay phases than QMCs of patches without phenol (Figure 83), similar to the prolongation of macroscopic decay time constants of excised patch recordings over 5-HT_{3A} (Barann et al., 2008; Witten, 2009).

The serotonin concentration dependence of phenol effects that have been shown by Witten for 5-HT_{3A} are visible on single channel level for the high conductance variant as well. The less serotonin is applied together with phenol, the stronger the effects on single channel kinetics (Figure 82). This suggests that one action of phenol is to interact with serotonin at the agonist binding site.

Surprisingly, phenol did not only influence kinetic values of single channel behavior of 5-HT_{3A}QDA channels, but also increased the single channel conductance (Figure 16). This can only be a partial explanation for the current increasing effect of phenol on macroscopic 5-HT_{3A} currents, which is only present at open channel and equilibrium application (Barann et al., 2008). First macroscopic recordings of 5-HT_{3A}QDA with phenol application (data not shown) even indicate much stronger enhancing effects of phenol on current peak amplitudes of the high conductance variant. Partly this can be due to the continuous presence of both phenol and serotonin during single channel recordings. Enhancing effects of phenol are masked by the increased equilibrium fraction of desensitized channels in the patch.

Overall, in contrast to propofol, phenol seems to stabilize the open state of the 5-HT_{3A}QDA channel and the channel stays activated longer. Neither a 12 % single channel current increase nor changes in open probabilities within clusters are sufficient to explain the strong enhancing effects of phenol on macroscopic peak currents. Similarly to the effects of propofol, the multitude of effects on open and closed durations does not sum up to significant changes in open probability within clusters. This indicates that the main effects of anesthetics on 5-HT_{3A}QDA kinetics can be found in cluster characteristics, such as the probabilities to enter and exit a cluster.

Implications for Future Substance Studies on Single Channel Level

Propofol and phenol introduced many changes to the single channel kinetics of the *human* 5-HT_{3A}QDA receptor. Inhibitory effects correlate with previously described inhibitory effects on macroscopic currents. For propofol, additional potentiating effects were revealed, which were suggested but could not be discriminated in macroscopic experiments.

Open probabilities within control clusters are very high (88 % – 94 % at 5-HT concentrations 30 nM – 3 µM). This raises the question, how substances increase macroscopic peak amplitudes, if within single channel clusters the maximum of activity seems to be reached just by binding the agonist. Some substances might increase single channel conductance. Another possible explanation would be that a substance increases the probability of a channel to start a cluster or decrease the probability to end a cluster. The latter option would mainly prolong the decay phase of macroscopic currents and lead to an increase of over all ion flux, the peak amplitude would not be much higher though. Indications for both can be found in the increased total open probability in recordings when phenol is present.

In order to not be limited to single channel activity within clusters, a way to determine the number of channels in a patch would have to be introduced. This could be done by recording macroscopic and microscopic currents from the same patch. Such a protocol will have to make sure that as well the large macroscopic as the tiny microscopic events are resolved properly.

A high number of recordings is needed due to high variability of channel activity (from patch to patch as well as over time) to be able to perform proper statistics. Thus future substance studies will be very time consuming, unless a way to record control and substance applications from the same patch is found.

As well the combination of macroscopic and microscopic current recordings as the combination of control and substance recordings on one patch require very stable excised patches that last over long time periods. To avoid channel activity rundown and effects and methodical artifacts that can come with it, it is essential to work with the lowest channel activity level possible, either by using low agonist concentrations or by using low transfection rates.

Conclusions

In the *human* $5HT_{3A}$QDA receptor channel a tentative/promising model for studies on single channel kinetics of ligand gated ion channels was found. Its control characterization requires a complex kinetic scheme for 5-HT_3 channel activity that includes at least two open states and three closed states within three types of clusters. The kinetics of *human* 5-HT_{3A}QDA are serotonin concentration dependent.

While there is considerable agreement between the macroscopic behavior of 5-HT_{3A}QDA channels and wild type receptors, there are some differences. Thus it is necessary to determine the effects of substances on the macroscopic currents of the mutant channel before one can proceed to single channel level.

The study of propofol (and its parent compound phenol) on both the macroscopic and single channel levels of *human* 5-HT_{3A}QDA receptors confirmed the complexity of anesthetic actions of these compounds. Complex actions of anesthetics on macroscopic kinetics of the receptor are composed of many actions on single channel kinetic properties such as open, closed and cluster durations and frequencies. In order to fully understand the effects of anesthetics, however, single channel studies are needed with related compounds to correlate the effects of functional groups on an anesthetic molecule with specific kinetic actions on single channels.

Abstract

5-HT_{3A} receptor channels have served in extensive macroscopic electrophysiological studies as a model to study effects of anesthetics and their related compounds on ligand-gated ion channels. Here, studies on the single channel level are pursued in order to provide a more detailed understanding of anesthetic induced effects on ion channels. Two high conductance forms of 5-HT_3 receptors are characterized and evaluated for their usefulness for single channel kinetic analysis of anesthetic interactions with ion channels.

Expression of human heteromeric 5-HT_{3AB} receptor channels was possible but problematic. There was evidence for functional co-existing 5-HT_{3A} homomers in cells transfected with both A and B subunits so that their individual properties could not be isolated. In addition, the proportion of functional heteromers decreased with the number of cell passages until none could be detected.

5-HT_{3A}QDA is the least modified high conductance mutant of homomeric 5-HT_{3A} receptor channels. Single channel data for *human* 5-HT_{3A}QDA receptor channels as a function of serotonin concentration confirm, in principle, the need for a complex kinetic model such as that proposed by Corradi et al. for *mouse* 5-HT_{3A}QDA receptor channels. The data also indicate the need for adjusting this model for the *human* 5-HT_{3A}QDA receptor.

The macroscopic characterization showed that 5-HT_{3A}QDA receptors are similar to wild-type 5-HT_{3A} receptors in their sensitivity to 5-HT and in their onset and offset kinetics, although the latter are accelerated and the rectification properties are changed. Thus, it is important to characterize the macroscopic effects of each substance on 5-HT_{3A}QDA receptors before proceeding to single channel measurements. Macroscopic studies with propofol and hexanol show mostly a high level of similarity between 5-HT_{3A} and 5-HT_{3A}QDA receptor channel behavior.

Propofol and phenol affected not just one but many aspects of 5-HT_{3A}QDA single channel kinetics. For propofol, the results confirmed not only the well-described inhibitory effects, but also provided direct evidence for an additional potentiating effect that had previously been indirectly inferred from macroscopic experiments.

Human 5-HT_{3A}QDA receptor channels are a suitable model for future substance studies at single channel level and provide additional insights into the diverse and complex effects of anesthetics on ligand-gated ion channels.

Attachments

List of Figures

Figure 1: Basic features of a neurotransmitter-gated ion channel, taken from N. Unwin 1993. 7
Figure 2: The architecture of the eukaryotic members of the pentameric ligand-gated ion channel super family. 11
Figure 3: Kinetic scheme for opening and closing of AChR 12
Figure 4: Kinetic scheme for opening and closing of mouse 5-HT_{3A}QDA channels, taken from (Corradi et al., 2009). 12
Figure 5: patch clamp configurations 20
Figure 6: Voltage application on the example of a 5-HT_{3A}QDA transfected excised outside out patch to record macroscopic currents. 24
Figure 7: Different solution application modes on excised outside out patches on the example of a 5-HT_{3A}QDA transfected patch. 25
Figure 8: Example for a macroscopic current of 5-HT_{3A} channels in an excised outside out patch, induced by 30 µM 5-HT. 30
Figure 9: Six traces of one 5-HT_{3AB} transfected patch, induced by 30 µM 5-HT at -100 mV. 33
Figure 10: All points histogram by plotting traces shown above. 34
Figure 11: Combined histograms of the same six 300 nM 5-HT recordings. 37
Figure 12: Duration components (ms) resulting from multiple Gaussian fits (formula 6) of closed duration histograms for individual patches at different serotonin concentrations. 38
Figure 13: Critical gaps (t_{gap}) between closed time components (C1-C7) 39
Figure 14: representative current trace over a stably 5-HT_{3A} transfected cell patch, induced by 30 µM 5-HT at -100 mV 40
Figure 15: I_{peak} of 5-HT induced currents over 5-HT_{3A} expressing membrane patches (n=15). 41
Figure 16: τ_{ON} and τ_{OFF} of 5-HT induced currents over 5-HT_{3A} expressing membrane patches (n=15) over the time since the patch was formed. 42
Figure 17: Recovery of 5-HT_{3A} from desensitization. 43
Figure 18: 5-HT concentration responses of stably 5-HT_{3A} transfected cell patches 44
Figure 19: representative trace of an outside out patch of stable 5-HT_{3AB} transfected HEK cell 45
Figure 20: representative trace of an outside out patch of stable 5-HT_{3AB} transfected HEK cell 46
Figure 21: 30 µM 5-HT induced peak currents (pA) at different dish ages (days). 47
Figure 22: Current amplitudes (pA) of single channel (sc) openings induced by 30 µM 5-HT at -100 mV. 47
Figure 23: Recovery from desensitization of 5-HT_{3AB} transfected cell patches. 48
Figure 24: Voltage dependence of currents of eleven 5-HT_{3AB} stably transfected cells induced by 30 µM 5-HT. 48
Figure 25: Voltage dependence of 5-HT_{3AB} currents induced by 30 µM 5-HT compared to different numbers of passages that cells went through before getting patched. 49
Figure 26: 5-HT_{3AB} transfected cell, traces of a patch at different voltages (-100 mV to +100 mV). Red trace at -100 mV was enlarged, single channel openings directed downwards. 49
Figure 27: 5-HT_{3AB} transfected cell, traces of a patch at different voltages (-100 mV – 100 mV). Red trace at -100 mV was enlarged. 49
Figure 28: ‘rectifying factor’ as calculated by formula (14) at different passages of different cell batches. 51
Figure 29: Concentration response curves for 20 individual patches of 5-HT_{3AB} stably transfected HEK293 cells. 52
Figure 30: Concentration response curves for different populations of patches of 5-HT_{3AB} stably transfected HEK293 cells. 53
Figure 31: 30 µM 5-HT induced current in an excised outside-out patch of a 5-HT_{3A}QDA transiently transfected HEK 293 cell at -100 mV. 54
Figure 32: I_{peak} of 5-HT induced currents over 5-HT_{3A}QDA expressing membrane patches (n=9) 55
Figure 33: Three 5-HT_{3A}QDA traces recorded over a time period of 30 minutes. 56
Figure 34: τ_{ON} and τ_{OFF} of 5-HT induced currents over 5-HT_{3A} expressing membrane patches (n=9) over the time since the patch was formed. 56

Figure 35: Comparing macroscopic current characteristics of 5-HT_{3A}, 5-HT_{3A}QDA and 5-HT_{3AB} channels. 57
Figure 36: Example of currents over the same 5-HT_{3A}QDA transfected patch, induced by 100, 30, 3 and 1 µM 5-HT at -100 mV 57
Figure 37: Dose response curves for serotonin on 5-HT_{3A} wt channels (from previous studies, as published in Brünker 2010) and on 5-HT_{3A}QDA channels. 58
Figure 38: Macroscopic currents from the same 5-HT_{3A}QDA transfected cell patch, induced by 30 µM 5-HT in a voltage range of -100 mV to +100 mV, in steps of 25 mV. 58
Figure 39: I-V curves for four individual patches. 59
Figure 40: IV curves for 5-HT_{3A} and 5-HT_{3A}QDA transfected cell membrane patches in comparison.. 59
Figure 41: Representative recording of a cell attached patch transiently transfected with 5-HT_{3A}QDA. 62
Figure 42: Magnified stretches from the recording shown in Figure 41. 62
Figure 43: Magnified stretches from the recording shown in Figure 41. 63
Figure 44: Example of a trace recorded at -80 mV induced by 30 nM 5-HT that includes three channel openings (indicated downwards). 63
Figure 45: Example of single channel amplitude analysis of one cell attached patch of a 5-HT_{3A}QDA transiently transfected cell. 64
Figure 46: Duration histograms for events from human 5-HT_{3A}QDA receptors, activated by 30 nM 5-HT, with superimposed fits (blue solid lines). 65
Figure 48: Combined duration histogram for closings of 5-HT_{3A}QDA channels at 30 nM 5-HT. 66
Figure 47: Current trace over a 5-HT_{3A}QDA transfected cell patch to depict a cluster. 66
Figure 49: Combined duration histogram for closings in 2+ clusters of 5-HT_{3A}QDA channels at 30 nM 5-HT 67
Figure 50: Fraction of individual channel openings that do not turn into a 2+ cluster for events from human 5-HT_{3A}QDA receptors at different 5-HT concentrations. 67
Figure 51: The number of openings in five individual recordings over time. 70
Figure 52: Example of a 2+ cluster duration histogram for one out of ten 30 nM 5-HT recordings. 72
Figure 53: Plotting time constants (ms) of fitting 2+ cluster duration histograms of individual patches at different serotonin concentrations. 72
Figure 54: Cluster duration histograms for ten combined patches, events were recorded at 30 nM 5-HT and -80 mV. 73
Figure 55: Cluster duration time constants (ms) and their fractional amplitudes at different 5-HT concentrations. 74
Figure 56: Predicted macroscopic decay based on cluster components. 75
Figure 57: Examples of macroscopic currents obtained by aligning and summing up clusters (blue) and their exponential fits (red). 76
Figure 58: Cluster durations of ten 30 nM recordings in relation to open durations. 78
Figure 59: An example of an open duration histogram for one out of ten 30 nM 5-HT recordings. 78
Figure 60: Resulting time constants (ms) of individual patches at different serotonin concentrations. 79
Figure 61: Open duration histograms and their fits (formula 6) for ten combined patches 80
Figure 62: Open duration histograms for different types of clusters of ten combined patches. 80
Figure 63: Open durations and their relative amplitudes for different types of clusters at different 5-HT concentrations. 81
Figure 64: Cluster durations of ten 30 nM recordings in relation to the number of openings in all clusters. 83
Figure 65: Fractional open probabilities within clusters for eight individual patches of 5-HT_{3A}QDA transfected cells. 84
Figure 66: Cluster durations of ten 30 nM recordings in relation to the fractional open probability in clusters. 85
Figure 67: Fractions of the three open components that start or end clusters (first + last) vs. fractions of longest open components of all events in all clusters at different 5-HT concentrations. 86
Figure 68: Closed duration histograms for ten combined patches 87
Figure 69: Closed durations and their relative amplitudes at different 5-HT concentrations. 88
Figure 70: Fractional open probabilities in 2+ clusters of ten 30 nM recordings in relation to the closed durations (ms) in 2+ clusters. 89
Figure 71: chemical structure of propofol 91
Figure 72: Example of macroscopic 5-HT_{3A}QDA currents exposed to 18 µM propofol. 91
Figure 73 : Closed, open and cluster duration histograms of complete recordings with 100 nM 5-HT and 18 µM propofol. 94
Figure 74: Aligning closed components (ms) for complete individual patches with and without propofol. 95

Figure 75: Event durations and their fractional amplitudes at different [5-HT] ± 18 µM propofol..... 96
Figure 76: Quasi Macroscopic Currents of recordings at 100 nM 5-HT + 18 µM propofol. 99
Figure 77: chemical structure of phenol 100
Figure 78: Activity of one complete cell attached recording with 3 µM 5-HT + 3 mM phenol in the recording pipette. 101
Figure 79: Closed duration histograms for complete combined patches under 3 µM and 30 nM 5-HT + 3 mM phenol and their fits (formula 6, black line)..... 103
Figure 80: Aligning closed components (ms) for complete individual patches with and without phenol at different [5-HT]. 104
Figure 81: Closed duration histograms for different 2+ clusters of combined patches under 3 µM and 30 nM 5-HT + 3 mM phenol and their fits (black line). 105
Figure 82: Event durations and their fractional amplitudes at different [5-HT] ± 3 mM phenol. 108
Figure 83: Quasi macroscopic currents for individual phenol experiments at different serotonin concentrations. 109
Figure 84: Representative trace of an outside out patch of a stable 5-HT_{3AB} transfected HEK cell. .. 113
Figure 85: Duration components (ms) resulting from multiple Gaussian fits (formula 6) of closed duration histograms for individual patches at different serotonin concentrations. 119
Figure 86: Open duration histograms for an individual recording of 30 nM induced single channel openings over human 5-HT_{3A}QDA, fitted with two (left) and three (right) exponential components. .. 124
Figure 87: Extended kinetic scheme for human 5-HT_{3A}QDA receptor channel activity. 125
Figure 88: Comparing macroscopic effects of propofol on 5-HT_{3A}QDA and effects of propofol on 5-HT_{3A} as found in (Witten, 2009). 126
Figure 89: Event durations and their fractional amplitudes at 100 nM 5-HT ± 18 µM propofol..... 128
Figure 90: Example of macroscopic 5-HT_{3A}QDA currents exposed to 1.5 mM n-hexanol. 148
Figure 91: comparing the macroscopic effects of 1.5 mM n-hexanol on 5-HT_{3A}QDA and 5-HT_{3A} channels as found in (Decker, 2010). 149

List of Tables

Table 1: List of used software..... 28
Table 2: List of equipment for the different setups that the experiments were conducted at..... 29
Table 3: Rectifying factors of nine individual patches and their average. 60
Table 4: Current amplitudes (pA) of single 5-HT_{3A}QDA channel events..... 64
Table 5: The medians of cluster durations within ten recordings at 30 nM 5-HT..... 69
Table 6: Event durations in 2+ clusters for 1st halves, 2nd halves and complete cell attached recordings of 5-HT_{3A}QDA channel activity induced by different serotonin concentrations. 71
Table 7: Decay time constants of quasi macroscopic currents built by aligning and summing long clusters of single channel events in cell attached patches compared with decay time constants of recorded macroscopic currents in outside-out patches..... 76
Table 8: Median open durations (ms) of 10 individual patches, exposed to 30 nM 5-HT..... 77
Table 9: Number of openings within clusters for the human 5-HT_{3A}QDA channels at different 5-HT concentrations. 83
Table 10: Medians of open probabilities and number of openings in clusters under different serotonin concentrations. 84
Table 11: Closed components (ms) and their fractions for different serotonin concentrations..... 90
Table 12: effects of open channel (-+) and equilibrium (++) application of 18 µM propofol on macroscopic currents of 5-HT_{3A}QDA channels. 92
Table 13: Total open probability in cell attached recordings with 100 nM 5-HT with and without 18 µM propofol..... 93
Table 14: mean single channel amplitudes (pA) of channel openings in 5-HT_{3A}QDA transfected cell patches. 93
Table 15: number of openings and open probabilities within clusters of 5-HT_{3A}QDA single channel recordings with and without 18 µM propofol..... 98
Table 16: Open probabilities of complete recordings including their 25 % and 75 % percentiles for combined recordings with 30 nM and 3 µM with and without 3 mM phenol..... 101
Table 17: Single channel amplitudes in recordings with and without 3 mM phenol..... 102
Table 18: Open probabilities (%) and number of openings within clusters for the human 5-HT_{3A}QDA channels at different 5-HT concentrations ± 3 mM phenol..... 108
Table 19: Concentration response characteristics of homomeric and heteromeric 5-HT_3 channels found by different groups..... 114
Table 20: Comparing the present with a previous study (Corradi et al., 2009)..... 123
Table 21: Exponential duration histogram components of combined dwell times of all events, normalized so that each patch gains the same weight. 145
Table 22: Exponential duration histogram components of combined dwell times of events in 2+ clusters, normalized so that each patch gains the same weight..... 146
Table 23: Exponential duration histogram components of combined dwell times of events in 5+ clusters, normalized so that each patch gains the same weight..... 147
Table 24: Effects of equilibrium (-+) and open channel (++) application of 1.5 mM n-hexanol on macroscopic currents of 5-HT_{3A}QDA channels. 148

List of Formuli

(1) 31
Macroscopic current fit (2 τ_{OFF})
(2) 32
Macroscopic current fit (1 τ_{OFF})
(3) 32
Weighted average of two decay constants
(4) 33
Gaussian fit of all-points histograms
(5) 35
Gaussian fit of duration histograms
(6) 35
Gaussian fit of duration histograms, transformed to log scale
(7) 36
Open probabilities
(8) 38
Critical gap time between components
(9). 41
Rundown: Decrease of I_{peak} (5-HT_{3A})
(10) 42
Rundown: Decrease of τ_{ON} (5-HT_{3A})
(11) 42
Rundown: Decrease of τ_{OFF} (5-HT_{3A})
(12) 43
Single exponential to fit recovery from desensitization (5-HT_{3A})
(13) 44
Sigmoidale dose response curve
(14) 50
Rectifying factor
(15) 55
Rundown: Decrease of I_{peak} (5-HT_{3A}QDA)
(16) 56
Rundown: Decrease of τ_{ON} (5-HT_{3A}QDA)
(17) 56
Rundown: Decrease of τ_{OFF} (5-HT_{3A}QDA)
(18). 74
Weighted average of cluster components
(19). 81
Weighted average of open components
(20). 88
Weighted average of closed components

References

Auerbach, A., and Akk, G. (1998). Desensitization of Mouse nicotinic acetylcholine receptor channels a two-gate mechanism. J. Gen. Physiol. *112*: 181–197.

Baptista-Hon, D.T., Deeb, T.Z., Lambert, J.J., Peters, J.A., and Hales, T.G. (2013). The minimum M3-M4 loop length of neurotransmitter-activated pentameric receptors is critical for the structural integrity of cytoplasmic portals. J. Biol. Chem. *288*: 21558–21568.

Barann, M., Dilger, J.P., Bönisch, H., Göthert, M., Dybek, A., and Urban, B.W. (2000a). Inhibition of 5-HT_3 receptors by propofol: equilibrium and kinetic measurements. Neuropharmacology *39*: 1064–1074.

Barann, M., Linden, I., Witten, S., and Urban, B.W. (2008). Molecular Actions of Propofol on Human 5-HT3A Receptors: Enhancement as Well as Inhibition by Closely Related Phenol Derivatives: Anesth. Analg. *106*: 846–857.

Barann, M., Meder, W., Dorner, Z., Brüss, M., Bönisch, H., Göthert, M., et al. (2000b). Recombinant human 5-HT_{3A} receptors in outside-out patches of HEK 293 cells: basic properties and barbiturate effects. Naunyn. Schmiedebergs Arch. Pharmacol. *362*: 255–265.

Barrera, N.P., Herbert, P., Henderson, R.M., Martin, I.L., and Edwardson, J.M. (2005a). Atomic force microscopy reveals the stoichiometry and subunit arrangement of 5-HT3 receptors. Proc. Natl. Acad. Sci. U. S. A. *102*: 12595–12600.

Beato, M., Groot-Kormelink, P.J., Colquhoun, D., and Sivilotti, L.G. (2004). The activation mechanism of alpha1 homomeric glycine receptors. J. Neurosci. Off. J. Soc. Neurosci. *24*: 895–906.

Belelli, D., Callachan, H., Hill-Venning, C., Peters, J.A., and Lambert, J.J. (1996). Interaction of positive allosteric modulators with human and Drosophila recombinant GABA receptors expressed in Xenopus laevis oocytes. Br. J. Pharmacol. *118*: 563–576.

Bonnet, V., and Bremer, F. (1952). [Synaptic potentials and central nervous system transmission]. Arch. Int. Physiol. *60*: 33–93.

Borgeat, A., and Stirnemann, H.R. (1998). [Antiemetic effect of propofol]. Anaesthesist *47*: 918–924.

Bouzat, C., Bartos, M., Corradi, J., and Sine, S.M. (2008). The Interface between Extracellular and Transmembrane Domains of Homomeric Cys-Loop Receptors Governs Open-Channel Lifetime and Rate of Desensitization. J. Neurosci. *28*: 7808–7819.

Brady, C.A., Stanford, I.M., Ali, I., Lin, L., Williams, J.M., E Dubin, A., et al. (2001). Pharmacological comparison of human homomeric 5-HT_{3A} receptors versus heteromeric 5-$HT_{3A/3B}$ receptors. Neuropharmacology *41*: 282–284.

Bremer, F., Bonnet, V., and Terzuolo, C. (1954). [Electrophysiologic study of the cortical auditory areas of the cat]. Arch. Int. Physiol. Biochim. *62*: 390–428.

Brünker, S. (2010). Differentielle pharmakologische Sensitivität von humanen 5-HT_3-Rezeptor-Subtypen. PhD Dissertation, Faculty of Medicine, University of Bonn (Bonn, Germany).

Chen, C., and Okayama, H. (1987). High-efficiency transformation of mammalian cells by plasmid DNA. Mol. Cell. Biol. *7*: 2745–2752.

Cheng, A., Bollan, K.A., Greenwood, S.M., Irving, A.J., and Connolly, C.N. (2007). Differential Subcellular Localization of RIC-3 Isoforms and Their Role in Determining 5-HT3 Receptor Composition. J. Biol. Chem. *282*: 26158–26166.

Colquhoun, D., and Sakmann, B. (1985). Fast events in single-channel currents activated by acetylcholine and its analogues at the frog muscle end-plate. J. Physiol. *369*: 501.

Corradi, J., Andersen, N., and Bouzat, C. (2011). A Novel Mechanism of Modulation of 5-HT3A Receptors by Hydrocortisone. Biophys. J. *100*: 42–51.

Corradi, J., Gumilar, F., and Bouzat, C. (2009). Single-Channel Kinetic Analysis for Activation and Desensitization of Homomeric 5-HT3A Receptors. Biophys. J. *97*: 1335–1345.

daCosta, C.J.B., and Sine, S.M. (2013). Stoichiometry for drug potentiation of a pentameric ion channel. Proc. Natl. Acad. Sci. *110*: 6595–6600.

Davies, P.A., Pistis, M., Hanna, M.C., Peters, J.A., Lambert, J.J., Hales, T.G., et al. (1999). The 5-HT3B subunit is a major determinant of serotonin-receptor function. Nature *397*: 359–363.

Decker, A.-M. (2010). Kinetische und pharmakologische Charakterisierung der molekularen Effekte von n-Alkanolen auf humane 5-HT_{3A} Rezeptoren. PhD Dissertation, Faculty of Medicine, University of Bonn (Bonn, Germany).

Decker, A.-M., Witten, S., Barann, M., and Urban, B.W. (2015). Fast and slow interactions of n-alkanols with human 5-HT_{3A} receptors: Implications for anesthetic mechanisms. Biochim. Biophys. Acta BBA - Biomembr. *1848*: 1524–1535.

Deeb, T.Z., Carland, J.E., Cooper, M.A., Livesey, M.R., Lambert, J.J., Peters, J.A., et al. (2006). Dynamic Modification of a Mutant Cytoplasmic Cysteine Residue Modulates the Conductance of the Human 5-HT3A Receptor. J. Biol. Chem. *282*: 6172–6182.

Dilger, J.P., Vidal, A.M., Mody, H.I., and Liu, Y. (1994). Evidence for direct actions of general anesthetics on an ion channel protein. A new look at a unified mechanism of action. Anesthesiology *81*: 431–442.

Eccles, J.C. (1964). The ionic mechanism of postsynaptic inhibition. Science *145*: 1140–1147.

Eccles, J.C., Schmidt, R., and Willis, W.D. (1963). Pharmacological studies on presynaptic inhibition. J. Physiol. *168*: 500–530.

Gyermek, L. (1995). 5-HT3 receptors: pharmacologic and therapeutic aspects. J. Clin. Pharmacol. *35*: 845–855.

Hales, T.G., Dunlop, J.I., Deeb, T.Z., Carland, J.E., Kelley, S.P., Lambert, J.J., et al. (2006). Common Determinants of Single Channel Conductance within the Large Cytoplasmic Loop of 5-Hydroxytryptamine Type 3 and 4beta2 Nicotinic Acetylcholine Receptors. J. Biol. Chem. *281*: 8062–8071.

Hapfelmeier, G., Tredt, C., Haseneder, R., Zieglgänsberger, W., Eisensamer, B., Rupprecht, R., et al. (2003). Co-expression of the 5-HT_{3B} Serotonin Receptor Subunit Alters the Biophysics of the 5-HT_3 Receptor. Biophys. J. *84*: 1720–1733.

Hodgkin, A.L., and Huxley, A.F. (1952). A quantitative description of membrane current and its application to conduction and excitation in nerve. J. Physiol. *117*: 500–544.

Hodgkin, A.L., and Katz, B. (1949). The effect of sodium ions on the electrical activity of the giant axon of the squid. J. Physiol. *108*: 37–77.

Hussy, N., Lukas, W., and Jones, K.A. (1994a). Functional properties of a cloned 5-hydroxytryptamine ionotropic receptor subunit: comparison with native mouse receptors. J. Physiol. *481*: 311–323.

Kapeller, J., Möller, D., Lasitschka, F., Autschbach, F., Hovius, R., Rappold, G., et al. (2011). Serotonin receptor diversity in the human colon: Expression of serotonin type 3 receptor subunits 5-HT3C, 5-HT3D, and 5-HT3E. J. Comp. Neurol. *519*: 420–432.

Kazama, T., Ikeda, K., and Morita, K. (1998). The pharmacodynamic interaction between propofol and fentanyl with respect to the suppression of somatic or hemodynamic responses to skin incision, peritoneum incision, and abdominal wall retraction. Anesthesiology *89*: 894–906.

Kelley, S.P., Dunlop, J.I., Kirkness, E.F., Lambert, J.J., and Peters, J.A. (2003a). A cytoplasmic region determines single-channel conductance in 5-HT3 receptors. Nature *424*: 321–324.

Krzywkowski, K., Davies, P.A., Feinberg-Zadek, P.L., Bräuner-Osborne, H., and Jensen, A.A. (2008a). High-frequency HTR3B variant associated with major depression dramatically augments the signaling of the human 5-HT3AB receptor. Proc. Natl. Acad. Sci. U. S. A. *105*: 722–727.

Krzywkowski, K., Davies, P.A., Irving, A.J., Bräuner-Osborne, H., and Jensen, A.A. (2008b). Characterization of the effects of four HTR3B polymorphisms on human 5-HT3AB receptor expression and signalling. Pharmacogenet. Genomics *18*: 1027–1040.

Livesey, M.R., Cooper, M.A., Deeb, T.Z., Carland, J.E., Kozuska, J., Hales, T.G., et al. (2008). Structural Determinants of Ca2+ Permeability and Conduction in the Human 5-Hydroxytryptamine Type 3A Receptor. J. Biol. Chem. *283*: 19301–19313.

Livesey, M.R., Cooper, M.A., Lambert, J.J., and Peters, J.A. (2011). Rings of Charge within the Extracellular Vestibule Influence Ion Permeation of the 5-HT3A Receptor. J. Biol. Chem. *286*: 16008–16017.

Lochner, M., and Lummis, S.C.R. (2010). Agonists and antagonists bind to an A-A interface in the heteromeric 5-HT3AB receptor. Biophys. J. *98*: 1494–1502.

Meiboom, M.F., Barann, M., Witten, S., Groeneveld, K., and Urban, B.W. (2013). Which agonist properties are important for the activation of 5-HT_{3A} receptors? Biochim. Biophys. Acta *1828*: 2564–2573.

Miles, T.F., Dougherty, D.A., and Lester, H.A. (2013). The 5-HT3AB Receptor Shows an A3B2 Stoichiometry at the Plasma Membrane. Biophys. J. *105*: 887–898.

Neher, E., and Sakmann, B. (1995). Single-Channel Recording (Springer).

Neher, E., Sakmann, B., and Steinbach, J.H. (1978). Nehr, Steinbach, Sakmann, 1978.

Nguyen, H.T., Li, K., daGraca, R.L., Delphin, E., Xiong, M., and Ye, J.H. (2009). Behavior and Cellular Evidence for Propofol-induced Hypnosis Involving Brain Glycine Receptors: Anesthesiology *PAP.*:

Niesler, B., Frank, B., Kapeller, J., and Rappold, G.A. (2003). Cloning, physical mapping and expression analysis of the human 5-HT3 serotonin receptor-like genes HTR3C, HTR3D and HTR3E. Gene *310*: 101–111.

Niesler, B., Walstab, J., Combrink, S., Möller, D., Kapeller, J., Rietdorf, J., et al. (2007). Characterization of the novel human serotonin receptor subunits 5-HT3C,5-HT3D, and 5-HT3E. Mol. Pharmacol. *72*: 8–17.

Noam, Y., Wadman, W.J., and Hooft, J.A. van (2008). On the voltage-dependent Ca2+ block of serotonin 5-HT3 receptors: a critical role of intracellular phosphates. J. Physiol. *586*: 3629–3638.

Peters, J.A., Cooper, M.A., Carland, J.E., Livesey, M.R., Hales, T.G., and Lambert, J.J. (2010). Novel structural determinants of single channel conductance and ion selectivity in 5-hydroxytryptamine type 3 and nicotinic acetylcholine receptors. J. Physiol. *588*: 587–596.

Pistis, M., Belelli, D., Peters, J.A., and Lambert, J.J. (1997). The interaction of general anaesthetics with recombinant GABAA and glycine receptors expressed in Xenopus laevis oocytes: a comparative study. Br. J. Pharmacol. *122*: 1707–1719.

Rayes, D., Rosa, M.J. De, Sine, S.M., and Bouzat, C. (2009). Number and Locations of Agonist Binding Sites Required to Activate Homomeric Cys-Loop Receptors. J. Neurosci. *29*: 6022–6032.

Rüsch, D., Musset, B., Wulf, H., Schuster, A., and Raines, D.E. (2007). Subunit-Dependent Modulation of the 5-Hydroxytryptamine Type 3 Receptor Open-Close Equilibrium by n-Alcohols. J. Pharmacol. Exp. Ther. *321*: 1069–1074.

Sigworth, F.J., and Sine, S.M. (1987). Data transformations for improved display and fitting of single-channel dwell time histograms. Biophys. J. *52*: 1047.

Sine, S.M., and Steinbach, J.H. (1987). Activation of acetylcholine receptors on clonal mammalian BC3H-1 cells by high concentrations of agonist. J. Physiol. *385*: 325–359.

Stevens, R. (2005). Modulation of Human 5-Hydroxytryptamine Type 3AB Receptors by Volatile Anesthetics and n-Alcohols. J. Pharmacol. Exp. Ther. *314*: 338–345.

Stewart, A., Davies, P.A., Kirkness, E.F., Safa, P., and Hales, T.G. (2003). Introduction of the 5-HT3B subunit alters the functional properties of 5-HT3 receptors native to neuroblastoma cells. Neuropharmacology *44*: 214–223.

Suchyna, T.M., Markin, V.S., and Sachs, F. (2009). Biophysics and structure of the patch and the gigaseal. Biophys. J. *97*: 738–747.

Tecott, L.H., Maricq, A.V., and Julius, D. (1993). Nervous system distribution of the serotonin 5-HT3 receptor mRNA. Proc. Natl. Acad. Sci. U. S. A. *90*: 1430–1434.

Unwin, Nigel (1993). Neurotransmitter Action: Opening of Ligand-Gated Ion Channels. Cell *10:* 31-41.

Urban, B.W., Bleckwenn, M., and Barann, M. (2006). Interactions of anesthetics with their targets: non-specific, specific or both? Pharmacol. Ther. *111*: 729–770.

Walstab, J., Hammer, C., Bönisch, H., Rappold, G., and Niesler, B. (2008). Naturally occurring variants in the HTR3B gene significantly alter properties of human heteromeric 5-hydroxytryptamine-3A/B receptors: Pharmacogenet. Genomics *18*: 793–802.

Witten, S. (2009). Molekulare Mechanismen von Phenol-Derivaten anligandengesteuerten Ionenkanälen. PhD Dissertation, Faculty of Mathematics and Natural Science, University of Bonn (Bonn, Germany).

Zeller, A., Jurd, R., Lambert, S., Arras, M., Drexler, B., Grashoff, C., et al. (2008). Inhibitory Ligand-Gated Ion Channels as Substrates for General Anesthetic Actions. In Modern Anesthetics, P.D. h c J. Schüttler, and P.D.D.H. Schwilden, eds. (Springer Berlin Heidelberg), pp 31–51.

Supporting Material

Time Constants and their Fractions for Combined Histograms

Table 21: Exponential duration histogram components of combined dwell times of **all events**, normalized so that each patch gains the same weight.
C = closed components, O = open components ,Cs = cluster components ,τ = time constant (ms), fr.amp = fractional amplitude
Control and propofol data based on t_{crit} 30ms, phenol data based on t_{crit} 300ms

30 nM 5-HT (10 patches)

	τ1	fr.amp 1	τ2	fr.amp 2	τ3	fr.amp 3	τ4	fr.amp 4	τ5	fr.amp 5	τ6	fr.amp 6	τ7	fr.amp 7	τ8	fr.amp 8	# events
C	0.17	0.31	0.99	0.14	5.8	0.05	57	0.03	456	0.07	2802	0.27	18338	0.12	x	x	3450
O	0.19	0.41	5.0	0.21	17	0.38											3450
Cs	0.19	0.42	10	0.31	44	0.27											1776

100 nM 5-HT (4 patches)

	τ1	fr.amp 1	τ2	fr.amp 2	τ3	fr.amp 3	τ4	fr.amp 4	τ5	fr.amp 5	τ6	fr.amp 6	τ7	fr.amp 7	τ8	fr.amp 8	# events
C	0.20	0.30	0.73	0.25	3.4	0.11	25	0.04	276	0.09	1674	0.14	14162	0.07	x	x	12627
O	0.26	0.37	7.9	0.30	18	0.33											12627
Cs	0.20	0.31	13	0.38	77	0.31											3525

300 nM 5-HT (6 patches)

	τ1	fr.amp 1	τ2	fr.amp 2	τ3	fr.amp 3	τ4	fr.amp 4	τ5	fr.amp 5	τ6	fr.amp 6	τ7	fr.amp 7	τ8	fr.amp 8	# events
C	0.15	0.39	1.0	0.14	5.3	0.19	74	0.08	x	x	1638	0.09	14214	0.08	109826	0.02	16294
O	0.24	0.29	2.2	0.14	33	0.57											16294
Cs	0.17	0.30	1.4	0.08	31	0.28	182	0.34									2651

3 µM 5-HT (7 patches)

	τ1	fr.amp 1	τ2	fr.amp 2	τ3	fr.amp 3	τ4	fr.amp 4	τ5	fr.amp 5	τ6	fr.amp 6	τ7	fr.amp 7	τ8	fr.amp 8	# events
C	0.14	0.38	0.79	0.21	2.7	0.13	44	0.05	252	0.07	1991	0.09	10529	0.14	x	x	4644
O	0.21	0.34	5.7	0.35	20	0.31											4644
Cs	0.17	0.32	25	0.47	128	0.21											1251

30 nM 5-HT + 3 mM phenol (4 patches)

	τ1	fr.amp 1	τ2	fr.amp 2	τ3	fr.amp 3	τ4	fr.amp 4	τ5	fr.amp 5	# events
C	0.12	0.88	2.2	0.03	42	0.02	2614	0.03	24188	0.05	2349
O	0.25	0.13	1.5	0.16	18	0.27	70	0.45			**2349**
Cs	0.14	0.24	1.1	0.09	67	0.23	389	0.43			**260**

3 µM 5-HT + 3 mM phenol (6 patches)

	τ1	fr.amp 1	τ2	fr.amp 2	τ3	fr.amp 3	τ4	fr.amp 4	τ5	fr.amp 5	# events
C	0.13	0.93	5.8	0.03	85	0.01	2044	0.01	11887	0.01	23059
O	0.32	0.14	5.1	0.26	22	0.60					**23059**
Cs	0.20	0.24	3.0	0.08	364	0.33	1996	0.35			**480**

100 nM 5-HT + 18 µM propofol (4 patches)

	τ1	fr.amp 1	τ2	fr.amp 2	τ3	fr.amp 3	τ4	fr.amp 4	τ5	fr.amp 5	# events
C	0.16	0.47	1.9	0.13	59	0.13	344	0.04	5927	0.03	8390
O	0.17	0.37	1.7	0.11	8.5	0.52					8390
Cs	0.18	0.34	2.3	0.08	26	0.58					4410

Table 22: Exponential duration histogram components of combined dwell times of **events in 2+ clusters**, normalized so that each patch gains the same weight.
C = closed components, O = open components ,Cs = cluster components, τ = time constant (ms), fr.amp = fractional amplitude
Control and propofol data based on t_{crit} 30ms, phenol data based on t_{crit} 300ms

30 nM 5-HT (10 patches)								
	τ1	fr.amp 1	τ2	fr.amp 2	τ3	fr.amp 3		# events
C	0.17	0.61	0.98	0.27	7.8	0.12		1674
O	0.23	0.34	12	0.66				2299
Cs	14	0.22	46	0.78				625

100 nM 5-HT (4 patches)								
	τ1	fr.amp 1	τ2	fr.amp 2	τ3	fr.amp 3		# events
C	0.21	0.45	0.83	0.39	6.5	0.16		9102
O	0.31	0.35	13.0	0.65				10806
Cs	22	0.40	86	0.60				1704

300 nM 5-HT (6 patches)								
	τ1	fr.amp 1	τ2	fr.amp 2	τ3	fr.amp 3		# events
C	0.15	0.54	1.0	0.19	6.4	0.27		13643
O	0.28	0.24	2.4	0.13	33	0.62		15234
Cs	35	0.31	196	0.69				1591

3 µM 5-HT (7 patches)								
	τ1	fr.amp 1	τ2	fr.amp 2	τ3	fr.amp 3		# events
C	0.15	0.52	1.0	0.36	7.4	0.12		3393
O	0.23	0.30	6.0	0.38	20	0.32		4078
Cs	31	0.70	156	0.30				685

30 nM 5-HT + 3 mM phenol (4 patches)								
	τ1	fr.amp 1	τ2	fr.amp 2	τ3	fr.amp 3		# events
C	0.12	0.97	2.5	0.03				2089
O	0.70	0.22	14	0.27	66	0.51		2244
Cs	1.5	0.07	86	0.17	400	0.75		155

3 µM 5-HT + 3 mM phenol (6 patches)								
	τ1	fr.amp 1	τ2	fr.amp 2	τ3	fr.amp 3		# events
C	0.13	0.95	5.6	0.03	83	0.01		22316
O	0.33	0.14	5.1	0.27	22	0.60		22885
Cs	3.2	0.06	361	0.45	1986	0.50		569

100 nM 5-HT + 18 µM propofol (4 patches)								
	τ1	fr.amp 1	τ2	fr.amp 2	τ3	fr.amp 3		# events
C	0.16	0.81	1.6	0.19				3980
O	0.16	0.28	1.5	0.12	8.4	0.60		5791
Cs	29	1.00						1811

Table 23: Exponential duration histogram components of combined dwell times of **events in 5+ clusters**, normalized so that each patch gains the same weight.
C = closed components, O = open components ,Cs = cluster components, τ = time constant (ms), fr.amp = fractional amplitude
Control and propofol data based on t_{crit} 30ms, phenol data based on t_{crit} 300ms

30 nM 5-HT (10 patches)								
	τ1	fr.amp 1	τ2	fr.amp 2	τ3	fr.amp 3		# events
C	0.16	0.58	0.95	0.32	7.5	0.10		885
O	0.26	0.32	12	0.68				1018
Cs	73	1.00						133

100 nM 5-HT (4 patches)								
	τ1	fr.amp 1	τ2	fr.amp 2	τ3	fr.amp 3		# events
C	0.23	0.48	0.90	0.38	6.2	0.14		7536
O	0.32	0.35	13	0.65				8304
Cs	113	1.00						768

300 nM 5-HT (6 patches)								
	τ1	fr.amp 1	τ2	fr.amp 2	τ3	fr.amp 3		# events
C	0.16	0.54	1.2	0.21	6.4	0.25		12415
O	0.31	0.24	2.3	0.13	34	0.63		13296
Cs	254	1.00						881

3 µM 5-HT (7 patches)								
	τ1	fr.amp 1	τ2	fr.amp 2	τ3	fr.amp 3		# events
C	0.15	0.57	1.1	0.32	6.0	0.12		2657
O	0.26	0.29	7.5	0.49	26	0.22		2916
Cs	94	1.00						259

30 nM 5-HT + 3 mM phenol (4 patches)								
	τ1	fr.amp 1	τ2	fr.amp 2	τ3	fr.amp 3		# events
C	0.12	0.97	2.3	0.03				1947
O	0.83	0.23	13.4	0.28	66	0.49		**2021**
Cs	595	1.00						**74**

3 µM 5-HT + 3 mM phenol (6 patches)								
	τ1	fr.amp 1	τ2	fr.amp 2	τ3	fr.amp 3		# events
C	0.13	0.95	5.8	0.03	81	0.01		22469
O	0.33	0.13	5.2	0.27	22	0.60		**22777**
Cs	623	0.61	2629	0.39				**308**

100 nM 5-HT + 18 µM propofol (4 patches)								
	τ1	fr.amp 1	τ2	fr.amp 2	τ3	fr.amp 3		# events
C	0.16	0.84	1.5	0.16				1611
O	0.15	0.27	0.49	0.11	8.0	0.63		1872
Cs	49	1.00						261

5-HT$_{3A}$ QDA – With n-Hexanol

Excised Outside-Out Patches

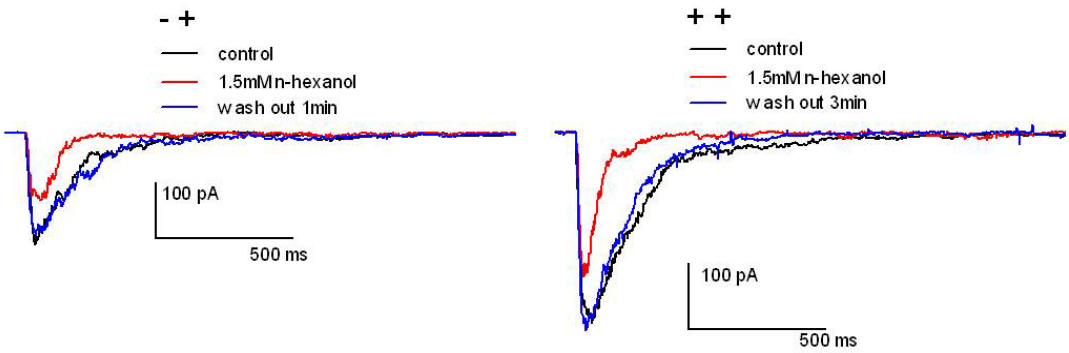

Figure 90: Example of macroscopic 5-HT$_{3A}$QDA currents exposed to 1.5 mM n-hexanol. Left: open channel application. Right: equilibrium application.

During open channel (-+) experiments, 1.5 mM n-hexanol was applied simultaneously with 5-HT. Equilibrium (++) experiments were conducted by exposing the patch to n-hexanol for a minute before a 5-HT pulse is added. Average values from control and wash out trace were used as control reference to take eventual rundown in account. Open channel and equilibrium application of 1.5 mM n-hexanol did not differ significantly from each other. Peak current amplitudes were suppressed to 67.7 % and 81 % of control respectively. As well as τ_{ON} as τ_{OFF} get faster when n-hexanol is applied, although for open channel application the reduction of τ_{ON} is not significant.

Table 24: Effects of equilibrium (-+) and open channel (++) application of 1.5 mM n-hexanol on macroscopic currents of 5-HT$_{3A}$QDA channels.
Peak reduction by -+ application to 67.7 % and the peak reduction by ++ application to 81 % was significant (P values of 0.0007 and 0.03 respectively). τ_{OFF} is reduced to 50 % (-+, P 0.0049) or 49.3 % (++, P 0.04). The onset did only change significantly at ++application (P 0.02). Paired two tailed t-tests.

condition		% of control	SD	n (=patches)
peak (pA)	-+	67.7***	1.5	3
	++	81.0*	6.2	3
τ_{ON}	-+	72.5	26.2	2
	++	64.0*	9.0	3
τ_{OFF}	-+	50.0**	6.1	3
	++	49.3*	18.0	3

Effects of n-hexanol on 5-HT$_{3A}$ channels are similar for both experimental modes. As well the peak current amplitudes as onset and decay phase of macroscopic currents are reduced by about half.

5-HT$_{3A}$QDA channels seem a little less sensitive to n-hexanol, but the tendencies are the same. Decker describes a time constant for the inhibiting effect of 21 ms and a partial recovery after 11.6 s (Decker, 2010), which explains that in the case of -+ application, hexanol is more inhibiting and causes a stronger reduction of the peak current. A similar effect can be seen here for the high conductance form.

Here gained macroscopic data of human 5-HT$_{3A}$QDA receptors under n-hexanol support again the high level of pharmacological similarity between the high conductance channel and its wild type.

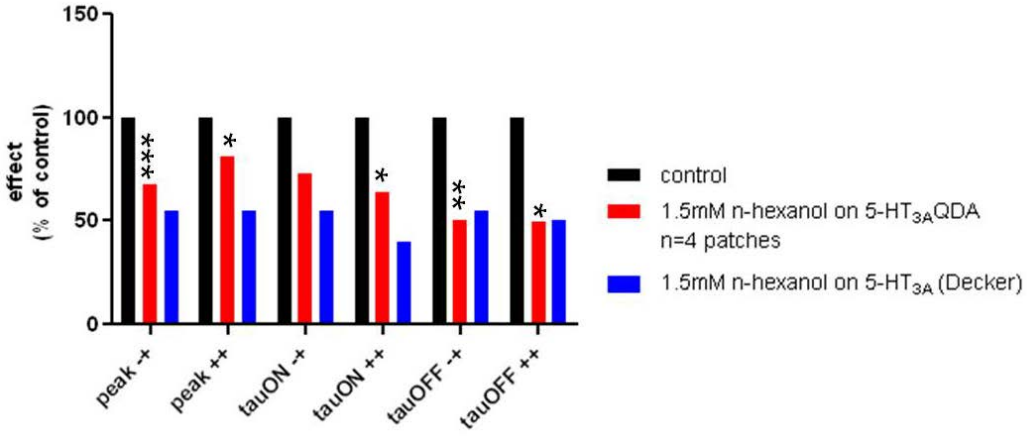

Figure 91: comparing the macroscopic effects of 1.5 mM n-hexanol on 5-HT_{3A}QDA and 5-HT_{3A} channels as found in **(Decker, 2010)**.
* shows significant differences of present n-hexanol study to its control. 5-HT_{3A}QDA data: Peak reduction by -+ application to 67.7 % and the peak reduction by ++ application to 81 % was significant (P values of 0.0007 and 0.03 respectively). τ_{OFF} is reduced to 50 % (-+, P 0.0049) and 49.3 % (++, P 0.04). The onset did only change significantly at ++application (P 0.02). Paired two tailed t-tests. 5-HT_{3A} data: taken from concentration response curves in **(Decker, 2010)**.

Acknowledgment

My deepest gratitudes go to Dr. Urban and Dr. Dilger. They did not only provide an interesting project topic, but supported me in all possible ways. This Thesis was only possible due to many (and many more!) stimulating discussions with them.

I want to thank Zita Dorner and Dr. Witten, who introduced me to 5-HT_{3A} channels and to my co-workers in Bonn and am very grateful for an always motivating and cheerful atmosphere in the laboratory of the Institute for Anesthesiology in Bonn.

During my stay at the Department of Anesthesiology in Stony Brook I felt always welcome and I want to thank Dr. Dilger for his constant support in various life – and lab-situations.

I thank Dr. Herzog for surveying this thesis with so much enthusiasm.

Thank you to everybody who brought me some coffee and some cheerful words every now and then.

Curriculum Vitae

Apr 2010 – Sep 2015	Doctoral thesis, Department of Anesthesiology, University Clinic Bonn molecular actions of anesthetica on the ligand-gated 5-HT_{3A} receptor (transfected HEK cells, macroscopic and single channel recordings)
Mar 2011 – Apr 2014	Research Scholar, Department of Anesthesiology, University Hospital Stony Brook, NY In cooperation with Department of Anesthesiology, University Clinic Bonn
Nov 2008 – Nov 2009	Scientific Assistant, Institute of Physiology and Pathophysiology, University Medical Center of the Johannis Gutenberg University Mainz thalamocortical and parasagital brain slices (animal: mice), patch clamp (whole cell, paired recordings, focal extracellular stimulation)
Mar 2007 – Mar 2008	Diplom thesis, Department of Membrane Biophysics, Institute of Botany, Technical University Darmstadt differential Rb^- and K^- conductivity of the viral potassium channel Kcv (voltage clamp, *Xenopus* oocytes)
Nov 2000 – March 2008	Technical University of Darmstadt, Darmstadt, Germany degree: Diplom Biologe (equiv. Master of Science), grade 1.4, major in plant physiology, animal physiology, ecology

Eidesstattliche Erklärung

Hiermit erkläre ich, dass ich die vorliegende Arbeit selbstständig angefertigt und keine anderen als die angegebenen Hilfsmittel und Quellen verwendet habe.

Kathrin Groeneveld, Bonn, September 2015